Design of a Latching Mechanism for Unloading a Rotary Compressor

by

Michael D. Webb

B.S. Mechanical Engineering
University of North Carolina at Charlotte, 1997

SUBMITTED TO THE DEPARTMENT OF MECHANICAL ENGINEERING IN PARTIAL FULFILLMENT OF THE REQUIREMENTS FOR THE DEGREE OF

MASTER OF SCIENCE IN MECHANICAL ENGINEERING
AT THE
MASSACHUSETTS INSTITUTE OF TECHNOLOGY

FEBRUARY 1999

© copyright 1999 Massachusetts Institute of Technology
All rights reserved

Signature of Author:_____
Department of Mechanical Engineering
January 15, 1999

Certified by:_____
Joseph L. Smith, Jr.
Professor of Mechanical Engineering
Thesis Supervisor

Accepted by:_____
Ain A. Sonin
Chairman, Department Committee on Graduate Students

MASSACHUSETTS INSTITUTE OF TECHNOLOGY
WITHDRAWN
JUL 12 1999
FROM
MIT LIBRARIES

ENG

Design of a Latching Mechanism for Unloading a Rotary Compressor

by

Michael D. Webb

Submitted to the Department of Mechanical Engineering on January 15, 1999 in partial fulfillment of the requirements for the Degree of Master of Science in Mechanical Engineering

ABSTRACT

The objective of this project was to develop an inexpensive means at achieving variable capacity in rotary air conditioning compressors. The current method at achieving variable capacity is to use a variable speed electric motor. This method actually uses high cost electronics to slow down the rotational speed of the electric motor and thus the pump drive shaft. This project developed a simple, mechanical mechanism which enables the compressor to achieve variable capacity without implementing these expensive motor controls.

The first chapter of the thesis starts by introducing the fundamental principles of how the latching mechanism works. Included in this chapter are explanations of major design issues such as the self-releasing concept. Chapters two and three then develop the static and dynamic equations needed to model the physics of the latching operation of the mechanism. Also included in these two chapters are details of the design including engineering drawings and material specifications.

The fourth chapter explains test data taken with the latching mechanism installed in a rotary compressor. Included in this chapter are test results from the mechanical operation of the mechanism. Also, there are air conditioning system test results from the implementation of the latching mechanism. Performance values such as COP and EER are recorded to better understand how well the latching mechanism was achieving variable capacity.

The final chapter presents the overall conclusions that were gained from this project. Also, suggestions are made for future mechanisms that could be made to improve upon the one discussed in this thesis.

Thesis Supervisor: Prof. Joseph L. Smith, Jr.
Title: Collins Professor of Mechanical Engineering

ACKNOWLEDGMENTS

I first wish to thank my advisor, Professor Joseph L. Smith, Jr., for the opportunity he gave me with this "hands-on" thesis project. I enjoyed working with him and he always made himself available when I needed help. I also believe he has increased my ability to approach engineering problems formally while, at the same time, helping me to build more physical intuition.

I thank Professor Wilson for his overall leadership and guidance with this project. I also would like to recognize Dr. Steven Umans and Dave Otten who helped with the solenoid coil design and the data acquisition system.

Both Mike Demaree and Bob Gertsen made themselves available in the shop of Building 41 whenever I needed to find tools or needed machining advice.

I would also like to thank Kevin Dunshee at Carrier in Syracus, NY. He helped me tremendously while I spent three weeks over the summer of 1998 at Carrier testing the latching mechanism. I also thank Carrier in general for its financial support of this project.

Finally, I would like to thank my father, George Webb, who instilled in me at an early age the desire to pursue engineering and the importance of an education.

TABLE OF CONTENTS

LIST OF FIGURES

LIST OF TABLES

NOMENCLATURE

A Differential equation constant (Equation 2.17)
A_1 Area of the cross section of the slider that is above the Neutral Axis (in^2)
A_{sur} Surface area of the slider on which there is oil film sliding resistance (ft^2)
a Shaft eccentricity (in)
a_s Variable in the reduced, nonlinear, differential equation used for the disengaging analysis of the slider
B Differential equation constant (Equation 2.18)
b Clearance distance between one side of the slider and the precision slot it travels in (ft)
b_s Variable in the reduced, nonlinear, differential equation used for the disengaging analysis of the slider
C Center of the rolling piston (a point)
C' Center of vain tip radius (a point)
CL Maximum edge to edge clearance between the left-most edge of the slider and the right-most edge of the latch on the vane stem (see Figure 2.15) (in)
c Distance from the Neutral Axis of the slider to the outer edge of the slider (in)
c_s Variable in the reduced, nonlinear, differential equation used for the disengaging analysis of the slider
D Resultant force of the solenoid disengaging force (FE) and the slider spring engaging force (S2) (lb)
d Discharge chamber (in^3)
d_s Variable in the reduced, nonlinear, differential equation used for the disengaging analysis of the slider
dP/dg Pressure gradient in g direction (see Figure 2.8) (lb/ft^2)/ft)
dT Total travel needed for the slider to engage the latch (in)

dx_{sp}/dt Velocity of the slider (ft/s)
du/dh Velocity gradient of the fluid between one side of the slider and the precision slot it travels in (1/s)
F Maximum resistive force acting on slider (lb)
FE Solenoid disengaging force (lb)
F_r The resultant force acting on the latch in the vane stem that is perpendicular to the line of contact between the latch and the slider (lb)
F_{vert} The h direction force component of F_r (lb)
f Frequency of compressor motor (Hz or rev/s)
g Axis direction
H Height dimension of the slider (in)
h Axis direction
I Moment of inertia of the entire cross-sectional area of the slider about it's Neutral Axis (in^4)
k Coil spring constant (lb/ft)

L Length between center of rolling piston (**C**) and the center of the vane tip radius (**C'**) (in)

M Maximum bending moment value in the slider when the slider is in the latched position (lb*in)

m Mass of the slider (lb*s^2/ft)

N.A. Nuetral Axis

O Center of the crankshaft (a point)

Q First moment of the area that acts about the N.A. of the slider (in^3)

S1, S2 Spring force values for engaging the slider into the latch (lb)

S3 Spring force value for the engaging of the slider. A first order linear equation combination of S1 and S2. (lb)

s Suction chamber (in^3)

T Width of the cross section of the slider (in)

t Time (s)

u Maximum velocity of the slider (ft/s)

V Summation of spring force plus gas discharge pressure force acting on the vane and vane stem. It is also the maximum shearing force across the cross section of the slider. (lb)

x Displacement of the vane and vane stem (in)

x1 Maximum coil spring compression displacement away from relaxed position (in)

x2 Minimum coil spring compression displacement away from relaxed position (in)

x(θ) Displacement of the vane and vane stem as a function of crank angle (in)

x(t) Displacement of the vane and vane stem as a function of time (in)

$\mathbf{x_s}$ Displacement of the slider when modeling with solenoid design 1 (in)

$\mathbf{x_{ss}}$ Displacement of the slider when modeling with solenoid design 2 (in)

$\mathbf{x_{sp}}$ Displacement of the slider when modeling with the spring force only (in)

$\mathbf{x_{sp}(t)}$ Displacement of the slider when modeling with the spring force only as a function of time (in)

$\dot{x}_s$ Reduction term which is the first derivative of displacement with respect to time (ft/s)

$\ddot{x}_{sp}$ Acceleration of the slider (For engaging analysis) (ft/s^2)

$\ddot{x}_s$ Acceleration of the slider (For disengaging analysis) (ft/s^2)

$\mathbf{y_b}$ Distance from the Nuetral Axis of the slider to the centroid of area A_1 (in)

τ Shearing stress of oil/freon mixture (lb/ft^2)

τ_{ave} Average value of the shearing stress across the cross section of the slider (lb/in^2)

τ_{max} Maximum value of the shearing stress found at the edges of the cross section of the slider (lb/in^2)

σ_m Maximum compressive stress in the slider (lb/in^2)

μ Viscosity of freon/oil mixture (lb*s/ft^2)

ω Angular speed of main crankshaft about center **O** (rad/s)

θ Crank angle (see Figure 2.2) (radians)

ϕ Vane to rolling piston angle (see Figure 2.2) (radians)

Δ Angle of the surface of contact between the slider and the latch in the vane stem with respect to the horizontal (degrees)

1. INTRODUCTION

This chapter contains three sections. The first section describes the operation of the two types of compressors and the motivation behind this project. The second section describes the operation of the rotary compressor and introduces the concept of the vane-latching mechanism. Section three describes the areas of the vane-latching mechanism on which this study has focused.

1.1 OPERATION OF THE ROTARY AND VARIABLE SPEED COMPRESSORS AND MOTIVATION BEHIND THIS PROJECT

Both the Carrier DB240 rotary compressor and the variable speed compressors compress and pump refrigerant 22 through the standard airconditioning cycle. The variable speed compressor can vary the mass flowrate of refrigerant 22 through the system where the model DB240 (and other similiar models) have a fixed mass flowrate. The variable speed compressor accomplishes this varying mass flowrate by reducing the electric compressor motor speed. This has many advantages including increased customer comfort due to a more constant cooling temperature, increased thermal efficiency, and reduced power consumption. The main disadvantage of the variable speed compressor is the high cost due to the variable speed characteristics of the electric compressor motor.

The motivation behind this project then became to develop a less expensive means at achieveing variable speed compressor performance. It was thought that since the variable speed compressor varied the mass flowrate of the refrigerant 22 in the system, a simple adaptation to the rotary compressor could accomplish the same thing.

This project was undertaken to develop a simple mechanism that could control the mass flow rate of refrigerant 22 in the Carrier model DB240 rotary compressor. The goals that were set for this project are:

1. Design and develop a mechanism that would allow for a controlled, varying mass flow rate of refrigerant in the Carrier DB240 rotary compressor.

2. Physically make this mechanism and implement it in a DB240 rotary compressor complete with control systems installed.

3. Throughly test the mechanism and analyze the results (both thermal and mechanical).

1.2 OPERATION OF THE CARRIER MODEL DB240 ROTARY COMPRESSOR AND INTRODUCTION OF THE VANE-LATCHING MECHANISM

A brief look at the basic operation of the rotary compressor, similiar to the Carrier DB240 compressor that is the focus of this study, will prove helpful in shedding some light on the idea behind the use of a vane-latching mechanism to achieve a variable mass flow rate.

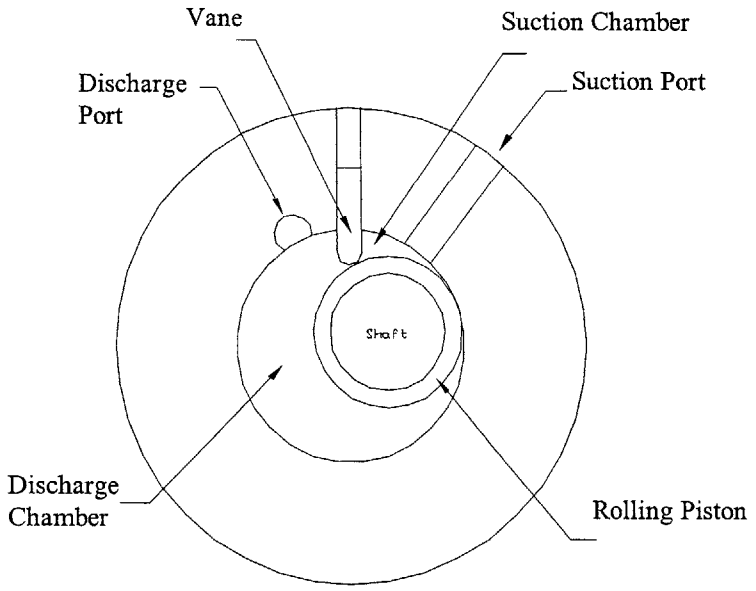

Figure 1.1

Figure 1.1 shows a very simple schematic of a rotary compressor, which basically consists of a cylindrical chamber linked to an inlet port and a pressure activated discharge valve. A rolling piston sits on an eccentric shaft driven by a motor. As it rolls, the piston contacts the wall of the cylindrical chamber forming a sealing point. A vane, which is pressure loaded during normal operation (by the fluid at discharge pressure and a spring), pushes against the rolling piston, thus forming a second sealing point and creating a closed discharge chamber whose volume decreases during the cycle, thus compressing the fluid.

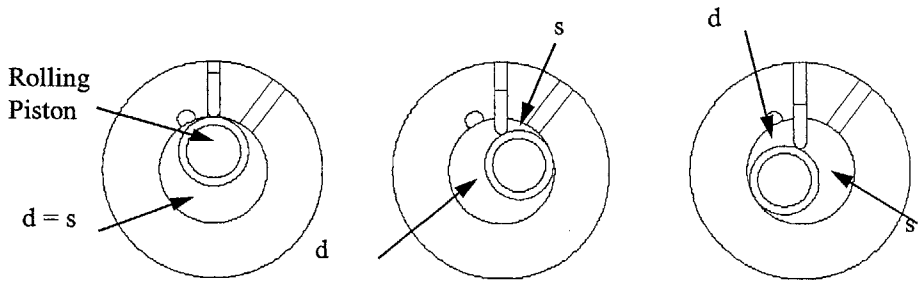

Figure 1.2 (Where d is discharge chamber and s is suction chamber)

The position of the rolling piston as the system goes through one complete revolution of the shaft is illustrated in Figure 1.2. The suction chamber (denoted by s) is always in contact with fluid at suction pressure via the inlet port. As soon as the rolling piston passes beyond the inlet port, a sealing point is formed thus trapping fluid at suction conditions within the closed discharge chamber (denoted by d). Further rotation of the piston causes this discharge chamber to continuously decrease in volume, thus building up fluid pressure in the chamber. Once the chamber exceeds the compressor discharge pressure, the pressure imbalance activates the discharge valve causing it to open, thus discharging the high pressure fluid. Once the piston reaches top dead center the two sealing points merge into one and the cycle is then repeated.

In order to achieve variable mass flow rate in this compressor the idea of lifting and holding the vane for a certain number of cycles was adopted. It can easily be understood that by lifting the vane the discharge chamber's seal is broken (See Figure 1.1). Discharge pressure can no longer build up and thus the discharge port will not open. The net result of this is a stop in the mass flow rate of the refrigerant 22 through the compressor. Then if the vane could be lifted and re-engaged at a controlled rate, the mass flowrate could also be controlled. Thus the modified rotary compressor would now equal the performance characteristics of the variable speed compressor. A previous attempt at designing a vane-lifting mechanism failed due to it's inability to disengage the vain at a fast enough rate. (Master of Science Thesis at MIT titled "Design of an Unloader for Rotary Compressors", June 1998) The result of this was audible noise as the rolling piston impacted the vane as the vane was being disengaged or "lifted."

In order to fix this problem the vane-latching mechanism was developed. Now, instead of "lifting" the vane, the vane is latched and held as the rolling piston passes the top dead center position (TDC) (See Figures 1.3, 1.4, and 1.5). Once again the discharge chamber's seal is broken and no refrigerant 22 flows through the system. The "latching" at the top dead center position is accomplished by applying an engaging force to the slider. The vane is latched at a position such that the vane will travel upward

approximately .020 in. every time the rolling piston rotates to the top dead center position. The "bumping" or displacing of the vane and vane stem .020in, while the slider is latched, is done on every revolution of the rolling piston. The .020in "bump" achieves two things: 1. it allows time for the slider to engage or extract and 2. it gives geometric clearance needed for the slider to engage or extract. These two design features are the heart of the mechanical self-synchronization concept developed for the latching and unlatching of the slider. In order to disengage the latching mechanism the force holding the slider in is reversed. The latch geometry is such that the slider will only disengage when the rolling piston comes to TDC and lifts the vane, and thus the vane stem, .020 in off the slider. Once disengaged the vane is free to follow the rolling piston as it passes away from TDC. The ability to engage and disengage the latching-mechanism at TDC prevents the rolling piston from having a heavy impact with the vane.

The force that is applied to the slider for engaging and disengaging is a combination spring force and solenoid force. The solenoid allows for electrical control of the timing of the engaging and disengaging of the latching mechanism.

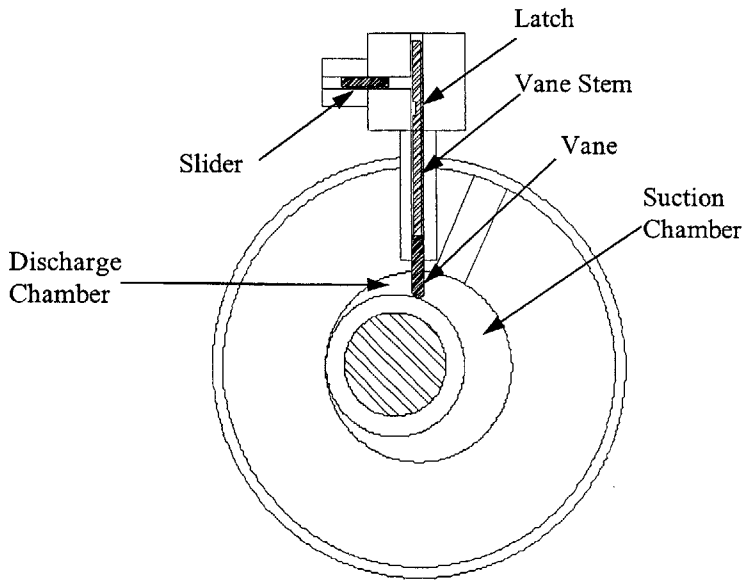

Figure 1.3 (Shows slider and latch disengaged; vane free to follow rolling piston)

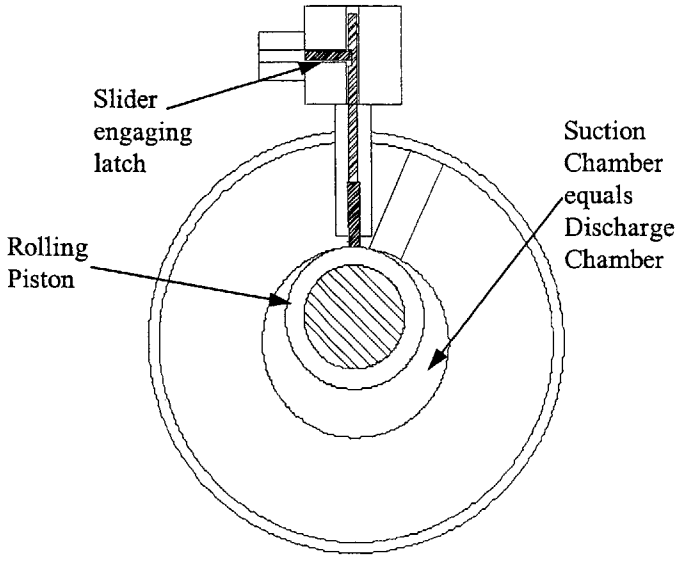

Figure 1.4 (Shows slider engaging latch in vane stem; note that this occurs where piston is at TDC)

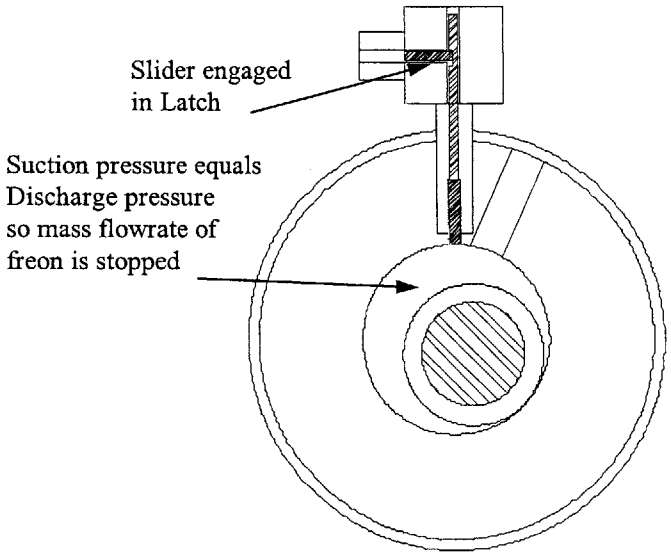

Figure 1.5 (Shows slider engaged in latched position; note that discharge chamber and suction chamber pressure are equal. Thus mass flowrate of refrigerant 22 through the compressor is now stopped.)

1.3 Focus of Study

The remaining chapters address issues related to the mechanics of the slider and the latch interface as well as the building and testing of the mechanism. Chapter two is devoted to the details of the design and analysis of the slider and latch system. Topics covered include motion, stress, and friction analysis on the slider. Chapter three deals with the manufacturing, construction, and implementation of the mechanism. Chapter four contains test and operation results (both of the mechanism and of the new thermal characteristics of the air conditioning system in general). Chapter five lists the major conclusions and recommendations for the implementation of this vane-latching mechanism.

2. DESIGN OF THE VANE-LATCHING MECHANISM

This chapter contains seven sections. Section one starts with a geometric description of the major mechanism parts and how they interact with one another. Section two deals with the analysis of the dynamics of the vane stem. This section sets the parameters that will have to be met by the slider in order for successfull latching to occur. Section three looks at the first part of the motion and dynamic analysis of the slider. Included in this section is the specification of the spring force necessary to engage the slider. Section four concludes the motion and dynamic analysis of the slider. Included in this section is the analysis of the unlatching force produced by the solenoid. Section five looks at the impact of friction on the operation of the slider. Section six contains a detailed load and stress analysis of the slider. Section seven describes the latch-slider interface geometry and the resulting force analysis.

2.1 Geometric Description And Part Identification

Figure 2.1A is shown in the following pages to better describe the major mechanism components and how they interact. Figures 1.3, 1.4, and 1.5 should also be referenced in order to understand the geometric positioning of all the mechanism parts relative to the crankshaft, rolling piston, vane, and compressor shell of the EDB240 rotary compressor. Notice in Figure 2.1A that all the components are numbered and then labeled in Table 2.1A. This is an assembly-type of drawing and includes phantom views of both the block and the solenoid. It is important to recognize that the other end of the vane stem (not shown) is connected directly to the vane in the compressor. Thus the entire assembly shown in Figure 2.1A resides outside the shell of the compressor. So in this view the vane stem reciprocates in the block as it follows the vane. When the compressor is at top dead center (TDC), the geometry is such that the slider (under action from the spring force) is free to engage itself into the notch in the vane stem. This prevents the vane stem (and thus the vane) from reciprocating and effectively unloads the compressor. In order to retract the slider and load the compressor, the solenoid produces a force opposing the spring force. The slider will not retract until the compressor reaches TDC however. It can be seen that the edges of the latch surfaces are inclined such as to avoid the extraction of the slider until the vane stem is lifted off the slider slightly. This small lift is referred to as "bump" and is equal to approximately .020in. The vane stem "bump" occurs in a very short period of time as the compressor approaches TDC. Physically what is happening is the rolling piston in the case of the compressor displaces the vane .020in as the crankshaft of the compressor approaches TDC. This in turn displaces the vane stem .020in. Once the slider has been extracted, the compressor is able to run loaded again. This is a very simple description of the operation of this mechanism. A more detailed description will follow later in Chapter 2.

Figures 2.1B and 2.1C both show cross section views of the solenoid. Both of these figures show more details than the view of the solenoid shown in Figure 2.1A. Figure

2.1B represents the solenoid configuration for Solenoid Design 1 and Figure 2.1C represents the solenoid configuration for Solenoid Design 2. It is important to notice in Figures 2.1A, 2.1B, and 2.1C that both spring options are shown (one for Solenoid Design 1 and one for Solenoid Design 2). Solenoid Design 1 uses the 3-arm beam springs shown engaging the slider in Figure 2.1A. Solenoid Design 2 uses the coil spring shown in Figure 2.1C. The main difference electrically/magnetically between Solenoid Design 1 and Solenoid Design 2 is that Solenoid Design 1 used a permanent magnet while Solenoid Design 2 does not. Also, the coil in Solenoid Design 1 is single wound while the coil in Solenoid Design 2 is double wound (2 wires fed onto the spool at the same time). The purpose for the permanent magnet in Solenoid Design 1 was to hold the slider extracted against the engaging spring force without having to run current through the coil. Due to problems that were encountered with the permanent magnet, the design was later changed to Solenoid Design 2. Here, current has to run through the coil in order to hold the slider extracted against the spring force.

The two cylindrical pieces that encase the solenoid (what is shown in Figure 2.1A) are made of ferrite in order to meet the magnetic design parameters for the solenoid.

It is important to understand that once the latching mechanism is fully assembled (see Figure 2.1A) the cylindrical ferrite piece comes in contact with the front face of the block (the face where the slider enters the block). The cylindrical ferrite pieces are held in place up against the block with the can (see drawing in Chapter 3). The bottom side of the block (the side where the vane stem is shown potruding) is sealed and attached to the shell of the rotary compressor with the flange (see drawing in Chapter 3). O-ring seals exist on all surfaces of the block that are shown open to the atmosphere in Figure 2.1A.

Table 2.1A (Parts Identification for Figure 2.1A)

Part Number	Part Name
1	Block
2	Vane Stem
3	Slider
4	Beam-Type Spring (2)
5	Solenoid (2 cylindrical ferrite pieces shown only

Table 2.1B (Parts Identification for Figure 2.1B)

Part Number	Part Name
1	Ferrite Piece (2 total)
2	Coil (Single Wound)
3	Spacer
4	Permanent Magnet

Table 2.1C (Parts Identification for Figure 2.1C)

Part Number	Part Name
1	Ferrite Piece (2 total)
2	Coil (double wound)
3	Pusher-Pin
4	Coil Spring
5	Spacer
6	Pole Piece
7	Green, Plastic, Ring Spacer

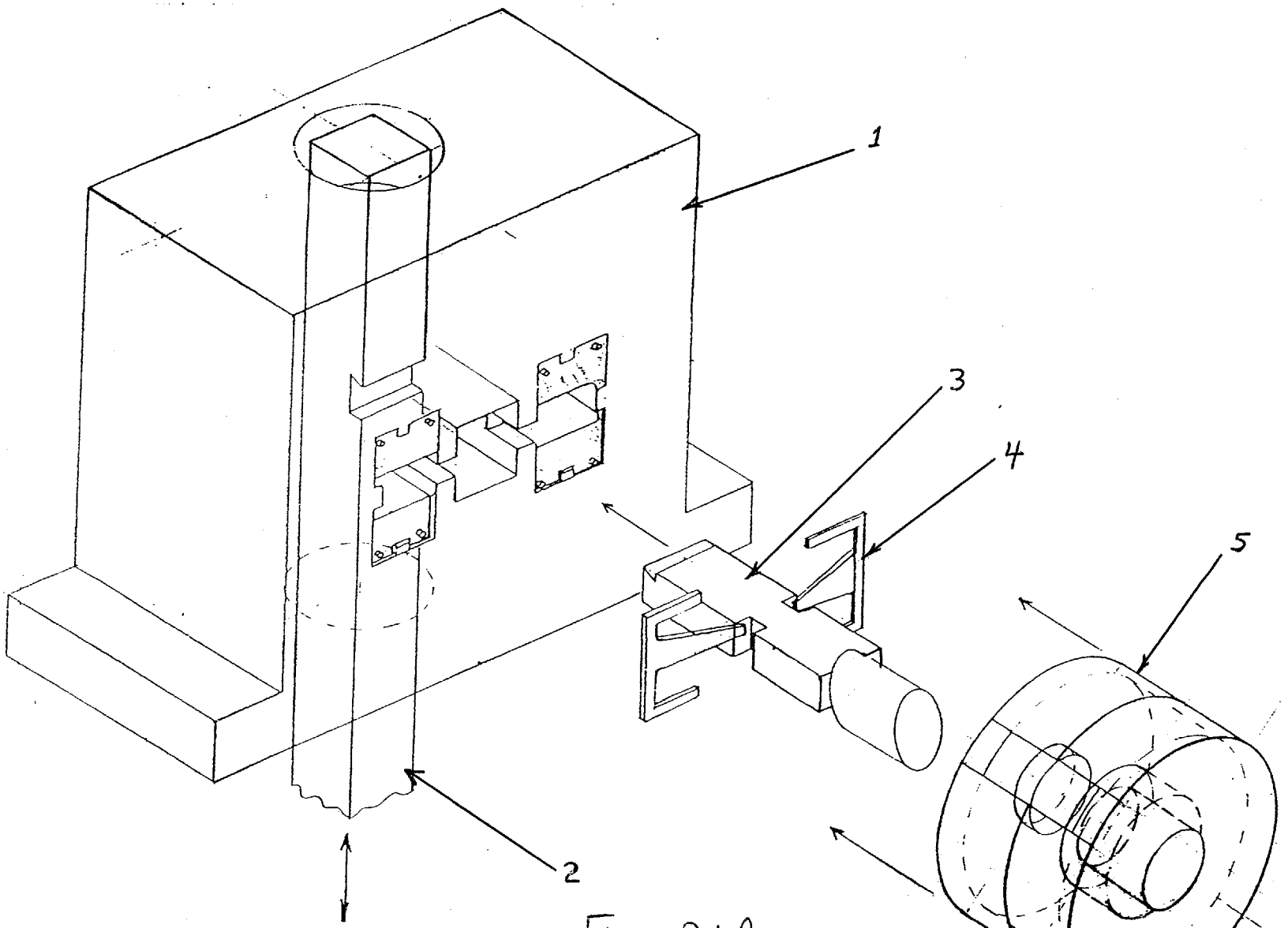

Figure 2.1 A

Scale: 1.66:1

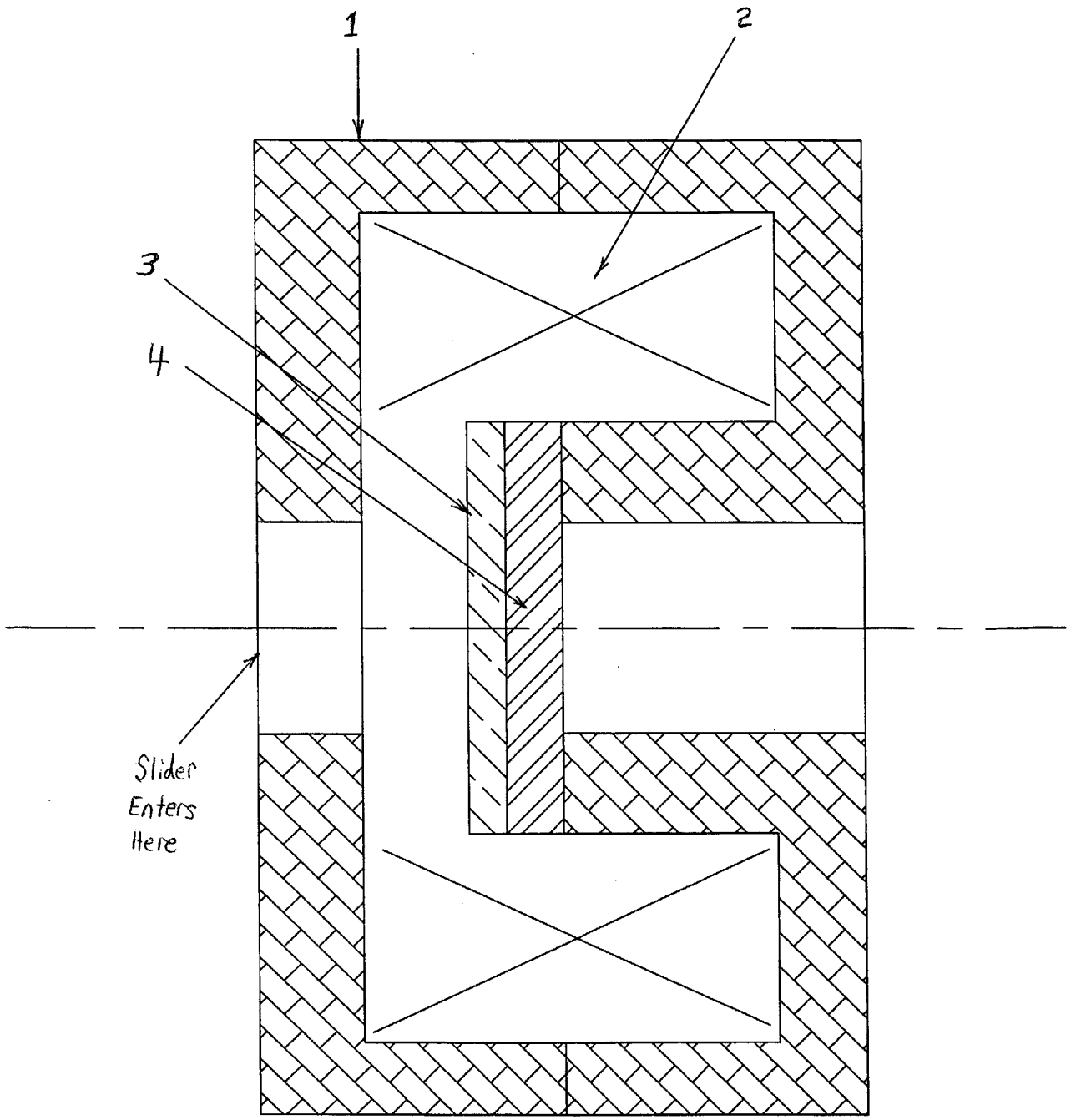

Cross Section of Solenoid Solenoid Design 1		
Comments: Figure 2.1B	Date: 12/16/98	Scale: 6:1

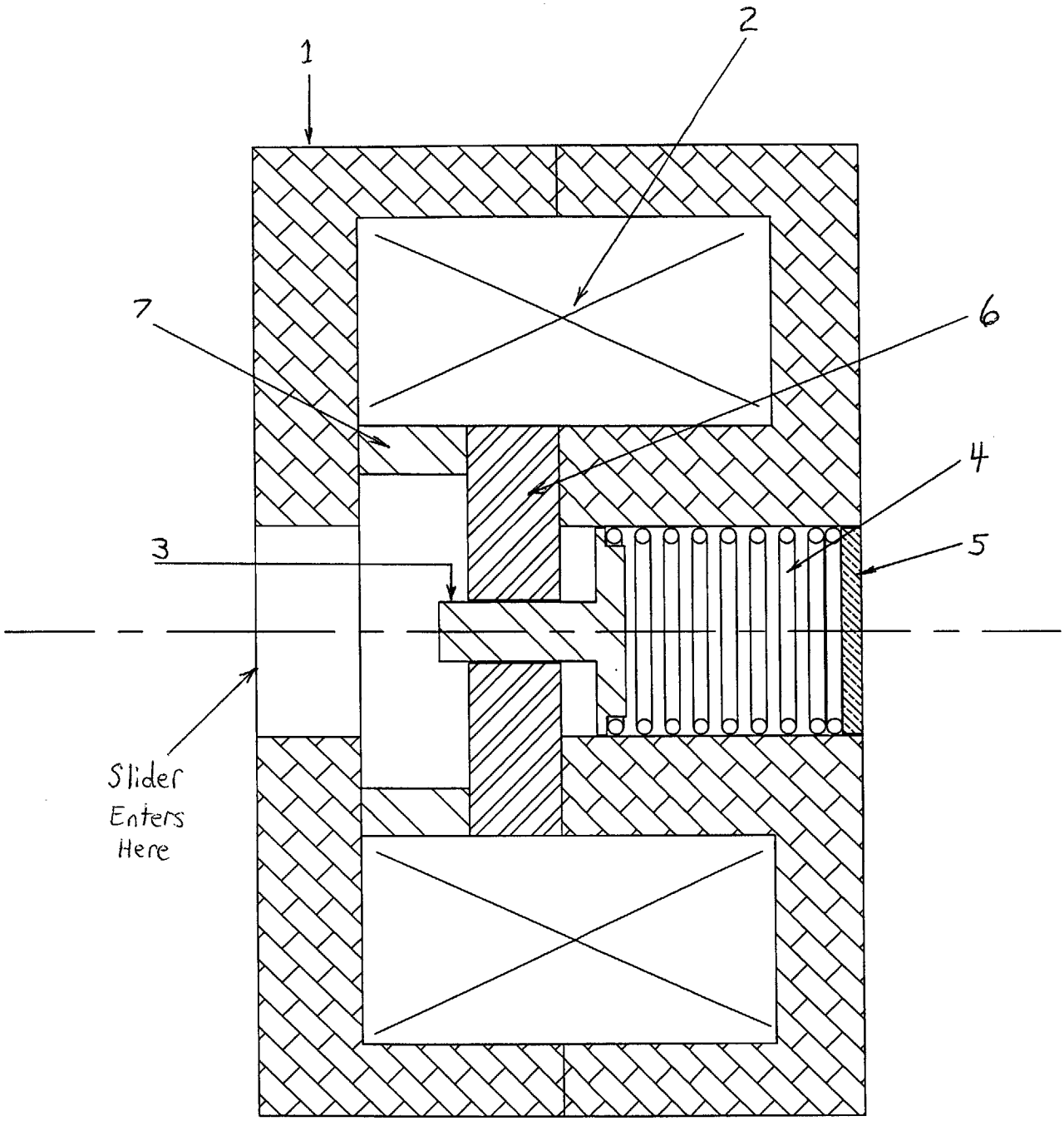

Cross Section of Solenoid Solenoid Design 2		
Comments: Figure 2.1C	Date: 12/16/98	Scale: 6:1

2.2 Analysis Of The Dynamics Of The Vane Stem

In order to successfully design the slider that will engage the latch on the vane stem, (see Figure 1.3, page 5) it is necessary to fully understand the dynamic characteristics of the rolling piston and the vane stem. Of particular interest is the position of the vane stem as a function of time. This section will concentrate on obtaining this result and thus define the dynamic parameters needed for the slider.

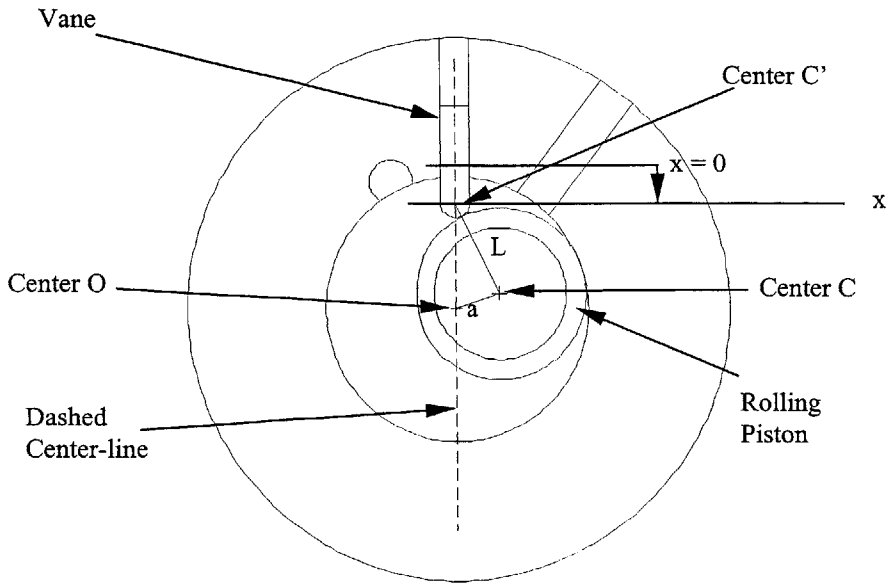

Figure 2.1 (Shows the slider-crank geometry of the rolling piston and the vane. Center C represents the center of the rolling piston, Center O represents the center of the crank shaft, and Center C' represents the center of the vane tip radius)

In Figure 2.1 it is easy to see that if the position of the vane as a function of time and crank angle θ (see also Figure 2.2) can be found, then the position of the vane stem as a function of time and crank angle θ is also known (they are equal). The parameters that are of concern are length a, length L, and ω (angular speed of the shaft about Center O). These parameters are listed below. They come from Carrier and apply to the model DB240 rotary compressor.

a = .199in (shaft eccentricity) **(2.1)**

L = .962in + .177in = 1.139in **(2.2)**

Equation 2.2 represents the summation of the rolling piston outside radius and the vane tip radius respectively.

Rotational speed is 3600rpm = 60 rev/sec = 60 hertz, thus...

$\omega = 2*(\pi)*f = 2*(3.14159)*60 = 377$ rad/sec = angular velocity of crank shaft **(2.3)**

f is the frequency and is equal to 60 rev/sec.

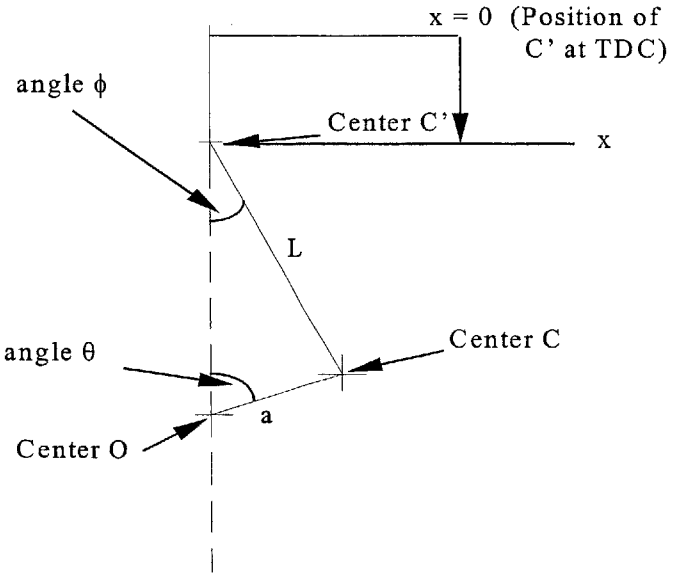

Figure 2.2 (Used for developing x(θ) and x(t), where x is the distance from the position of C' at TDC to Center C' at time t)

From the geometry in Figure 2.2 it can be seen that...

$$a + L = x + L*(\cos(\phi)) + a*(\cos(\theta)) \quad \textbf{(2.4)}$$

where x is the distance from the position of C' at TDC to Center C' at time t.

It can also be seen that...

$$\sin(\phi) = (a/L)*\sin(\theta) \quad \textbf{(2.5)}$$

From trigonometry...

$$\cos^2(\phi) + \sin^2(\phi) = 1 \quad \textbf{(2.6)}$$

Now, by substituting Equation 2.5 into 2.6 and solving for $\cos(\phi)$ yields...

$$\cos(\phi) = (1 - (a^2/L^2)*(\sin^2(\theta))^{1/2} \quad \textbf{(2.7)}$$

Substituting Equation 2.7 into 2.4 and solving for x yields...

$$x(\theta) = a + L - a*\cos(\theta) - (L^2 - a^2 \sin^2(\theta))^{1/2} \quad \textbf{(2.8)}$$

where x is the distance from the position of C' at TDC to Center C' at time t, θ is the crank angle measured in radians, and a and L are the distance parameters described in Figures 2.1 and 2.2 which have values given in Equations 2.1 and 2.2 respectively.

In order to relate the crank angle (θ) to the angular velocity (ω) and time t, the following equation is used...

$$\theta = \omega*t \quad \textbf{(2.9)}$$

where t is the time measured in seconds.

Substituting Equation 2.9 into Equation 2.8 yields the following...

$$x(t) = a + L - a*\cos(\omega t) - (L^2 - a^2 \sin^2(\omega t))^{1/2} \quad \textbf{(2.10)}$$

where x is the distance from the position of C' at TDC to Center C' at time t, ω is the angular speed of the crank shaft which has a constant value given by Equation 2.3, a and L are the distance parameters described in Figures 2.1 and 2.2 which have values given in Equations 2.1 and 2.2 respectively, and t is the time in seconds.

It was decided that the latching of the vane stem will occur during approximately .020in of vane stem displacement from TDC. In order to set the parameters for the dynamic analysis of the slider, the time period in which the vane stem is in the x = .020in range needs to be calculated. Using Equation 2.8 and employing trial and error techniques it

was found that at θ equal to .43 radians $x(\theta)$ was equal to .021in. Thus, this value of θ met the design criteria well. Now, using Equation 2.11 below, the total time span for engaging the slider into the vane-stem latch can be calculated. Notice that the total time is multiplied by a factor of two to account for both the approach and departure of the vane-stem from TDC.

$$t = (\theta/\omega)*2 \qquad \textbf{(2.11)}$$

Where t is the time in seconds, θ is the crank angle (.43 radians for the latching case), and ω is the angular velocity of the crank shaft and is measured in radians/second (377rad/s, a constant value). Substituting these values into Equation 2.11 yields the following result...

$$t = .00228 \text{ seconds} \qquad \textbf{(2.12)}$$

which represents the total time needed to engage the slider into the latch in the vane stem.

2.3 MOTION AND DYNAMIC ANALYSIS OF THE SLIDER PART 1

Since the time required for engagement of the slider into the latch has been calculated (Section 2.2), a detailed dynamic and motion analysis of the slider is needed. This section will present the methods for solving the parameters that govern the dynamic analysis of engaging the slider into the latch. The maximum velocity of the slider will also be calculated for the purpose of friction analysis in Section 2.5. This section will conclude with a description of the necessary spring force specifications that are required to engage the slider. The following design criteria will be useful.

$$m = .0001657 \ (lb*s^2)/ft = .00001381 \ (lb*s^2)/in \quad \textbf{(2.13)}$$

$$dT = x1 - x2 = .070in \quad \textbf{(2.14)}$$

$$t = .00228 \text{ seconds} \quad \textbf{(2.15)}$$

Where m is the design mass of the slider, dT is the total travel needed for the slider to engage the latch, x1 represents the maximum coil spring compression displacement away from the relaxed position, x2 represents the minimum coil spring compression displacement away from the relaxed position, and t is the time period in which the slider must engage the latch (Note that Equation 2.15 is equal to Equation 2.12).

Figure 2.3, below, shows a general schematic that includes the main parameters that govern the slider motion. Note that this is not a detailed drawing of the slider/spring/pusher-pin/pole piece system. However it will do fine for the purpose of obtaining the appropriate modeling equations.

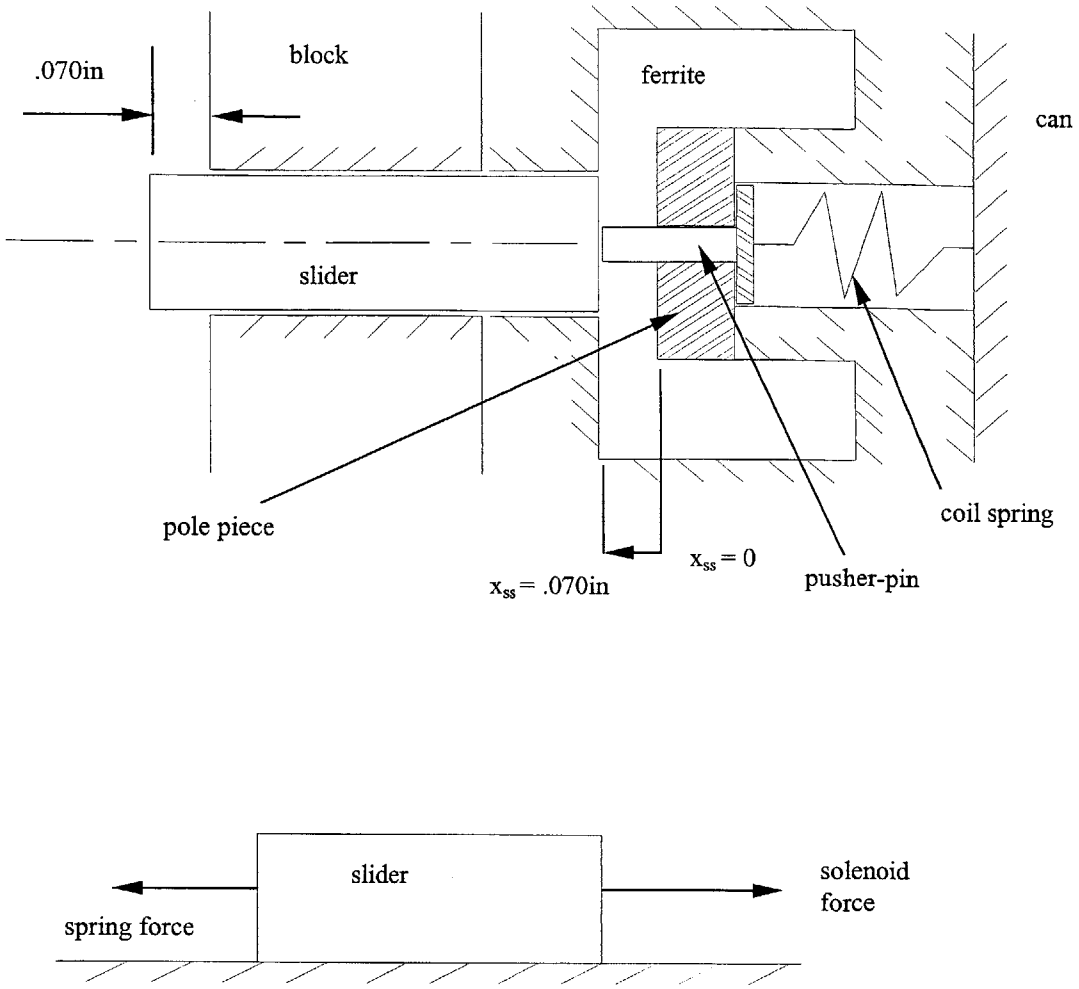

Figure 2.3 (The top view shows the basic geometry for the modeling of the slider dynamics. Note the positive direction of displacement is away from the pole piece. x_{ss} is measured from the edge of the pole piece closest to the slider to the nearest edge of the slider. The bottom view shows a free body diagram of the slider when the solenoid force is applied)

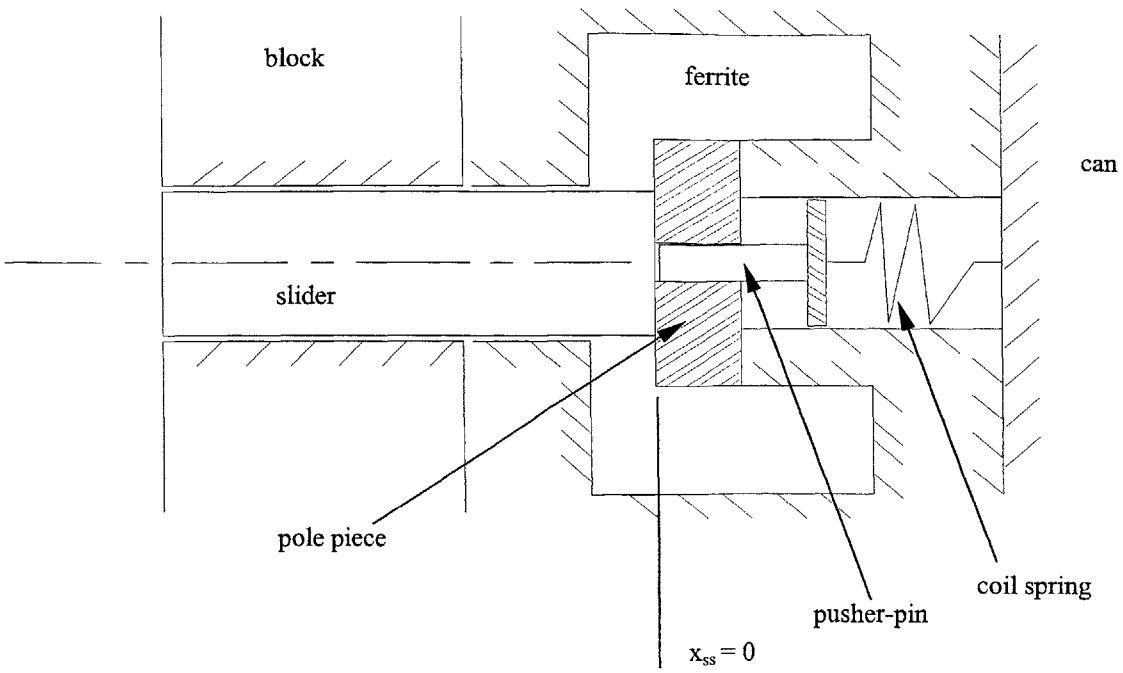

Figure 2.4 (This shows the slider in the fully disengaged position and up against the pole piece. x_{ss} is equal to zero in this schematic. Note that the spring is at maximum compression.)

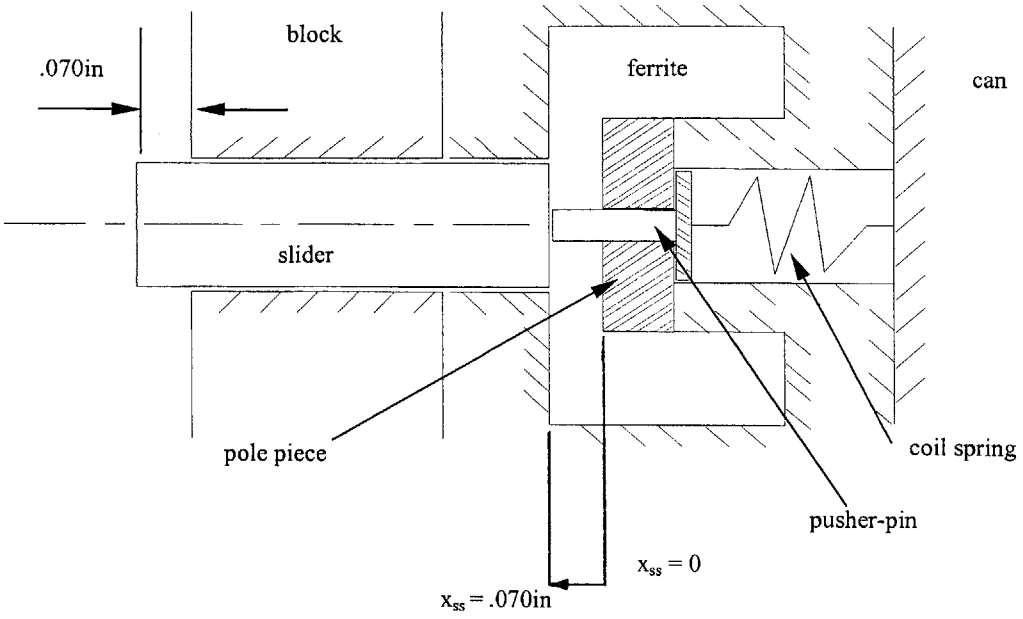

Figure 2.5 (This shows the slider in the fully engaged or latched position. The spring is now at minimum compression. Note the slider total travel dimension (x_{ss} is equal to .070 inches here). The sign convention stays the same as in Figures 2.3 and 2.4.)

Thus, by looking at Figures 2.3, 2.4, and 2.5, the slider motion can be described as follows; the slider starts at a displacement value of x_{ss} = 0in (fully disengaged) and travels a distance of .070in to end at a displacement values of x_{ss} = .070in (fully engaged).

The first step in the analysis is to calculate the necessary engaging spring force. To do this the value of the spring constant, k, will be solved for. This will allow for the specification of the linear force range that is needed to accelerate the slider into the latch within the time period specified by Equation 2.15. When the slider is having the spring force applied to it to engage the latch the solenoid force is zero (no voltage). At this point the spring is then free to push the slider in the positive x_{ss} direction (see Figure 2.4) away from the pole piece and into the latch. It is important to understand that the initial slider position is in contact with the pole piece. To set up the equation for the engaging analysis, Figure 2.6, below, will be used.

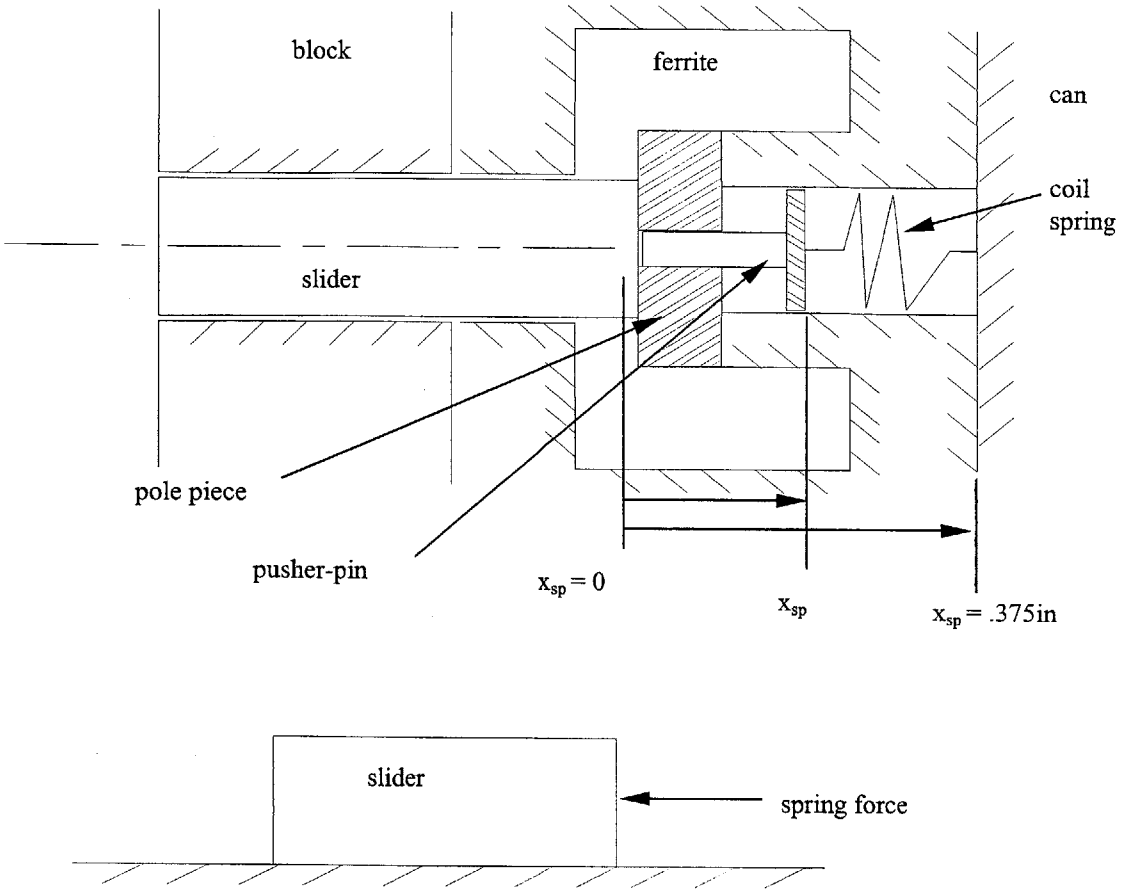

Figure 2.6 (The top view shows the slider/spring interface. Note the positive x_{sp} direction is reversed from Figure 2.3 and applies to Equations 2.16 through 2.28 only. The bottom view shows the free body diagram of the slider.)

Note that in Figure 2.6 the positive x_{sp} direction is reversed from that of Figure 2.3. This is done just for the modeling of the engaging of the slider. It applies to Equations 2.16 through 2.28 only. Once the appropriate spring force is obtained, it will be combined with the solenoid force and will have the sign convention shown in Figure 2.3.

Now, by applying Newton's law of motion to the slider spring combination...

$$m\ddot{x}_{sp} + kx_{xp} = 0 \qquad \textbf{(2.16)}$$

where m is the mass of the slider in $(lb*s^2)/ft$, $\ddot{x}_{sp}$ is the acceleration of the slider in ft/s^2, k is the spring constant in lb/ft, and x_{sp} is the displacement of the slider away from the equilibrium position in ft. The general real solution of Equation 2.16 is...

$$x_{sp}(t) = A\cos[(k/m)^{1/2}(t)] + B\sin[(k/m)^{1/2}(t)] \qquad \textbf{(2.17)}$$

where $x_{sp}(t)$ is the displacement of the slider from the equilibrium position as a function of time, k is the spring constant in lb/ft, m is the mass of the slider in $(lb*s^2)/ft$, t is the time in seconds, and A and B are arbitrary constants that must be solved for by applying boundary conditions. Now in order to solve Equation 2.17 for k, the following boundary conditions must be applied.

Intial Boundary Conditions:

$m = .0001657\ (lb*s^2)/ft = .00001381\ (lb*s^2)/in$ **(2.18)**

$t = 0$ **(2.19)**

$x1 = .0208ft = .250in$ **(2.20)**

$dx_{sp}/dt = 0\ ft/s$ **(2.21)**

By substituting these values into Equation 2.17 the arbitrary constants A and B can be solved for.

$A = .0208ft = .250in$ **(2.22)**

$B = 0$ **(2.23)**

The initial boundary conditions apply to the slider with the spring under maximum compression (in the direction of positive x_{sp} in Figure 2.6). Note that the assumed value of x1 (Equation 2.20) was chosen in an effort to obtain a practical value of k, the spring constant, that is feasible based on the design and geometry constraints of the spring. Once k is calculated, the maximum compression force, the minimum compression force and the linear range of force needed to accelerate the mass will be known.

The final boundary conditions are listed below.

$t = .00228$ seconds **(2.24)**

$x2 = .015ft = .180in$ **(2.25)**

These final boundary conditions represent the time required to engage the slider into the latch (note that Equation 2.24 = Equation 2.15 = Equation 2.12) and also specify the total slider travel length (.070in = x1 - x2).

By substituting Equations 2.22, 2.23, 2.24, and 2.25 into Equation 2.17, k can be solved for.

$k = 18.84\ lb/ft = 1.57\ lb/in$ **(2.26)**

Now, in order to calculate the maximum velocity of the slider the equation of velocity as a function of time needs to be calculated. Taking the derivative of Equation 2.17 results in...

$$dx_{sp}/dt = A*[(k/m)^{1/2}(-\sin(t*(k/m)^{1/2})] + B*[(k/m)^{1/2}\cos(t*(k/m)^{1/2})] \quad \textbf{(2.27)}$$

where dx_{sp}/dt is the velocity of the slider in ft/s, A and B are the arbitrary constants given in Equations 2.22 and 2.23 respectively, m is the mass of the slider in $(lb*s^2)/ft$, k is the spring constant given in Equation 2.26 in lb/ft, and t is the time in seconds. The maximum velocity of the slider will occur just before the slider becomes latched (at t = .00228s). Substituting Equations 2.18, 2.22, 2.23, 2.24, and 2.26 into Equation 2.27 yields the following result.

$$u = -4.443 \text{ ft/s} = -58.6 \text{ in/s} \quad \textbf{(2.28)}$$

Equation 2.28 represents the maximum velocity obtained by the slider. Note that the negative sign is correct according to the sign convention given in Figure 2.6. These values will be positive when used later in accordance with the sign convention described in Figure 2.3.

By multiplying Equation 2.26 by Equations 2.20 and 2.25 the linear force range can be obtained.

$$S1 = .393 \text{ lb} \quad \textbf{(2.29)}$$

$$S2 = .283 \text{ lb} \quad \textbf{(2.30)}$$

S1 represents the force the spring must apply under maximum compression (slider fully disengaged and against the pole piece). S2 represents the force the spring must apply once the slider is completely engaged or latched. The spring forcing function is linear with respect to displacement and has a slope defined by Equation 2.26. Both of these force values are positive with respect to the x_{ss} direction given in Figure 2.3.

2.4 MOTION AND DYNAMIC ANALYSIS OF THE SLIDER PART 2

This section concludes the motion and dynamic analysis of the slider by combining the spring force and the solenoid force for the disengaging of the slider. This section is split into two parts. The first part covers the first solenoid design which included a permanent magnet. The majority of the analytical work was done on this design. The second part covers the new and existing solenoid design which does not include a permanent magnet. The objective of this section is to calculate the necessary solenoid force needed to completely disengage the slider from the latch in the time period given by Equation 2.12. This section will conclude with a detailed description of the force values calculated for the first solenoid design and an operating description of the second solenoid design.

It is important to note that all references to "positive force" and "negative force" in this section will be according to the sign convention shown in Figure 2.3 in Section 2.3.

SOLENOID DESIGN 1: USING A PERMANENT MAGNET

In order to calculate the necessary energized magnet force needed to disengage (or unlatch) the slider, the relationship between the permanent magnet force and the spring force must be fully understood. Table 2.2, below, lists experimentally obtained force values acting on the slider from the permanent magnet. It also lists the spring force values calculated in Section 2.3 as well as the permanent magnet force values multiplied by a constant (2.25). These 2.25x values will be used as a first order analysis for modeling the extraction of the slider with an energized magnet. The basis for multiplying the permanent magnet force values by a constant came from the advice of Dr. Steve Umans. Having had previous experience with solenoids, he figured that the true energized magnet would reflect similar force versus displacement data as the non-energized permanent magnet but at just a higher magnitude. The actual value of 2.25 was chosen simply because it is physically possible to energize the permanent magnet to 2.25 times the values shown in the second column of Table 2.2. Also it serves as a good starting point for the iteration process because it "looks" like it may work. The values in Table 2.2 are used in Figures 2.8 and 2.9. Listed in Table 2.1 are some of the specifications for Solenoid Design 1.

Table 2.1 (Specifications of Solenoid Design 1)

Resistance Value (ohms)	6.5
Type of Winding	Single wound
Operating Voltage	35+
Type of Wire	Number 28 (insulated)
Permanent Magnet	Yes

Table 2.2 (Experimentally Obtained Force vs Displacement Values For Solenoid Design 1)

Displacement x_s (in) (x_s is measured from the edge of the perm. magnet to the edge of the slider)	Permanent Magnet Force (lb)	Spring Force From Section 2.2 (lb)	2.25x Permanent Magnet Force (lb)
0	1.53		3.4425
.028	1.055		2.374
.04		.393	
.053	.697		1.568
.07	.548		1.233
.085	.359		.8078
.106	.307		.6908
.11		.283	
.124	.216		.486

Note: x_s is equal to .040 inches when the slider is fully disengaged. See Figure 2.7.

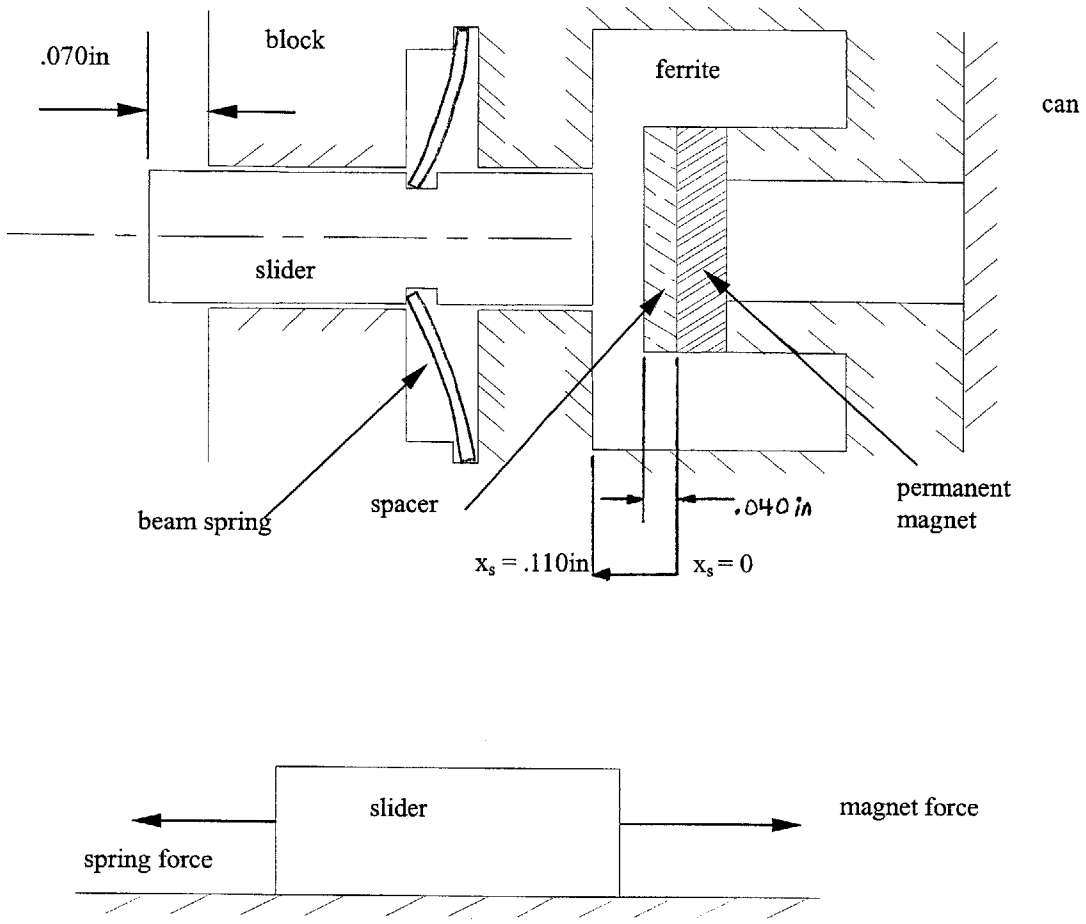

Figure 2.7 (This design is used in Solenoid Design 1 Notice that for this analysis x_s is measured from the edge of the permanent magnet to the edge of the slider. This schematic shows the slider in the fully engaged position. x_s = .110in)

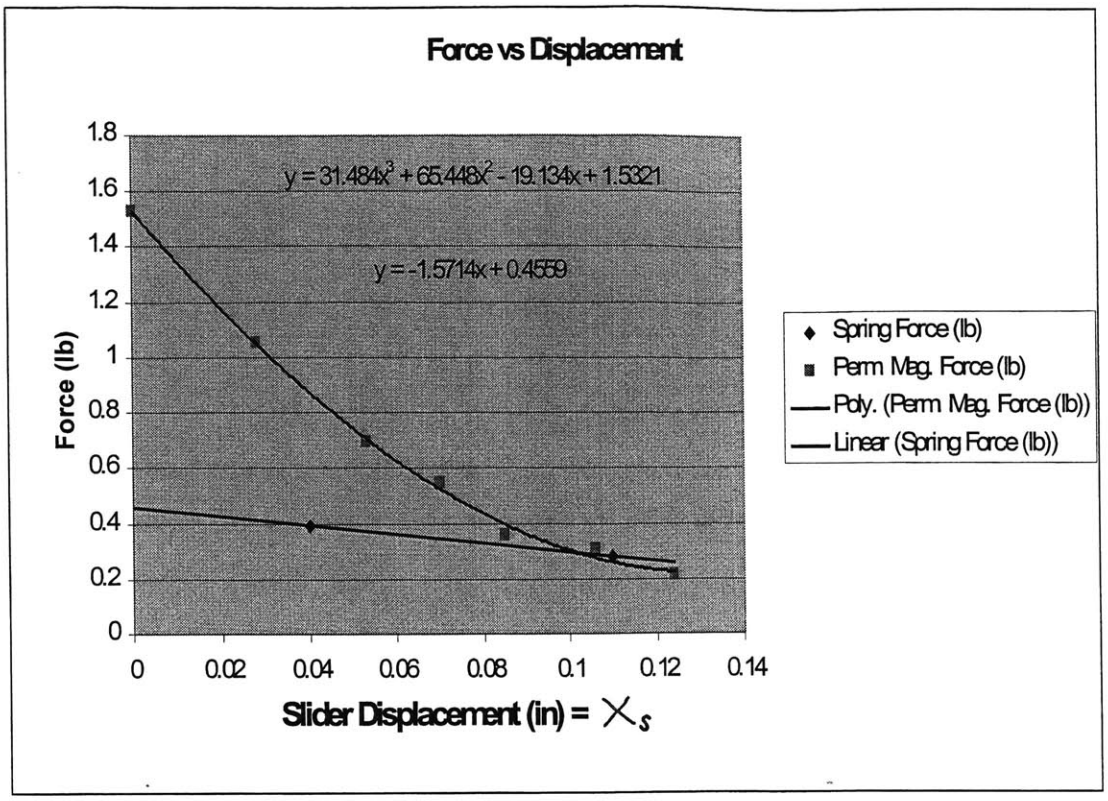

Figure 2.8 (This shows the linear force curve of the spring and the experimentally obtained data points which correspond to the permanent magnet force on the slider.)

For this disengaging analysis, x_s is the distance measured between the edge of the permanent magnet and the edge of the slider with the positive direction indicated in Figure 2.7. Thus, by looking at Figure 2.7, it can be concluded that the slider is fully disengaged (unlatched) at a displacement value of x_s equal to .040in (since the spacer is .040in thick). Note that in this first design the pole piece shown in Figure 2.3 was replaced with a non-magnetic spacer that was .040in thick. Also, in place of the pusher-pin, there was a permanent magnet that was in contact with the spacer. See Figure 2.7 above.

So in Figure 2.8 the slider starts at a displacement value of x_s = .040in and travels a distance of .070in to end at a displacement value of x_s = .110in (the slider is in the fully latched position here). Notice that the permanent magnet force is higher than the spring force at a displacement value of .040in. This is to allow the permanent magnet force to hold the slider in the unlatched position until the permanent magnet field is killed by application of current to the coil in the demagnetizing direction. When the permanent magnet field is killed the permanent magnet force values in Figure 2.8 go to zero. This allows the spring to engage the slider in the latch as described in Section 2.3. Once the

slider has become latched the permanent magnet field is restored. Notice, at this latched position, that the spring force is greater than the permanent magnet force keeping a net positive force on the slider. This ensures that the slider will not come unlatched.

In order to disengage the slider from the latched position, the magnet force must become greater than the spring force. In fact, the magnet force must be large enough to ensure that the slider becomes fully disengaged in a time period of .00228 seconds (Equation 2.12).

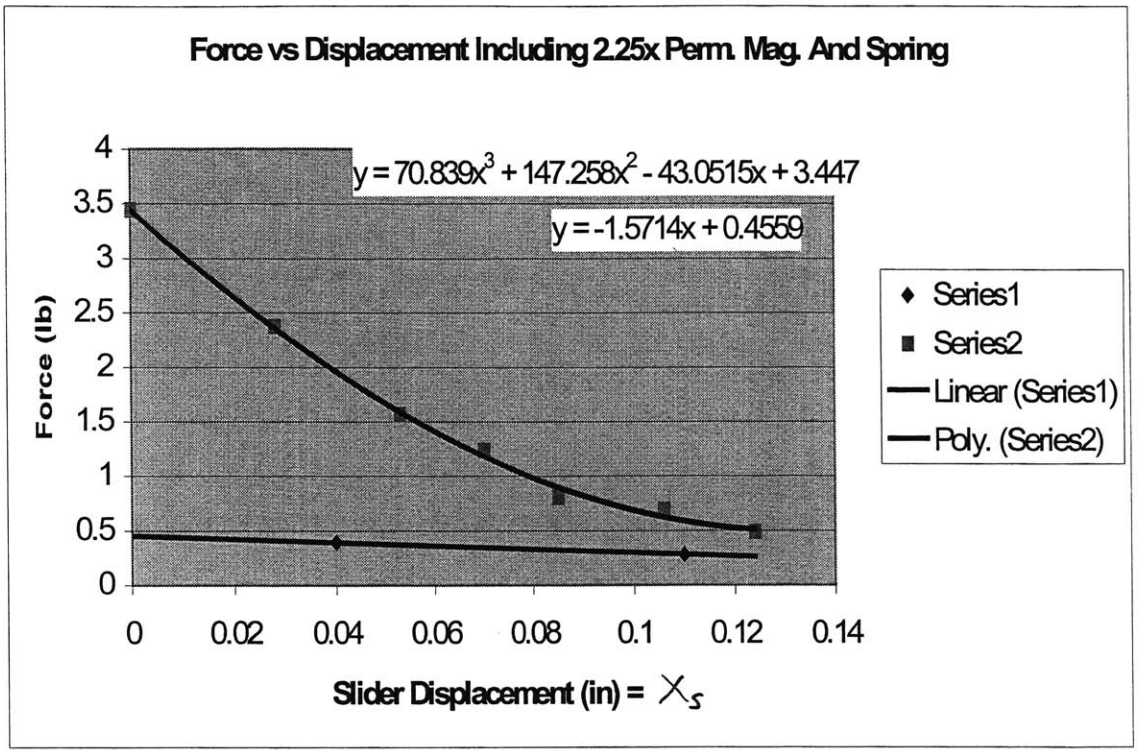

Figure 2.9 (This shows the linear force curve of the spring and a possible energized magnet curve (2.25x) that was fit using a third order polynomial.)

In Figure 2.9 the energized magnet force versus displacement data has been plot and has been curve fit using a third order polynomial. This energized magnet force versus displacement plot represents magnet force values of 2.25 times those given in Figure 2.8 above. This method of simply multiplying the experimentally obtained permanent magnet force values by a constant is done as a simple approximation. Dr. Steve Umans did a Finite Element Analysis (FEA) of this first design and that is covered later. The linear spring force versus displacement has also been plot. The first equation is...

$$FE = 70.839x_s^3 + 147.258x_s^2 - 43.0515x_s + 3.447 \qquad \textbf{(2.31)}$$

where FE is the energized magnet force (lb) and x_s is the displacement away from the permanent magnet (in) according to the sign convention given in Figure 2.7.

The linear equation governing the spring force as a function of displacement is also given below...

$$S3 = -1.5714x_s + .4559 \quad \textbf{(2.32)}$$

where S3 represents the spring force (lb) and x_s is the displacement away from the permanent magnet (in). Equation 2.32 comes from the values calculated in Section 2.3 and listed under Equations 2.26, 2.29, and 2.30.

In order to model the dynamics of the slider being disengaged Figure 2.7 will be referred to. Applying Newton's law of motion to the slider, the spring force, and the energized magnet force yields the following equation...

$$m\ddot{x}_s - S3 + FE = 0 \quad \textbf{(2.33)}$$

where m is the mass of the slider ($lb*s^2/ft$) whose value is given in Equation 2.13, $\ddot{x}_s$ is the acceleration of the slider (second derivative of displacement with respect to time), S3 is the spring force function given in Equation 2.32 , and FE is the energized magnet force function given in Equation 2.31. Substituting the values in Equations 2.31 and 2.32 into Equation 2.33 yields the following.

$$m\ddot{x}_s - (-1.5714x_s + .4559) + (70.839x_s^3 + 147.258x_s^2 - 43.0515x_s + 3.447) = 0 \quad \textbf{(2.34)}$$

Simplifying Equation 2.34 and reducing the order of the differential equation to a system of two first order equations results in the following...

$$m\dot{x}_s + (70.839)x_s^3 + (147.258)x_s^2 + (-41.480)x_s + 2.9911 = 0 \quad \textbf{(2.35)}$$

where m is the mass of the slider ($lb*s^2/ft$), $\dot{x}_s$ is the reduction term which is the first derivative of displacement with respect to time, and x_s is the displacement of the slider away from the magnet (in) according to the sign convention given in Figure 2.7.

Even though the differential equation was simplified into the form shown in Equation 2.35 above, it represents a nonlinear system which proves highly nontrivial to solve by hand. Therefore, this equation was solved using a numerical solving technique in MATLAB. The MATLAB code is listed in the Appendix. In order to understand the variables a_s, b_s, c_s, and d_s in the MATLAB code the following equation form was adopted.

$$m\dot{x}_s + (a_s)\, x_s^3 + (b_s)x_s^2 + (c_s)x_s + (d) = 0 \quad \textbf{(2.36)}$$

For the given FE, the constants a_s, b_s, c_s, and d_s are listed below.

$$a_s = 70.839 \quad \textbf{(2.37)}$$

$$b_s = 147.258 \quad \textbf{(2.38)}$$

$$c_s = -41.480 \quad \textbf{(2.39)}$$

$$d_s = 2.9911 \quad \textbf{(2.40)}$$

Solving the first order system of differential equations given in Equations 2.35 using MATLAB gives a net slider displacement of .080in in a time span of .0023 seconds. This clearly indicates that if the energized magnet extracting force can realistically reach the values demonstrated in Figure 2.9 then Solenoid Design 1 will work.

In an effort to obtain a more accurate model of the energized magnet extracting force Dr. Steve Umans did a FEA analysis on Solenoid Design 1. In order to reduce the number of iterations that would have to be run, he set the analysis to achieve a force of .486lb at a displacement of x_s equal to .110in. This parameter was chosen as a starting point by looking at the 2.25x permanent magnet force value at a displacement of x_s equal to .124in (see Table 2.2). The results of Dr. Umans analysis are shown below in Table 2.3 and Figure 2.10.

Table 2.3 (FEA Analysis Force vs Displacement Values For Solenoid Design 1)

Displacement x_s (in)	Permanent Magnet Alone (lb)	Permanent Magnet With Aiding Current (lb)
.040	.699	1.617
.055	.636	1.318
.070	.442	1.053
.090	.291	.701
.110	.203	.496

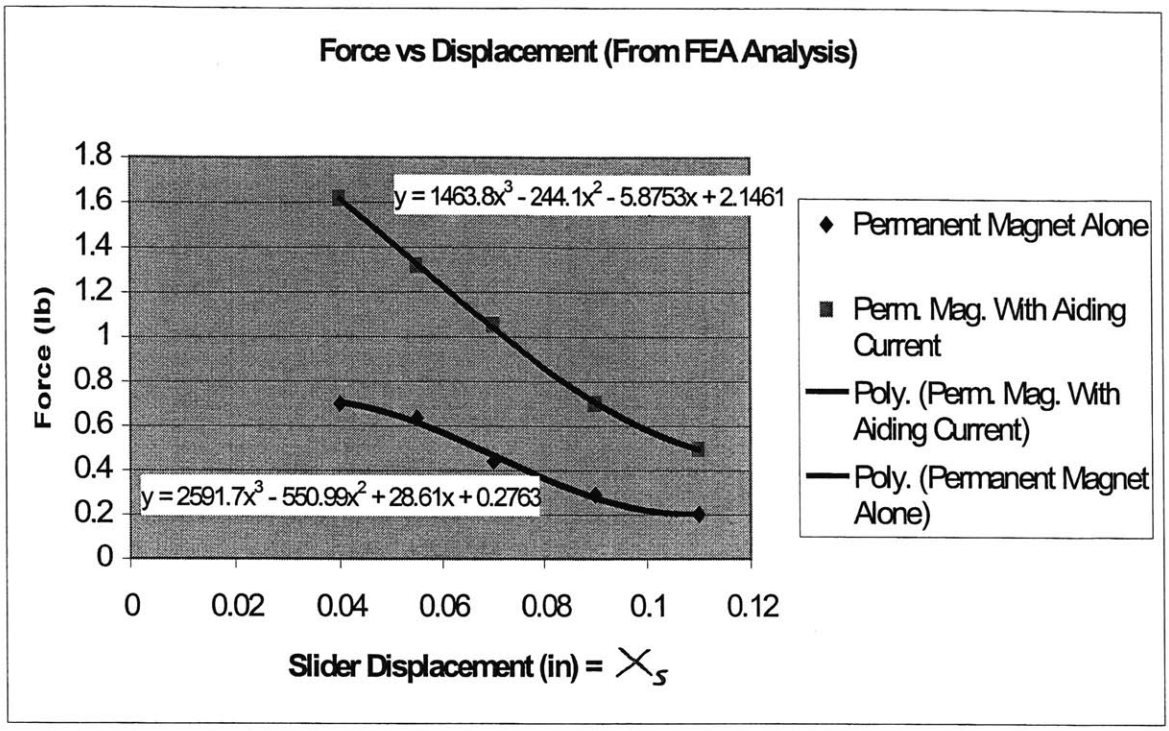

Figure 2.10 (This plot shows the Force vs Displacement values shown in Table 2.3 above. Displacement is equal to x_s here also. These values represent the FEA analysis on Solenoid Design 1)

The values in Figure 2.10 were also curve fit using a third order polynomial. Those equations are shown above in Figure 2.10. Using the same analysis technique on the FEA values as was demonstrated in Equations 2.31, 2.32, and 2.33 and using the same value for S3 (the spring force does not change) results in the following equations…

$$FE = 1463.8x_s^3 - 244.1x_s^2 - -5.875x_s + 2.146 \qquad \textbf{(2.41)}$$

Where FE now represents the energized magnet force (lb) using FEA values and x_s is the displacement of the slider away from the permanent magnet (in). Substituting the values in Equations 2.32 and 2.41 into Equation 2.33 results in the following equation…

$$m\ddot{x}_s - (-1.5714x_s + .4559) + (1463.8x_s^3 - 244.1x_s^2 - 5.875x_s + 2.146) = 0 \qquad \textbf{(2.42)}$$

Simplifying Equation 2.42 and reducing the order of the differential equation to a system of two first order equations results in the following…

$$m\ddot{x}_s + (1463.8)x_s^3 + (-244.1)x_s^2 + (-4.3039)x_s + (1.6902) = 0 \quad \textbf{(2.43)}$$

where m is the mass of the slider ($lb*s^2/ft$) whose value is given in Equation 2.13, $\ddot{x}_s$ is the acceleration of the slider (second derivative of displacement with respect to time), S3 is the spring force function given in Equation 2.32, $\dot{x}_s$ is the reduction term which is the first derivative of displacement with respect to time, x_s is the displacement of the slider away from the permanent magnet (in) according to the sign convention given in Figure 2.7, and FE is the energized magnet force function given in Equation 2.41.

By using the format shown in Equation 2.36 the new values for a_s, b_s, c_s, and d_s can be found.

$$a_s = 1463.8 \quad \textbf{(2.44)}$$

$$b_s = -244.1 \quad \textbf{(2.45)}$$

$$c_s = -4.3039 \quad \textbf{(2.46)}$$

$$d_s = 1.6902 \quad \textbf{(2.47)}$$

Using these new FEA based values to solve the differential equation given in Equation 2.43 gives a net slider displacement of .0515in in a time period of .0023 seconds. Once again MATLAB was used to solve Equation 2.43. This new displacement result is lower than the required .070in of slider travel needed in .0023 seconds. This indicates that the slider will not come unlatched during one revolution of the rolling piston.

At this point it was decided the best thing to do was to go ahead and put the latch mechanism together and test it with Solenoid Design 1. As is discussed in Chapter 4, the results of Solenoid Design 1 proved unsatisfactory. The above FEA analysis, with its predicted unsatisfactory result, would prove to be the case in real world testing. Other problems were also discovered relating to the permanent magnet and the high operating temperatures of the compressor.

SOLENOID DESIGN 2: NO PERMANENT MAGNET AND DOUBLE WOUND COIL

Table 2.4 (Specifications of Solenoid Design 2)

Resistance Value (ohms)	1.8
Type of Winding	Double wound
Operating Voltage (V)	25
Type of Wire	Number 28 (insulated)
Permanent Magnet	No

Due to the inability of Solenoid Design 1 to properly extract the slider in .0023 seconds and also due to other problems, it was decided to adopt a different solenoid design. With the aid of Professor Wilson and Dave Otten, it was experimentally determined that Solenoid Design 1 was not producing enough extracting force. In order to obtain more extracting force a new, double wound solenoid design was adopted. By double winding the coil the basic wire cross section was doubled and the length of wire that could be wound in the given volume of the coil was cut in half. This lowered the total resistance of the coil by approximately 70% (see Tables 2.1 and 2.4). By applying the same voltage to Solenoid Design 2 as was applied to Solenoid Design 1 the current used by Solenoid Design 2 was now larger in magnitude (Since Voltage = Current * Resistance). This allows Solenoid Design 2 to produce more unlatching force on the slider with the same magnitude of applied voltage to the solenoid coil.

Due to the time constraint that the project was under, no official analysis was done on Solenoid Design 2 to determine the extracting force acting on the slider as a function of displacement. Instead, the solenoid was simply built according to the specifications given in Table 2.4 and experimentally tested in the latching mechanism. As is discussed in Chapter 4, this design also proved somewhat unsatisfactory. It appeared that the solenoid was unable to extract the slider within one stroke of the compressor. Dr. Umans simply doubled the time (from .020 seconds to .040 seconds) that the unlatch voltage signal is applied to the solenoid. This adjustment appears to have worked and the solenoid is now able to unlatch the slider consistently.

2.5 ANALYSIS OF FRICTION ON THE OPERATION OF THE SLIDER

The objective of this section is to calculate the maximum resistive force acting on the slider as it is in motion to engage the latch. The slider and the entire latch mechanism operate in an oil and refrigerant 22 saturated environment. Thus the important parameter is to calculate the sliding resistance due to the presence of an oil film surrounding the slider.

Of use will be the following parameters...

$$b = .003in = .00025ft \tag{2.48}$$

$$u = 4.883\ ft/s = 58.6\ in/s \tag{2.49}$$

where b is the clearance distance between one side of the slider and the slot in which it travels and u is the maximum velocity of the slider (from Equation 2.28).

It can be seen from Figure 2.11 that the part of the slider that will have a resistive force applied to it is the rectangular part with dimensions .240in X .100in X .400 in (.240in into the page and .100in thick). This rectangular part is the part that guides the slider during latching and unlatching. It is also the load bearing part during the time in which the slider is latched. Figure 2.11, below, shows a simple front view of the slider and the slot it travels in and labels the part that has the resistive force applied to it.

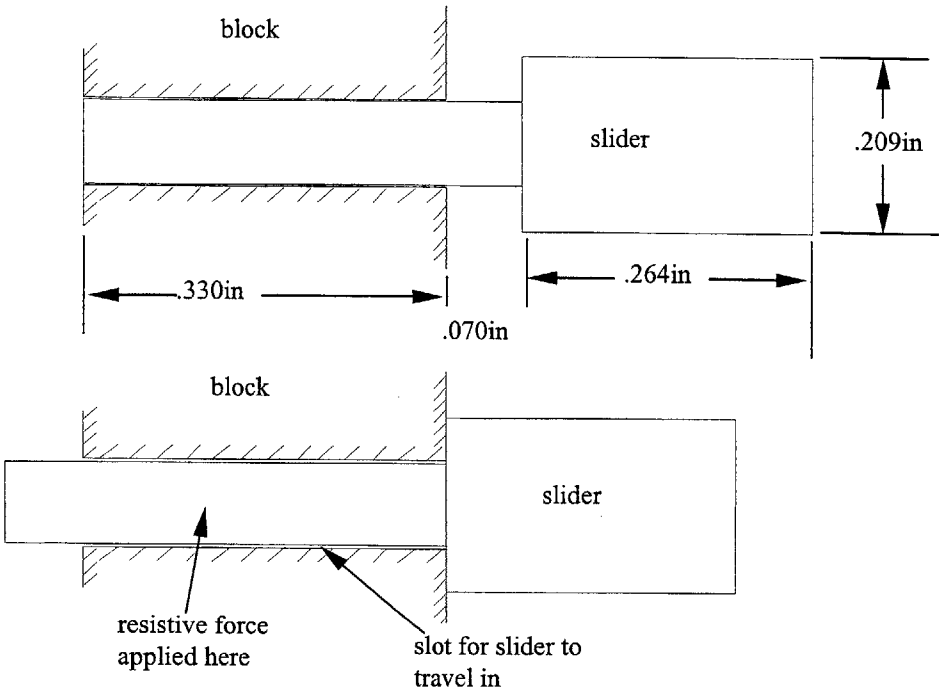

Figure 2.11 (This shows a simplified front view of the slider and the slot in which it travels. The top view shows the unlatched position while the bottom view shows the latched position. The rectangular part has dimensions .400in X .100in X .240in.)

Notice that the slot that the slider travels in is only .330in in length however. This reduces the net surface contact area for sliding resistance to...

$$A_{sur} = [(.330in)*(.240in)*2] + [(.330in)*(.100in)*2] = 2244in^2 = .00156ft^2 \quad \textbf{(2.50)}$$

where A_{sur} is the total surface area affected by sliding resistance.

Figure 2.12, below, shows a viscous fluid trapped between two plates. The top plate has a force applied to it and is traveling with a constant velocity while the lower plate is fixed. This figure will be used to set up the governing equations needed to calculate the net resistive force on the slider.

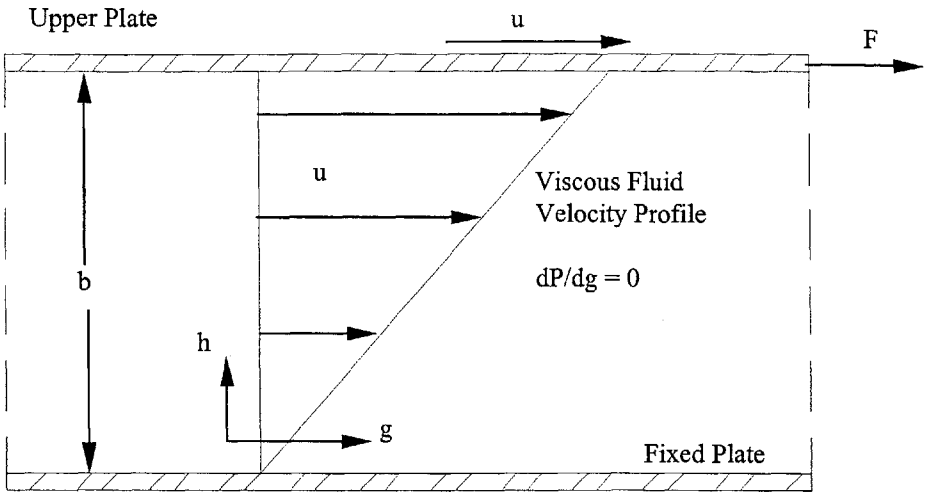

Figure 2.12 (This shows a viscous fluid between two parrallel plates. The top plate has a force F applied to it and it has a constant velocity u. The bottom plate is fixed. Note the sign convention)

In Figure 2.12, above, it is assumed that there is no pressure gradient in the g direction. In other words dP/dg = 0. The resisting force on the upper plate can written as...

$$F = \tau * A_{sur} \qquad \textbf{(2.51)}$$

where F is the resisting force on the upper plate, τ is the shearing stress of the fluid, and A_{sur} is the surface area of the upper plate or slider. The shearing stress is defined by...

$$\tau = \mu * (du/dh) \qquad \textbf{(2.52)}$$

where μ is the viscosity of the fluid and du/dh is the velocity gradient of the fluid between the two plates. The variable du/dh can be defined as follows...

$$du/dh = u/b \qquad \textbf{(2.53)}$$

where u is the velocity of the top plate (or maximum velocity of the slider) and b is the distance between the two plates. For the case of the slider, the velocity gradient between the two plates will be considered linear. The value of the viscosity of the oil/refrigerant 22 mixture came from a Daniel plot of Zerol 300/R22 at a pressure of 170psia and a temperature of 90 degrees F, and is given below in Equation 2.54. This temperature and pressure represents a good average operating condition for the vane-latching mechanism.

$$\mu = 1.0737 \times 10^{-5} \ (lb*s)/ft^2 \qquad \textbf{(2.54)}$$

Now that the viscosity of the oil/refrigerant 22 mixture has been found, the velocity gradient between the upper and lower plate can be found. Substituting Equations 2.48 and 2.49 into 2.53 results in

$$du/dh = [4.883 \text{ ft/s}]/.00025\text{ft} = 19532.0 \text{ 1/s} \quad \textbf{(2.55)}$$

where du/dh represents the velocity gradient of the oil/refrigerant 22 fluid between the surface of the slider and the slot in which it travels. Note that the velocity value of 4.883 ft/s in Equation 2.55 represents the maximum velocity of the slider found in Section 2.3. Now, substituting Equation 2.54 and Equation 2.55 into Equation 2.52 results in the following...

$$\tau = .2097 \text{ lb/ft}^2 \quad \textbf{(2.56)}$$

where τ represents the shearing stress of the oil/refrigerant 22 fluid at the interface of the slider. One final substitution of Equation 2.56 and Equation 2.50 into Equation 2.51 results in the final result...

$$F = (.2097 \text{ lb/ft}^2)*(.00156\text{ft}^2) = .000327 \text{ lb} \quad \textbf{(2.57)}$$

where F represents the maximum resistive force acting on the slider as it is in motion to engage the latch. In relation to the spring and magnet forces needed to engage and disengage the slider, this force is small enough to be considered negligible.

2.6 LOAD AND STRESS ANALYSIS OF THE SLIDER

The objective of this section is to calculate the maximum operating stresses that the slider will encounter. The stress calculations will be split up into a shear stress analysis, and a bending stress analysis.

The maximum stresses that the slider will be subject to will occur during latching. These stresses will originate from the discharge gas pressure acting on the vane and vane stem and from the latch impacting the slider (static plus dynamic forces). However, since the velocity of the vane stem, and thus the latch, is very low near top dead center, the dynamic effect is negligible. Thus the following stress calculations will be derived from a static force analysis. Figure 2.13, below, shows a simplified view of the slider interfacing with the latch. Note that the specific latch geometry is not shown here. However, for the purpose of calculating the maximum shear and bending stresses within the slider, it will do fine.

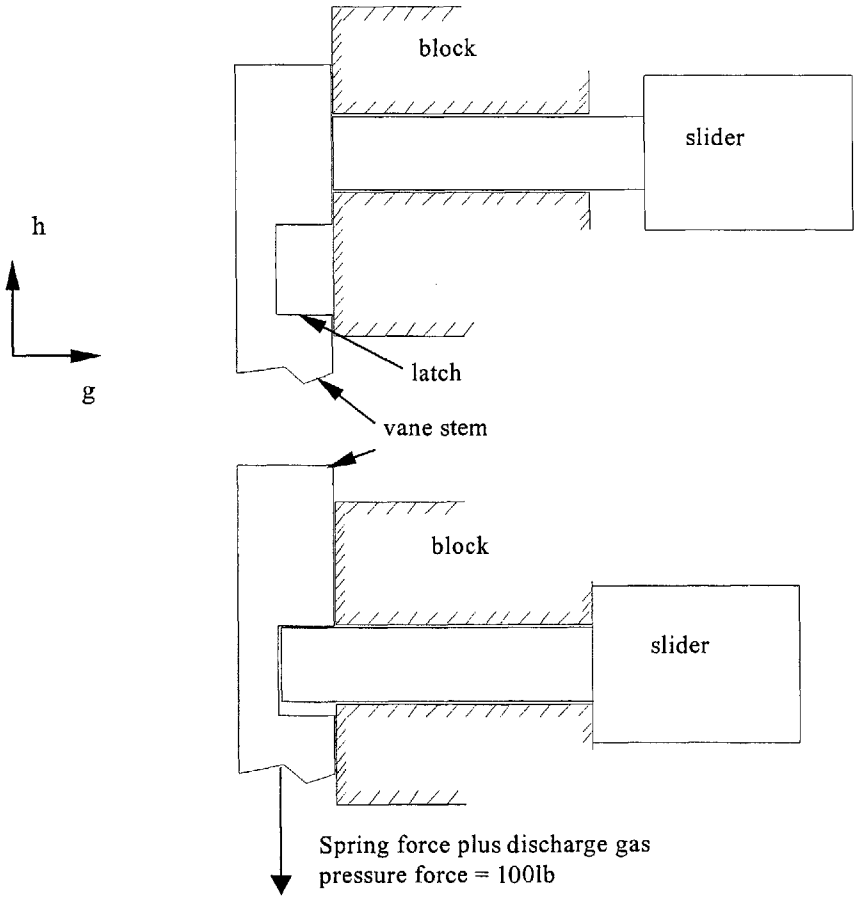

Figure 2.13 (This shows another simplified front view of the slider and the latch in the vane stem. The top view shows the slider disengaged or unlatched while the bottom view shows the slider in the latched position.)

A free body diagram of the slider in the latched position is shown below in Figure 2.14. Several assumptions were made in the analysis at this point...

$$V = 100 \text{ lb} \tag{2.58}$$

where V is the force acting in the negative h direction on the vane stem (see Figure 2.13). This force represents the sum of the vane spring force plus the discharge gas pressure force acing on the vane and vane stem. The vane spring force is not a design feature of this mechanism. The spring was originally designed by Carrier for the model DB240 to keep the vane in contact with the rolling piston during start-up and low discharge pressure conditions. The vane spring force alone loads the vane stem with a 7.0 lb force in the negative h direction when the rolling piston is at top dead center. Also, the assumption was made that the slider does not distort or deflect during loading. Thus, the slider becomes slightly "cocked" in it's travel slot creating line contact loads as shown below in Figure 2.14.

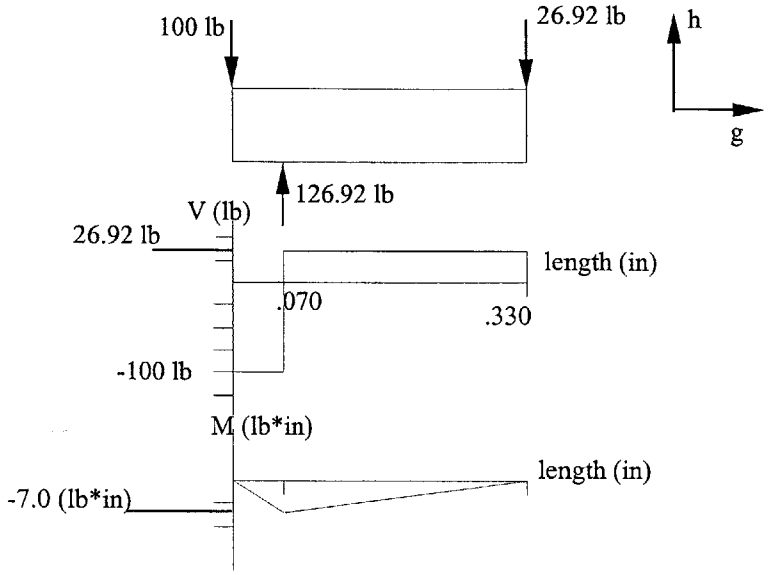

Figure 2.14 (The top view shows a free body diagram of the slider. The resultant line contact loads are representative of the latched position. The bottom two views are the shear and bending moment diagrams of the slider)

Since the latching distance of the slider is so short (.070 in) the shear stress analysis will be done first. Figure 2.15, below, shows a cross-section side view of the rectangular portion of the slider and is used to point out the needed dimensions.

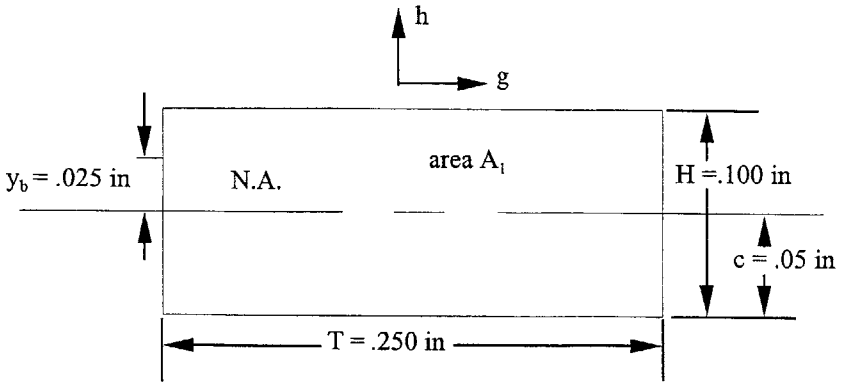

Figure 2.15 (This shows a cross-section side view of the rectangular portion of the slider.)

The maximum shear stress is going to occur from the point where the 100 lb load is applied up to .070 in where the slider first enters the slot (from shear diagram, Figure 2.14). Looking at Figure 2.15, above, the maximum shear stress occurs at the nuetral axis (N.A.) and out at the edges of beam. In order to calculate the shear stress, the following equations are used...

$$\tau_{ave} = (V*Q)/(I*T) \quad \textbf{(2.59)}$$

$$\tau_{max}/\tau_{ave} = 1.692 \quad \textbf{(2.60)}$$

where τ_{ave} (lb/in^2) is the average value of the shearing stress in the negative h direction (Figure 2.15) across the cross section of the slider, τ_{max} (lb/in^2) is the maximum value of the shearing stress in the negative h direction found at the edges of the cross section, V is the maximum shearing force (lb), Q is the first moment of the area that acts about the neutral axis (in^3), I is the moment of inertia of the entire cross-sectional area about the neutral axis (in^4), and T is the width of the cross section (in). Equation 2.60 is used to find the maximum shearing stress at the edges of the cross section. The ratio is used as a correction factor since the slider is not considered to be a "tall, narrow, rectangular beam". In order to calculate Q and I, the following equations are used...

$$Q = A_1*y_b \quad \textbf{(2.61)}$$

$$I = (1/12)*(T)*H^3 \quad \textbf{(2.62)}$$

where T is the width of the cross-section (in), H is the heigth of the cross-section, A_1 is the area of the cross-section that is above the nuetral axis (in^2), and y_b is the distance from the nuetral axis to the centroid of area A_1. Substituting the values in Figure 2.15 into Equations 2.61 and 2.62 ,above, results in the following values.

$$Q = (.250in*.050in)*(.025in) = .000313in^3 \quad \textbf{(2.63)}$$

$$I = (1/12)*(.250in)*(.100in)^3 = .000021in^4 \quad \textbf{(2.64)}$$

Now, by substituting Equations 2.58, 2.63, 2.64 and the value of T in Figure 2.15 into Equation 2.59, the average shearing stress can be solved for.

$$\tau_{ave} = 5961.9\ lb/in^2 \quad \textbf{(2.65)}$$

One final substitution of Equation 2.65 into Equation 2.60 results in the value of the maximum shearing stress.

$$\tau_{max} = (1.692)*(5961.9\ lb/in^2) = 10087.5\ lb/in^2 \quad \textbf{(2.66)}$$

In order to calculate the maximum compressive and tensile stresses in the slider, the maximum value of the bending moment in the slider must be known. This can be found by refering to the bending moment diagram in Figure 2.14.

$$M = 7.0\ lb*in \quad \textbf{(2.67)}$$

M is the maximum bending moment value when the slider is in the latched position. Due to the geometry of the slider and the nature of the loading, the maximum compressive and tensile stresses in the slider will be equal in magnitude. So, for the sake of this analysis, the maximum compressive stress will be calculated. The maximum compressive stress occurs on the underside (underside in the negative h direction in Figures 2.13 and 2.14) and is given by the following equation...

$$\sigma_m = (M*c)/I \quad \textbf{(2.68)}$$

where σ_m is the maximum compressive in the slider (lb/in^2), M is the maximum bending moment induced in the slider (Equation 2.67), c is the distance from the nuetral axis to the outer edge of the slider (see Figure 2.15), and I is the moment of inertia of the entire cross-sectional area about the neutral axis (Equation 2.64). By substituting Equations 2.67 and 2.64 and the value of c given in Figure 2.15 into Equation 2.68, the maximum compressive stress in the slider can be found.

$$\sigma_m = 16666.7\ lb/in^2 \quad \textbf{(2.69)}$$

The values given by Equations 2.66 and 2.69 show that the induced stresses in the slider are small. Comparing these stresses to the material specifications of air-hardened tool steel it can be seen that these stresses are well within acceptable operation limits.

2.7 DESIGN OF THE LATCH-SLIDER INTERFACE GEOMETRY AND THE RESULTING FORCE ANALYSIS

A required design parameter of the slider and the latch in the vane stem is that of keeping the vane stem lifted (latched) until the rolling piston reaches top dead center and releases the latch mechanism. In order to accomplish this it is necessary to prevent the slider from being disengaged by the solenoid disengaging force until the rolling piston is at top dead center. This can be accomplished by proper design of the latch-slider interface geometry. This section describes the operating parameters that the latching system must operate within and also describes the latch-slider interface geometry that will meet these parameters.

There is no synchronized timing of the unlatching signal to the solenoid and the position of the rolling piston. When a signal is sent to the solenoid causing it to energize and apply the solenoid disengaging force, the rolling piston may or may not be at top dead center (See Figures 1.4 and 1.5). For example, say the rolling piston is in a position equivalent to that shown in Figure 1.5 and the electromagnetic disengaging force is activated. If the slider were to disengage from the the latch in the vane stem, the vane would be driven down by the spring and the discharge gas pressure force. As the vane would be translating downward the rolling piston would continue in it's steady rotational motion and impact the vane. At this point, normal, loaded operation of the compressor would continue. However, this impact condition of the vane with the rolling piston is unacceptable since it produces an audible noise. Eliminating this noise was one of the original goals of this project (see Section 1.2).

Thus the parameter for the latch-slider interface geometry is simple: design a latch-slider interface geometry such that the slider will not disengage, even with the solenoid disengaging force applied, until the rolling piston reaches top dead center.

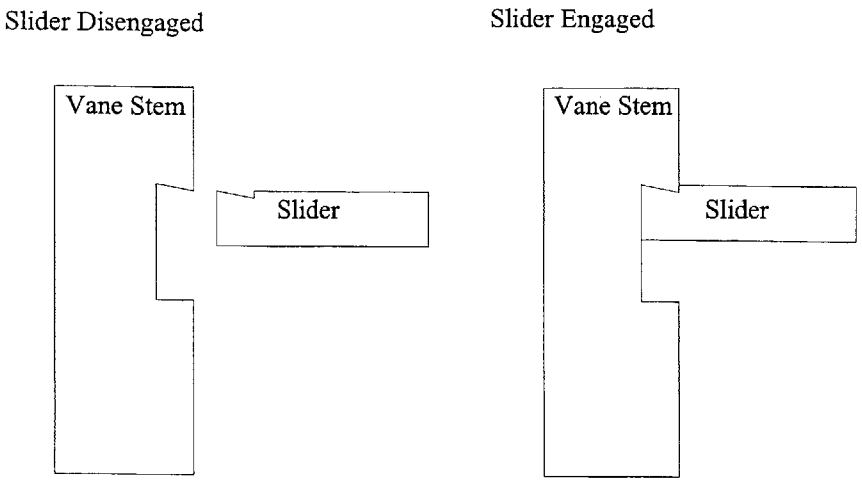

Figure 2.16 (The left view shows the slider disengaged from the latch in the vane stem. The right view shows the slider engaged with the latch in the vane stem. The slots that the vane stem and the slider travel in are not shown for the sake of clarity.)

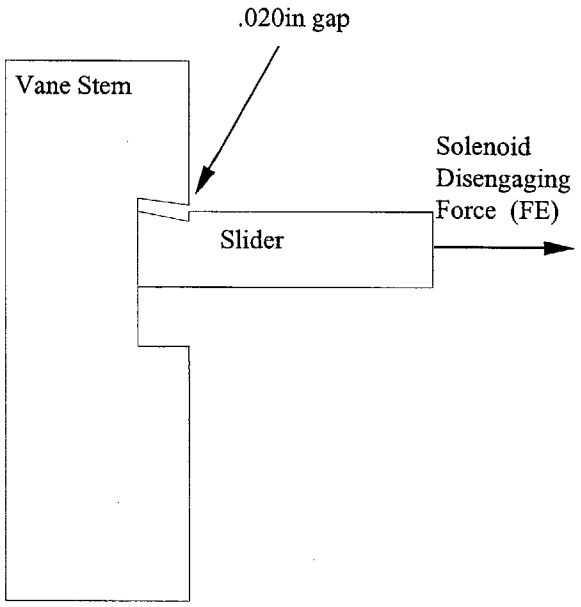

Figure 2.17 (This shows a close up view of the vane stem and the slider. This position is equivalent to that shown in Figure 1.4. i.e.; The rolling piston is at top dead center and the solenoid disengaging force is now able to disengage the slider.)

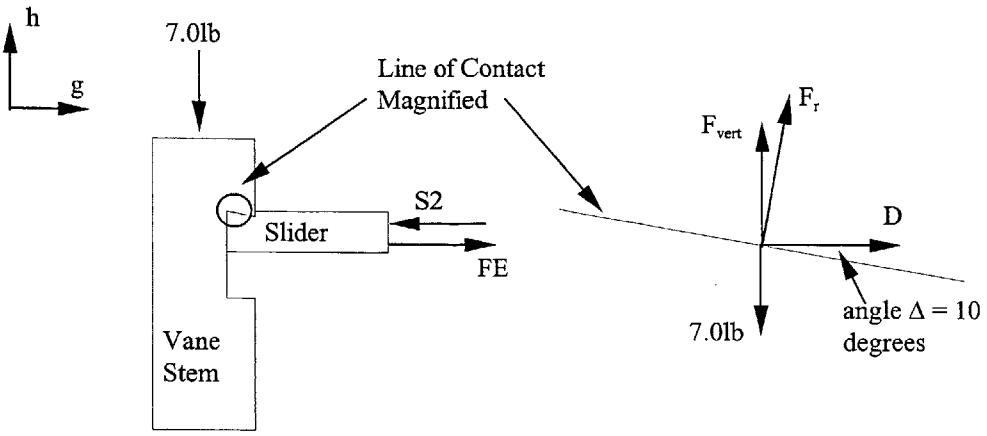

Figure 2.18 (This shows the vane stem under the 7 pound vane spring force (negative h direction) and D, the resultant force of the solenoid disengaging force (FE) and the slider spring-engaging force (S2). The right side shows a magnified view of the latch contact surface with the respective forces acting on it.)

Figure 2.16 on the previous page shows the slider engaged and disengaged from the latch. In Figure 2.17, also on the previous page, the slider is engaged. However, the .020in gap that is shown represents the situation when the rolling piston is at top dead center (See Figure 1.4). Recall from Section 2.2 that the .020in of gap was an original design feature. Even when the vane stem is latched and in the unloaded position the vane stem will be displaced .020in in the h direction every time the rolling piston approaches and leaves top dead center. It is during this interval that the solenoid disengaging force is able to disengage (or unlatch) the slider from the vane stem.

The right side view of Figure 2.18, above, shows the force balance on the contact surface of the latch in the vane stem (equal and opposite forces act on the slider surface). The force D is the resultant force of the solenoid disengaging force (FE) and the slider spring-engaging force (S2). It is important to note that the value of D is a constant value only at the point where the slider is in the fully engaged position. By utilizing the value of S2 given in Equation 2.30, estimating the value of FE (no official calculations were ever done on the new solenoid force values), and summing those forces according to the sign convention given in Figure 2.3, the absolute value of D can be solved for.

$$D = ABS\ (S2 - FE) \qquad \textbf{(2.70)}$$

$$D = ABS\ (283\ lb - 1.3lb) = 1.02\ lb \qquad \textbf{(2.71)}$$

The resultant force acting on the latch in the vane stem, F_r, acts perpendicular to the surface of contact shown in Figure 2.18. D is the net disengaging force described above in Equations 2.70 through 2.71. F_{vert} is the vertical component of F_r. The 7.0 lb force

acting in the negative h direction is the vane spring force that was described in Section 2.6. In most cases the force acting on the vane stem in the negative h direction will be greater in magnitude than 7.0 lb. However, for the purpose of this calculation, the minimum value of 7.0 lb will be used. In order for the slider to be prevented from becoming unlatched until the rolling piston reaches top dead center F_{vert} must be smaller in magnitude than 7.0 lb. In order to ensure this the angle Δ, which represents the angle of the surface of contact between the slider and the latch in the vane stem with respect to the horizontal, can be calculated. From the geometry of Figure 2.18, the following equation can be developed.

$$\tan (90-\Delta) = F_{vert}/D \qquad \textbf{(2.72)}$$

By setting F_{vert} equal to 7.0 lb (the minimum condition in order to prevent the slider from disengaging), and substituting the value in Equation 2.71 for D, the value of Δ in Equation 2.72 can be solved.

$$\tan (90-\Delta) = 7.0 \text{ lb}/1.02 \text{ lb} \qquad \textbf{(2.73)}$$

$$\Delta = 8.3 \text{ degrees} \qquad \textbf{(2.74)}$$

It was decided that for ease of manufacture the angle Δ would be set to 10 degrees. This is shown in Figures 2.16 through 2.18. Therefore, with this angle applied to the latch-slider interface geometry the slider will not disengage until the rolling piston reaches top dead center.

There is a particular problem with this new latch-slider interface geometry. With the angle Δ set equal to 10 degrees as shown in Figure 2.18 the net clearance between the slider and the latch in the vane stem is reduced. The spring force parameter (Section 2.3) was calculated based on a square latch geometry ($\Delta = 0$ degrees). Both the square latch geometry and the new latch geometry are shown below in Figure 2.19. With the square latch geometry, the net displacement of the vane and vane stem of .020in from top dead center (when latched) is equal to the net clearance between the slider and the latch in the vane stem.

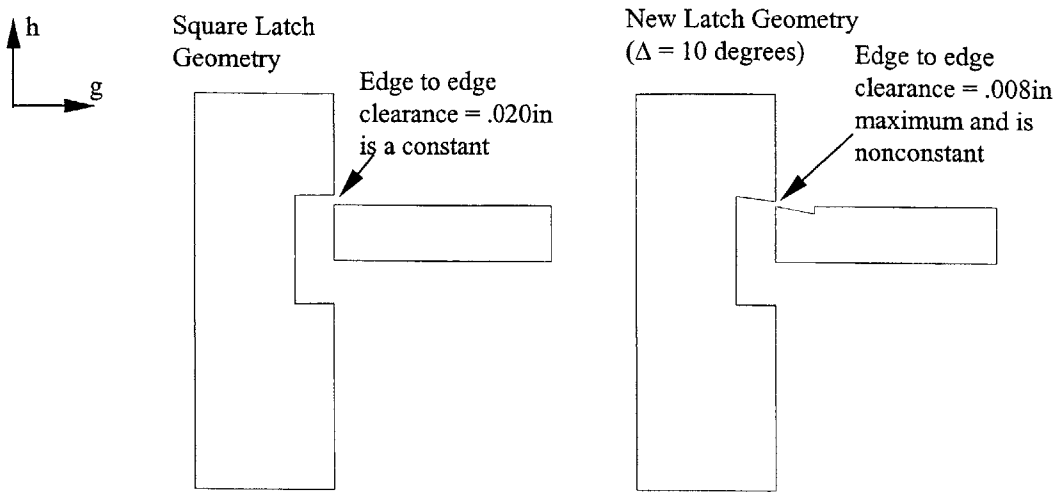

Figure 2.19 (The left view shows the square latch geometry. The right view is equivalent to Figure 2.17 but just with the slider disengaged. Both views represent the vane stem displaced the designed .020in from rest position. i.e. equivalent to the position shown in Figure 2.17 with the rolling piston at top dead center)

In Figure 2.19, above, the terminology "edge to edge" clearance refers to the maximum h direction clearance between the left-most edge of the slider and the right-most edge of the latch in the vane stem. Obviously, this maximum clearance condition occurs when the rolling piston is at top dead center. It is easy to notice that the square latch geometry keeps a constant, maximum h direction clearance of .020in along the length of the slider. In order to calculate the edge to edge clearance due to the new latch geometry Figure 2.20, below, will be referenced.

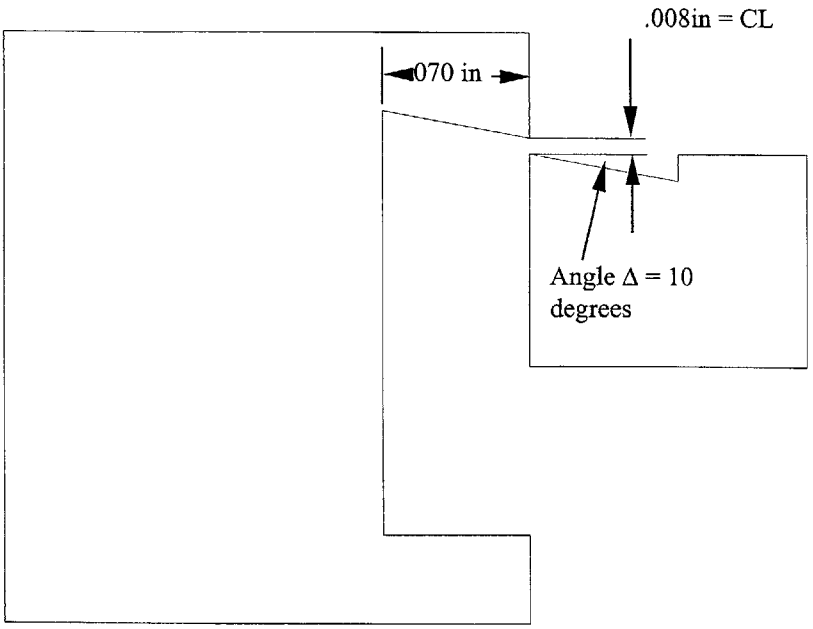

Figure 2.20 (This shows a close-up view of the new latch geometry and how the edge to edge clearance value is calculated. Again, this is representative of the rolling piston at top dead center.)

From the geometry shown above the edge to edge clearance (denoted as CL) can be calculated.

$$CL = .020in - (.070in)*(\tan(10^{\circ})) = .008in \quad \textbf{(2.75)}$$

This new edge to edge clearance value is substantially less than the original design parameter of .020in. So, if the slider is attempting to engage the latch in the vane stem, it will have much less time to fully engage than was originally designed for. As mentioned previously, the spring engaging and and estimated solenoid disengaging force parameters were designed for a full .020in of maximum edge to edge clearance. Thus, it is inevitable that the new latch geometry will not allow the slider to fully engage the latch within one revolution of the rolling piston. It will now take two, maybe three revolutions for the slider to fully engage the latch.

3. DESIGN AND CONSTRUCTION DETAILS OF THE MECHANISM

This chapter contains four sections. The objective of this chapter is to explain construction technique, list material specifications, explain overall functional design considerations, and show full mechanical drawings (where feasible) of the major mechanism components. Section one starts with the modification of the vane and the construction of the vane stem. Section two looks at the design and construction details of the block. Section three explains the design and construction details of the slider and the spring/pusher-pin combination. Section four contains detailed mechanical drawings of the major mechanism parts. It may be useful to refer back to Figures 1.3 through 1.5 to understand the orientation of some of the mechanism parts.

3.1 Modification Of The Vane And Construction Of The Vane Stem

In order to latch and hold the vane near top dead center (TDC), a way of attaching the vane stem to the vane had to be accomplished. This was done by cutting a small key-hole in the vane and cutting the matching key geometry in the vane stem. The key and key-hole geometry is designed to allow a slight "rocking" movement of the vane stem relative to a stationary vane. This keeps binding or "cocking" of the vane from occurring while it travels in its slot and is attached to the vane stem. This key and key-hole geometry was also carefully designed with small radii at all profile changes in order to try and reduce high stress concentrations. Due to the hardness of the vane and the high precision required in cutting the key and key-hole geometry a CNC wire EDM machine was used to cut the two fitting profiles.

The stock for the vane stem was originally purchased as precision square rod with a cross section dimension of .255 x .255 in. It was then precision ground down to a cross section dimension of .250 x .250 in as required to fit in the square broached hole in the block (See Section 3.2 for details on the block). Once this was accomplished it was necessary to cut the latch geometry in the vane stem. The fundamental design objectives of this latch geometry are discussed in Chapter 2, Section 7. The location of the latch cut out relative to the very bottom of the vane stem (where the key geometry is cut) is especially crucial. This precision location will determine the ability to meet the initial design criteria of .020in of vane and vane stem "bump" when the slider is latched. Of course the absolute relativity of the latch cut out in the vane stem to that of the slider location in the block determines the "bump" magnitude. For this reason the description of the precision locating and cutting of the latch in the vane stem will be discussed in detail in Section 2 of this chapter. It is important to note, however, that the critical location of the latch cut out is not shown on the accompanying drawing in Section 4. This is due to the nature of how it was jigged up and cut and then quickly assembled to begin testing. No time was available to go back and document it's location.

Table 3.1 (Specifications on the Vane and Vane Stem)

Object	Material Specification	Supplier
Vane	M2 Tool Steel, Through Hardened to Rockwell hardness 60C-65C	Carrier
Vane Stem	AISI Type A2, Air Hardened Steel	MSC

3.2 Design And Construction Details Of The Block

The block is the piece of the mechanism that houses both the vane stem and the slider. The bottom of the block is attached to the flange by means of four, #4 bolts. Sealing between the block and the flange is accomplished by means of a #17 neoprene O-ring. The flange is then welded around the outside diameter of a hole in the compressor shell. Thus, in operation, the vane stem protrudes through the compressor shell, into and through the flange, and into it's guided slot in the block. Perpendicular to the flange, the can is mounted to the side of the block. Sealing between the can and the block is accomplished by means of a #25 neoprene O-ring. It is important to remember that parts of the slider are in both the block and the can at all times. The block guides the slider and takes the load of the latched vane stem while the can houses both the solenoid and the spring and pusher pin which insert and extract the slider. The top and back-side of the block are sealed with cover plates that have O-ring grooves and O-rings. The top cover plate utilizes four, #6 bolts and a #17 O-ring while the back plate utilizes four, #4 bolts and a #25 O-ring.

The guide-slots in the block for the both the vane stem and the slider are .250in square slots. These slots are perpendicular to each other and were made by pressing a square, .250in broach through drilled pilot holes. The square slots were chosen in order to prevent rotation of the latch cut out in the vane stem relative to the slider.

As was mentioned in Section 1, the location of the latch cut out relative to the location of the slider in the block is especially crucial. In order to have some flexibility in locating the slider relative to the latch cut out in the vane stem, it was decided that shims would be used on two sides of the slider. Thus the slider height and in turn the "bump" height of the vane stem could be adjusted by varying shim thickness. Small ear type tabs were machined into the profile of the shims in order to keep them from falling into the square, broached slot that the vane stem travels in.

In order to achieve .020in of vane stem "bump" the following procedure was used; 1.The bolted shell compressor was half assembled with the cast iron cylinder and the lower bearing flange precision mounted in the bolted shell, 2. The vane and the rolling piston were placed in the cast iron cylinder, 3. The vane stem was inserted through the flange and the compressor shell and attached to the vane, 4. The upper bearing flange was mounted to the cast iron cylinder, 5. The block was then slid over the vane stem and clamped to the flange, 6. The whole assembly was then mounted on a precision-flat cast iron table with the direction of vane and vane stem travel perpendicular to the surface of the table, 7. Since the vane stem was not pre-cut yet, it extended beyond the top of the block even at bottom dead center. A dial indicator was used on the top of the vane stem in conjunction with hand cranking the shaft of the compressor to position the vane and vane stem at top dead center (TDC), 8. Once TDC was located, a vertical vernier was used to measure the distance from the top of the block to the top of the vane stem, 9. The block was then removed from the flange and vane stem, 10. By inserting a piece of square key

stock into the slot for the slider and utilizing a depth micrometer, the distance from the top of the block to the intersection of the centerlines of the broached vane-stem slot and the slider slot could be found, 11. The vane stem was then taken out of the compressor and placed in an endmill, 12. The latch cut out in the vane stem was then located by summing the distances in Step 8 and Step 10 and measuring off that distance from the top of the vane stem (the end where the vertical vernier measurement was made).

The shims that precision locate the slider in it's slot in the block were precision ground to try and achieve the .020in of "bump". Due to lack of experience and lack of shop tooling, the actual vane stem bump turned out to be .017in.

Table 3.2 (Specifications on the block and shims)

Object	Material Specifications	Machining Operation	Bump displacement
Block	Pipe Flange Steel	Vertical End Mill and Broach	
Shims	Pipe Flange Steel	Vertical End Mill and Surface Grinder	.017in

3.3 Design And Construction Details Of The Slider and Spring/Pusher-Pin Combination

The design goal of the spring and pusher-pin combination is to supply the latching force to the slider whereas the solenoid coil provides the unlatching and unlatched holding force to the slider. It will be useful to refer back to Figures 2.1A, 2.1B, and 2.1C during the following explanation. The slider, the coil, the spring, the pole piece, the pusher-pin, and the spring spacer all lie along the longitudnal axis of the solenoid coil. All the pieces are housed in the can except for the slider which is, at all times, housed in both the block and the can. When the can is assembled to the block, the front face of the block provides the retainment on the ferrite pieces, the coil, and the spring/pusher-pin assembly needed to keep spring precompression on the slider engaging spring.

Both the pusher-pin and the pole piece contact the slider. The pole piece, which rests in contact with the ferrite structure in the center of the coil, only contacts the slider when the slider is in the disengaged position. The pole piece also completes the magnetic circuit to the slider when the slider is in the disengaged position. The pusher-pin is guided by both the pole piece and the cylindrical ferrite structure lying along the centerline of the solenoid coil. The pusher-pin is constructed out of stainless steel to prevent unwanted magnetic forces from acting on it. The pole piece houses the pin part of the pusher-pin (the part that actually contacts the slider) while the ferrite structure houses the base part of the pusher-pin (the part that contacts the engaging spring). A small .065in hole was drilled in the center of the pole piece to accommodate the pin part of the pusher-pin. The base part of the pusher-pin has a fan blade type of geometry. It consists of four blades, each ninety degrees apart. Each blade is approximately .040in wide. This blade type geometry prevents the base part of the pusher-pin from acting like a dash pot damper when the center-line oriented cylindrical ferrite structure fills with compressor oil.

The spring is a coil type compression spring and is compressed between the base of the pole piece and a spring spacer on the inside surface of the can. Further details on the compression spring can be found in Table 3.3, below. The spring spacer was made out of aluminum for ease of manufacture.

As was mentioned back in Chapter 2 the coil is double wound with #28 insulated wire. It was hand wound on a nylon bobbin by utilizing a slow turning lathe. The coil was then coated with epoxy to prevent the wires from coming loose. This proved to be especially effective during assembly of the coil and the spring/pusher-pin combination. See Chapter 2, Section 4 for more details on the coil.

The entire coil and slider-engaging spring assembly is housed between two cylindrical pieces of ferrite. The ferrite is then contained in the can and retained in the can by the front face of the block. This is accomplished by assembling the can to the block. It is important to note that one of the ferrite pieces (the one in contact with the block when fully assembled) has its center structure machined down to accommodate the slider and

the pole piece. In place of the center structure of the ferrite piece is a plastic spacer that helps provide the assembled precompression force needed to hold the pole piece and the engaging spring assembly in place.

Table 3.3 (Slider Engaging Spring Specifications)

Type	Linear Spring Constant	Spring Outside Diameter	Spring Wire Size	Spring Free Length
Coil, Compression	5.70lb/in	.180in	.016in	.375in

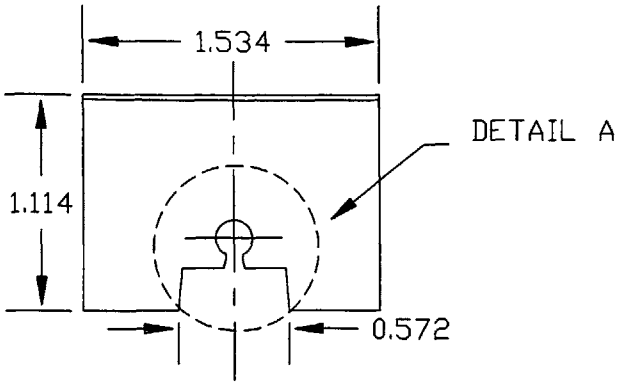

FRONT VIEW

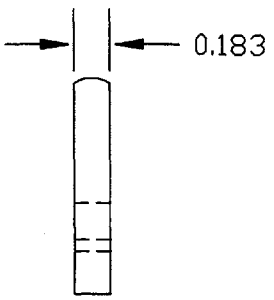

SIDE VIEW

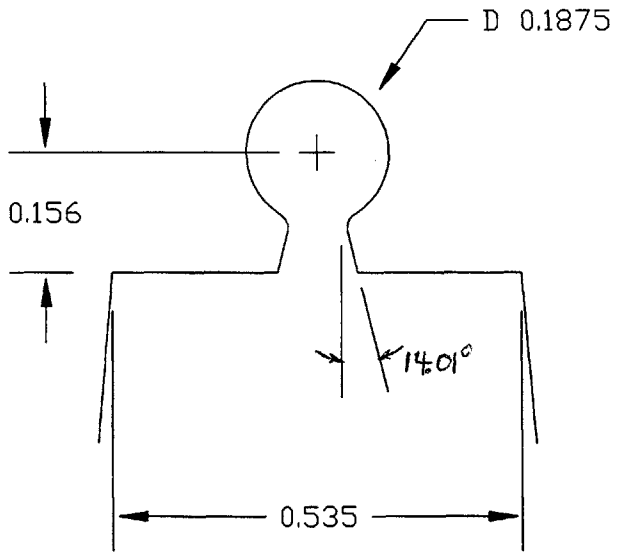

DETAIL A

NOTES:

1. Front and side views
   Scale: 1:1
   Detail A magnified 4x
2. All dimensions in inches, angle in degrees

VANE MODIFICATIONS	
Comments: Figure 3.1	Date 3/10/98

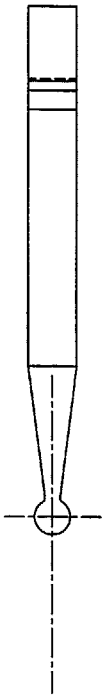

FRONT VIEW

SIDE VIEW

NOTES:

1. Front and side views drawn to scale.

2. Scale is 1:1

Vane Stem Modifications	
Comments Figure 3.2	Date 3/10/98

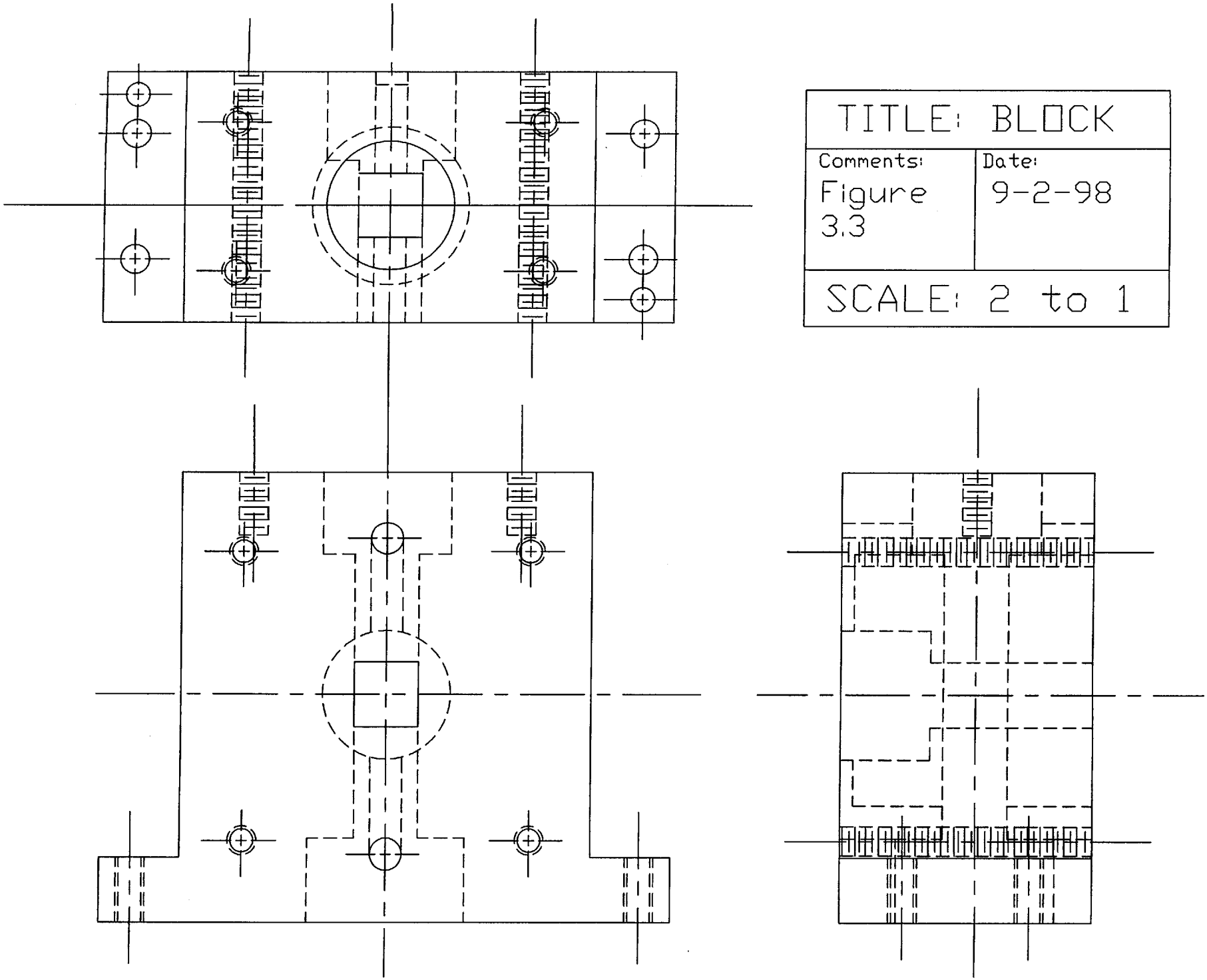

TITLE: BLOCK	
Comments: Figure 3.3	Date: 9-2-98
SCALE: 2 to 1	

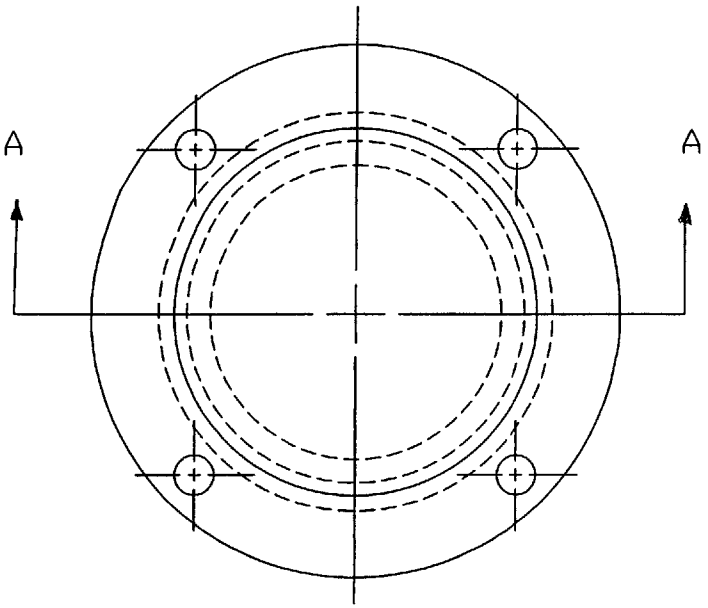

TITLE: CAN	
Comments: Figure 3.4	Date: 2-20-98
SCALE: 1.5 TO 1	

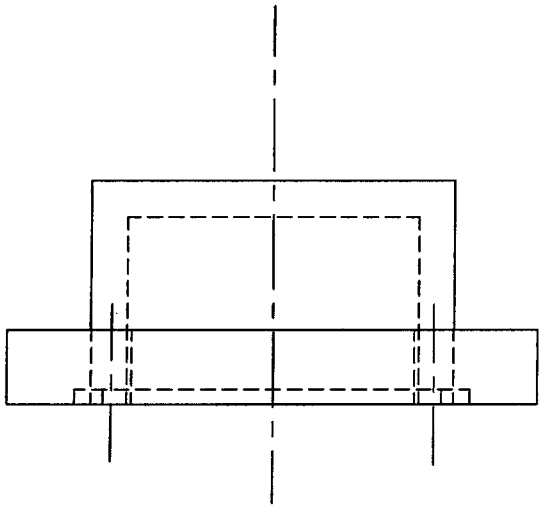

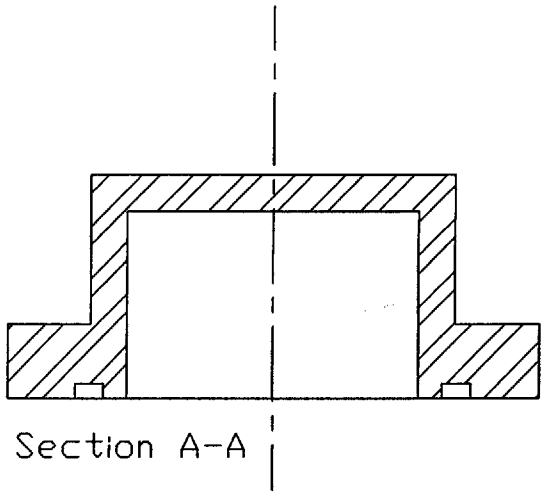

Section A-A

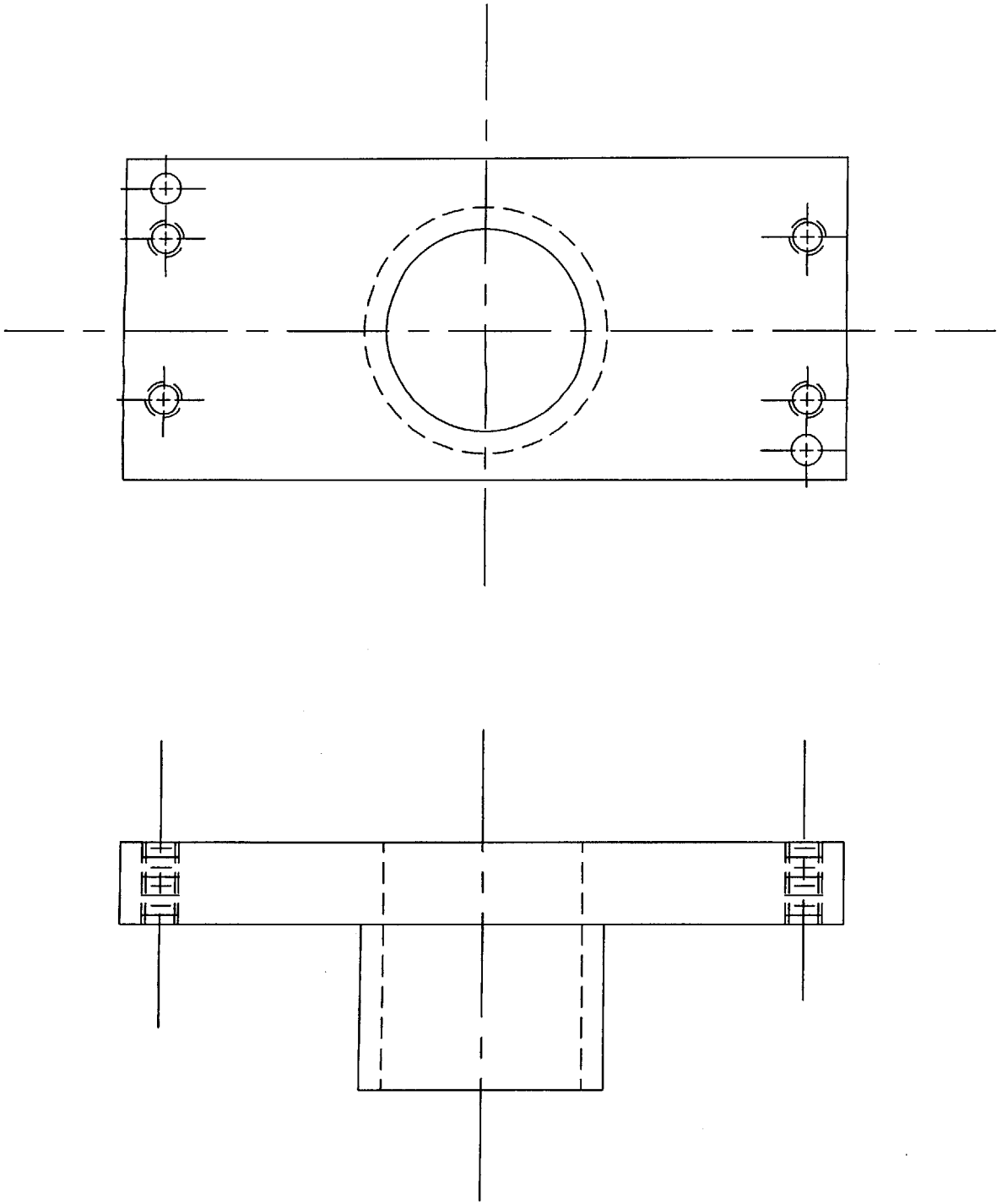

TITLE: FLANGE
DATE: 1-27-98
SCALE: 2 to 1

4. TESTING OF THE MECHANISM

This chapter is split into two major sections. The first section contains test data and results on the mechanical operation of the latching mechanism. Included in this section is a description of the beam type, slider engaging springs that were used with solenoid design 1. Also included, are full test data and results on both solenoid design 1 and solenoid design 2. The second section addresses the thermodynamic test data taken from an air conditioning system utilizing the latching mechanism compressor. Trends in data such as refrigerant mass flow rate, temperature, and pressure as a function of time are observed and recorded in this section. Also included in this section is air side test data for the evaluation of the performance of the latching mechanism compressor in a duct-free split system. Performance parameters measured and calculated include EER and COP.

4.1 Test Data And Results On The Mechanical Operation Of The Latching Mechanism

The preliminary testing of the latching mechanism in the compressor consisted of running the compressor on dry nitrogen. This was done to avoid the time consumption of assembling the compressor into a system and then charging it with refrigerant 22.

The first tests that were run on the latching mechanism utilized solenoid design 1. There were two, identical springs used to engage the slider with solenoid design 1 (one on each side of the slider). Each spring was a combination beam and torsion spring. There were three spring thicknesses that were experimented with: .006in, .008in, and .010in. Each spring had a constant thickness across its entire cross section. Figure 4.1, below, shows a top, front, and right side view of one of the springs before prebending. The springs operated by being held in a cavity in the block and were constrained by the first ferrite piece in the can. The spherical raises on the springs represent contact points by pins or ferrite that supply the constraint force on the springs so they can operate. The long middle beam actually contacted a slot in the slider (one spring on each side of the slider). The middle beam and the two arm beams supplied the bending resistance while the center beam supplied the torsion resistance. The middle beam was prebent a certain amount to obtain the necessary slider engaging spring force. This amount, along with the necessary thickness of the springs, was calculated using simple rectangular beam equations for both the bending and torsion cases. Once the springs were made out of flat, spring steel stock, the necessary prebend amount needed on the middle beam of each spring was experimentally determined. This experimental set-up consisted of placing two springs in their cavities in the block, clamping the springs at the points indicated in Figure 4.1, and using weights and a pulley system to deflect the middle beams. The middle beam deflection was then measured using a vertical vernier. Two weights were used on the .010in thick springs while just one weight was used on the .008in and .006in thick springs. The results of these experiments are shown below in Table 4.1.

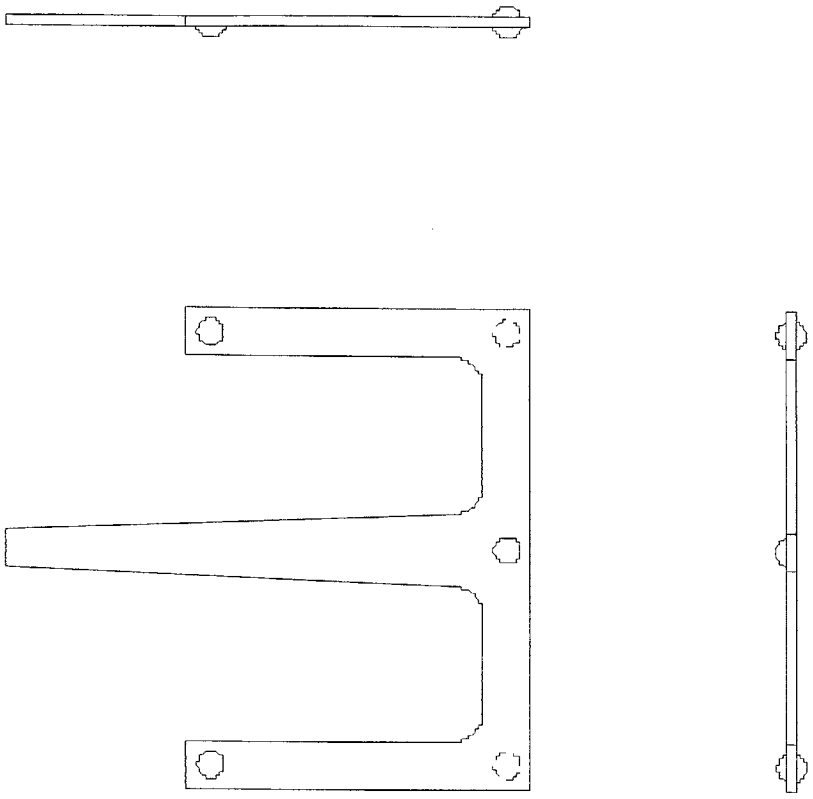

Figure 4.1 (This shows a top, front, and right side view of one beam type spring used with solenoid design 1. The spherical raises indicate clamping points by either pins or a ferrite piece in the can needed to constrain the spring during operation.)

Table 4.1 (This lists the experimentally measured beam spring displacement as a function of force)

Spring Thickness	Measured Middle Beam Deflection (2 springs)	Force
.010in	.100in	.7lb
.010in	.030in	.28lb
.008in	.064in	.28lb
.006in	.205in	.28lb

FIRST SET OF TESTS USING SOLENOID DESIGN 1 AND BEAM TYPE SPRINGS

Test 1 (Last week of May, 1998)

Mechanism Specifications:

1. two, .008in thick, beam type springs with middle beam bent .110in (calculated/extrapolated force range over .070in of slider travel, .17lb to .48lb)
2. one thick permanent magnet (.059in thick)
3. one .040in thick plastic spacer between permanent magnet and slider
4. Power Supply (Field Killing so the slider can latch), 13.5V
5. Power Supply (Energizing Electromagnet) 35V
6. Solenoid control box set at various settings

Using the above specifications, the mechanism was assembled onto the compressor. The compressor was located in Building 41 and was operated on dry nitrogen only (no refrigerant 22). When the mechanism was assembled the slider was unlatched (slider against the spacer). When regular operation was attempted, the slider would not latch. The top portion of the compressor was then disassembled and the compressor was slowly hand-cranked while the solenoid was connected to Dr. Umans control box. The slider did latch. Unlatching was then attempted while hand-cranking. Unlatching was successful even with unlatching current pulse times as low as 1.5ms (.0015s).

Test 2 (Last week of May, 1998)

Mechanism Specifications: same as those in Test 1

It was thought that the slider was not latching due to a pressure difference across the slider (high pressure on the latch side of the slider and a lower pressure on the permanent magnet side of the slider). This high pressure on the latch side of the slider was believed to originate from the vane stem compressing the dry nitrogen in the block as the vane and vane stem approached top dead center (TDC). In order to relieve the pressure difference, holes and slots were drilled in the block to vent the pressure in the top portion of the block to compressor discharge pressure. The latch mechanism and the compressor were then reassembled in Building 41 and the compressor was run on dry nitrogen. Once again the mechanism was assembled with the slider unlatched (slider against the spacer). When regular operation was attempted, the slider would not latch. No more tests were attempted with the .008in thick, beam type springs. It was decided that more spring force was needed to engage the slider under regular operation.

Test 3 (June 10, 1998)

Mechanism Specifications:

1. two, .010in thick, beam type springs with middle beam bent .140in (calculated/extrapolated force range over .070in of slider travel, .5lb to 1.0lb)
2. one thick (.059in thick) permanent magnet
3. one thin (.029in thick) permanent magnet
4. one .010in thick plastic spacer between permanent magnet and slider
5. Power Supply (Field Killing so the slider can latch), 13.5V
6. Power Supply (Energizing Electromagnet) 35V
7. Solenoid control box set at various settings

After Test 2 it was decided that there was simply not enough spring engaging force acting on the slider. For this reason, the .008in thick beam type springs were replaced with .010in thick beam type springs. Due to the increased slider spring engaging force, the permanent magnet force had to be increased. Thus a second, thinner permanent magnet was added. Consequently, a thinner plastic spacer was needed to keep the slider properly aligned. The latch mechanism and the compressor were then reassembled in Building 41 and the compressor was run on dry nitrogen. The mechanism was assembled with the slider unlatched (slider against the spacer). The slider did latch and unlatch properly under regular compressor operation.

Test 4 (June 11, 1998)

Mechanism Specifications: same as those in Test 3 plus

1. Solenoid control box set to cycle at 10.0 seconds @ 50% duty cycle

The latch mechanism and the compressor were then assembled into the duct-free split system in the heat transfer lab. The mechanism was assembled with the slider unlatched (slider against the spacer). The system was charged with R22 freon. When regular operation was attempted, a new phenomena was observed. The slider would latch then miss an unlatch solenoid pulse (stay latched). Then, on the next unlatch solenoid pulse the slider would come unlatched. This phenomena of the slider skipping one unlatch pulse continued somewhat consistently. As the period and duty cycle on Steve's box were changed the unlatch skipping pattern continued. The duty cycle was then turned completely off and the compressor was allowed to run loaded for several minutes. After approximately ten minutes the slider latched and the compressor began to run unloaded. This latching occurred without supplying a current to the coil to kill the permanent magnet field. The presumed reason for this occurring was an increase in permanent magnet temperature (due to the compressor shell heating while the compressor operated under full load) and thus a weakening of the permanent magnet force. When the permanent magnet force became weak enough for the spring force to overcome it, the slider became latched.

Conclusions of Tests 1 Through 4

Test 1 and Test 2 demonstrated that the slider latching and unlatching force required was more than that calculated in Chapter 2. There are two possible explanations for this. First, the actual vane and vane stem bump was measured at .017in. Since this is less than the .020in that the calculations were based on, the time required to engage or disengage the slider will be less than .0023s. Second, as described in Chapter 2, Section 6, the slider and latch cut out geometry are such that more time is needed to engage or disengage the slider even if there was .020in of vane and vane stem bump. Two conclusions can also be drawn from Test 3 and Test 4. First, even with slightly more powerful springs and a more powerful permanent magnet, latching and unlatching problems continued. Second, the performance of the permanent magnet seriously degraded when the compressor heated to normal operating temperature. It was decided that at this point that both the permanent magnet design and the beam spring design had to be changed. The beam springs were replaced with a linear coil spring and the permanent magnet was replaced with a coil only solenoid. The coil only solenoid would provide both slider holding current (when the slider was unlatched) and slider extracting force.

SECOND SET OF TESTS USING SOLENOID DESIGN 2 AND LINEAR COIL SPRING

Note that Tests 5 through 17 contain a single wound coil. Even though Solenoid Design 2 is described in Chapter 2 as having a double wound coil, the double wound coil does not appear until Test 18. The pusher-pin also has a different base geometry for Tests 5 through 11 than described in Chapter 3. For Tests 5 through 11 the base of the pusher-pin is a solid, thin piston (no fan blade geometry until Test 12). The other fundamental, mechanical design properties of Solenoid Design 2 (i.e. the pole piece and linear coil spring) remain the same from Test 5 through 22.

Test 5 (June 21, 1998)

Mechanism Specifications:

1. Compression-type coil spring with .016in wire size, .625in free length, k = 3.27 lb/in, and .180in OD (outside diameter). Spring has force specifications of 1.28lb with slider unlatched and 1.05lb with slider latched
2. No spring spacer in bottom of can
3. Single wound coil (6.5 ohm)
4. Pusher-pin and pole piece
5. Brass pole piece retaining spacer (between pole piece and ferrite)
6. Power Supply (for slider extraction) 35+V
7. Solenoid control box set at various settings

The latch mechanism and the compressor were assembled in Building 41. With the top cover of the block removed, the compressor was hand-cranked over while the solenoid

was connected to Dr. Umans' control box. The system would latch but not unlatch. The reason for this was simple. There was not enough unlatching current available for the given coil resistance (large power supply maxed out at 35+V) to extract the slider against the new coil spring. At this point it was decided to use a shorter, stiffer spring with a maximum compressed force less than or equal to 1.0lb (spring force on the slider when it is completely unlatched).

Test 6 (June 23, 1998)

Mechanism Specifications:

1. Compression-type coil spring with .016in wire size, .250in free length, k = 9.39 lb/in, and .180in OD (outside diameter). Spring has force specifications of .995lb with slider unlatched and .34lb with slider latched
2. .090in spring spacer in bottom of can
3. Single wound coil (6.5 ohm)
4. Pusher-pin and pole piece
5. Brass pole piece retaining spacer (between pole piece and ferrite)
6. Power Supply hooked through Dr. Umans' box; operating on 20ms (.020s) pulses, unlatch holding current = .300A to .400A, unlatching voltage as low as 10.0 V, Solenoid control box period = 4s @ 50% duty cycle

The block, can, slider, and solenoid were assembled and placed out on the table for separate testing (not assembled onto the compressor). While Dr. Umans' control box was connected to the solenoid, a phenomena of the slider "bouncing" was observed. This "bouncing" is described as the slider traveling through the .070in of unlatching distance and then immediately returning to the latched position. In other words, it would not stay unlatched. Several conclusions were drawn at this point. First, this bouncing could be do to not enough unlatch holding current. Second, the spring force on the slider in the latched position is very low. This could cause the slider to reach a very high velocity when impacting the pole piece. Finally, the brass retaining pole piece spacer could be causing some unneeded eddy currents. In order to address these concerns it was decided to switch springs and replace the brass pole piece retaining spacer with a plastic one.

Test 7 (June 23, 1998)

Mechanism Specifications:

1. Compression-type coil spring with .016in wire size, .375in free length, k = 5.70 lb/in, and .180in OD (outside diameter). Spring has force specifications of .998lb with slider unlatched and .60lb with slider latched
2. .034in spring spacer in bottom of can
3. Single wound coil (6.5 ohm)
4. Pusher-pin and pole piece
5. Green, plastic pole piece retaining spacer (between pole piece and ferrite)
6. Power Supply hooked through Dr. Umans' box; operating on 20ms (.020s) pulses, unlatch holding current = .300A to .400A, unlatching voltage as low as 21.0 V, Solenoid control box period = 4s @ 50% duty cycle

The block, can, slider, and solenoid were assembled and placed out on the table for separate testing (not assembled onto the compressor). While Dr. Umans' control box was connected to the solenoid, the "bouncing" phenomena occurred again. A small weight was rested on the slider. When this was done the "bouncing" phenomena was eliminated and the slider would latch and unlatch properly. The mass of the small weight was .042lb. In order to model the system with this weight magnitude, it was decided to reduce the spring force by an amount equal to or greater than .042lb.

Test 8 (June 24, 1998)

Mechanism Specifications:

1. Compression-type coil spring with .016in wire size, .375in free length, k = 5.70 lb/in, and .180in OD (outside diameter). Spring has force specifications of .918lb with slider unlatched and .52lb with slider latched
2. .020in spring spacer in bottom of can
3. Single wound coil (6.5 ohm)
4. Pusher-pin and pole piece
5. Green, plastic pole piece retaining spacer (between pole piece and ferrite)
6. Power Supply hooked through Dr. Umans' box; operating on 20ms (.020s) pulses, unlatch holding current = .400A, unlatching voltage as low as 21.0 V, Solenoid control box period = 10s @ 50% duty cycle

The block, can, slider, and solenoid were assembled and placed out on the table for separate testing (not assembled onto the compressor). While Dr. Umans' control box was connected to the solenoid, the bouncing phenomena did not occur. The slider successfully latched and unlatched. The only thing that was changed from Test 7 was the spring. It's

applied force to the slider was reduced by .08lb by putting a smaller spring spacer in the bottom of the can.

Test 9 (June 24, 1998)

Mechanism Specifications: same as those in Test 8 except that the unlatching voltage was increased to and held at 30.0V

The block, can, slider, and solenoid assembly from Test 8 was assembled onto the compressor. A hand-crank test was performed. The slider latched and unlatched successfully.

Test 10 (June 24, 1998)

Mechanism Specifications: same as Test 9 except the compressor was hooked into the duct-free split system in the heat transfer laboratory and the system was charged with refrigerant 22.

Due to the nature of the new solenoid design the compressor started with the slider in the latched position (compressor unloaded). Several tests were then conducted while the compressor was running in the system. 1. With the solenoid connected to Dr. Umans' control box, the slider would not unlatch. The unlatch holding current was set at .400A while the unlatching voltage was adjusted between 20.0V and 35.0+V. 2. The large power supply (the one that supplies the unlatching voltage) was connected straight to the solenoid. By doing this Dr. Umans' control box was bypassed. When the leads were quickly "touched" together the slider would not unlatch. The voltage on the large power supply was adjusted between 10.0V and 35.0+V. 3. The large power supply was reconnected to Dr. Umans' control box which was in turn connected to the solenoid. The period on Dr. Umans' control box was changed to 1.0s @ 50% duty cycle. With Dr. Umans' control box attempting to unlatch the slider, the power was shut off to the compressor motor. As the motor coasted down to zero rpm an attempt was made to listen and hear if the slider came unlatched. It was determined that the slider did not come unlatched. The unlatching voltage was maintained at 35.0+V while the unlatch holding current was set at .400A during the coast down time. As a result of the slider not unlatching, it was decided to evacuate freon from the system and remove the compressor from the system.

Test 11 (June 24, 1998)

Mechanism Specifications: same as Test 9 and Test 10 except the compressor was removed from the air conditioning system described in Test 10.

The top cover of the compressor was removed and the top cover of the block was removed exposing the vane stem. The compressor was tilted to prevent oil from pouring out of the top of the block. Several tests were then conducted while the compressor was

hand-cranked. Note, at this time the slider was still in the latched position. 1. The slider would not unlatch. The unlatch holding current was set at .400A. The unlatching voltage was set to 20.0V. 2. The unlatching voltage was slowly driven up to 35.0V. Between 35.0V and 35.0+V the slider unlatched and began to cycle (latch and unlatch according to the time set on Dr. Umans' control box. 3. The unlatching voltage was then slowly reduced. The slider quit latching and unlatching when the unlatching voltage got between 25.0V and 20.0V.

Conclusions of Tests 5 Through 11

Tests 5 through 9 demonstrated that the dynamics of the slider are very sensitive to the spring force that is used to engage the slider. The "bouncing" phenomena was eliminated by reducing the spring force by .08lb (see Tests 7 and 8). At this point, it can be concluded that the "bouncing" phenomena was caused by a spring that was too strong when the slider was unlatched. The weaker that the spring was while the slider was unlatched, the greater the possibility that the unlatch holding current would hold the slider unlatched. This would then prevent the slider from unlatching and bouncing off the pole piece back to the latched position again. A close analysis of Test 11 will explain why the slider failed to latch and unlatch. The base of the pole piece was a solid piston that was operating in the cylinder of the ferrite mold. By taking apart the mechanism and filling the ferrite cylinder with oil, it could be seen that the base of the pusher pin was acting just like a piston in an oil-filled piston-cylinder damper. This oil damping was the reason the slider was not extracting in Test 10. In order to fix this problem, the base of the pusher-pin would be modified from a solid piston to a four-bladed fan geometry. This new geometry would allow the oil in the ferrite cylinder to flow around the base of the pusher pin as it translated with the spring and the slider.

Test 12 (June 25, 1998)

Mechanism Specifications:

1. Compression-type coil spring with .016in wire size, .375in free length, k = 5.70 lb/in, and .180in OD (outside diameter). Spring has force specifications of .918lb with slider unlatched and .52lb with slider latched
2. .020in spring spacer in bottom of can
3. Single wound coil
4. Fan blade pusher-pin base geometry and pole piece
5. Green, plastic pole piece retaining spacer (between pole piece and ferrite)
6. Power Supply hooked through Dr. Umans' box; operating on 20ms (.020s) pulses, unlatch holding current = .400A, unlatching voltage between 20.0V and 30.0V, Solenoid control box period = 8s @ 50% duty cycle

The block, can, slider, and solenoid were assembled and placed out on the table for separate testing (not assembled onto the compressor). This was the first test with the new fan blade geometry on the base of the pusher-pin. The slider successfully latched and unlatched.

Test 13 (June 25, 1998)

Mechanism Specifications: same as those in Test 12

The block, can, slider, and solenoid assembly from Test 12 was assembled onto the compressor. A hand-crank test was performed. The slider latched and unlatched successfully.

Test 14 (June 25, 1998)

Mechanism Specifications: same as those in Test 12 except the unlatching voltage was increased to 35.0+V

The compressor from Test 13 was completely assembled into the air conditioning system in the heat transfer laboratory. Once again, the compressor was started with the slider in the latched position. When the solenoid was connected to Dr. Umans' control box the slider did not unlatch. The unlatching voltage was increased to maximum (35.0+V). The slider still would not unlatch.

Test 15 (June 25, 1998)

Mechanism Specifications: same as those in Test 12 and Test 14 except that Dr. Umans' box was disconnected from the solenoid

With Dr. Umans' control box disconnected, the large power supply was directly connected to the solenoid. This was accomplished by setting the power supply to maximum voltage (35.0+V) and "touching" the leads together. The slider successfully unlatched and then latched again. It was noticed that the amp meter reading on the large power supply read a larger amplitude when "touching" the leads together versus having the solenoid and power supply connected to Dr. Umans' control box.

Test 16 (July 1, 1998)

Mechanism Specifications: same as those in Test 12 and Test 15 except that Dr. Umans' control box was reconnected to the solenoid

Professor Wilson and Dave Otten went through Dr. Umans' control box and fixed a possible over-currenting problem. At this point, the compressor was still connected into the air conditioning system from Test 13. Several experiments were then run. 1. Dave Otten connected a digital oscilloscope to the output of Dr. Umans' box. Of concern was

the magnitude of the unlatching voltage and the unlatching current. The unlatching current = 4.5A at an unlatching voltage = 40.0V. 2. The compressor was then started and the slider began to unlatch and latch at an inconsistent rate (as compared to when it should according to Dr. Umans' control box). As time went on the slider unlatching and latching operation became highly inconsistent. This was believed to be due to the compressor heating up to operating temperature and thus heating the coil in the solenoid. 3. A quick experiment was also done by separately decreasing the holding current (on the small power supply) and the unlatching voltage (on the large power supply). It was concluded that decreasing the holding current had negligible effect on the inconsistent operation of the slider while decreasing the unlatching voltage increased the rate at which the slider "missed" the unlatch cycle.

Test 17 (July 2, 1998)

Mechanism Specifications: same as those in Test 12 and Test 16 except that Dr. Umans' control box period = 3.0s @ 50% duty cycle

Tests on the solenoid and Dr. Umans' control box were continued from the previous test. Some measurements were first made with the compressor cold (before motor start up). These measurements were made by Professor Wilson using his digital oscilloscope. 1. Coil resistance = 6.5ohms (measured with hand held voltmeter). 2. Output data from Dr. Umans' control box to the solenoid (while pulsing) is shown below in Table 4.2.

Table 4.2 (These three measurements were made by setting the voltage output on the large power supply at three different settings; each setting at a higher voltage than the previous).

Large Power Supply Setting #	Output Voltage to Solenoid Coil	Output Current to Solenoid Coil
Setting 1	11.6V	1.7A
Setting 2	32.8V	4.8A
Setting 3	39.2V	6.0A

The voltage and current readings in Table 4.2 verify the 6.5ohm coil resistance measured in (1.) with the hand held voltmeter. 3. The compressor was then started in the air conditioning system. As the compressor ran and warmed up, Dr. Umans' box was set to cycle the slider. Table 4.3, below, lists the data observed and taken during the time the compressor was started until it was turned off.

Table 4.3 (This lists data observed and recorded when the compressor was turned on. The current measurements were made with a digital oscilloscope).

Time (min:s) from time compressor was started	Current Reading	Unlatching Voltage read straight off the large power supply	Compressor Shell Surface Temperature	Comments
0:00	5.5A	35.0+V	No Reading (N.R.)	Slider latching and unlatching somewhat consistently
1:00	5.0A	35.0+V	N.R.	Note reduction in current
1:40	5.0A	35.0+V	N.R.	Slider still latching and unlatching somewhat consistently
2:40	4.0A	35.0V	N.R.	Reduced Unlatching Voltage/ Slider operating less consistently
7:40	5.2A	35.0+V	N.R.	Increased Unlatching Voltage back to max/Slider began to operate somewhat consistently again
9:13	3.8A	30.0V	110^0F	Reduced Unlatching Voltage/Slider operating less consistently
13:50	2.9A	20.0V	115^0F	Reduced Unlatching Voltage More/ Slider completely stopped working
20:34	5.05A	35.0+V	125^0F	Unlatching Voltage increased back to max/slider began to work somewhat consistently again

It is important to define the terms "somewhat consistently" and "less consistently" when referring to performance evaluations of the slider given in Table 4.3. "Somewhat consistently" is defined as the slider latching and then skipping an unlatch cycle. On the next unlatch cycle the slider would unlatch properly. "Less consistently" is defined as the slider latching and then skipping two or three unlatch cycles. On the third or fourth unlatch cycle the slider will then unlatch. These terms are defined somewhat loosely, but they were the only gage that was available to measure slider performance. It was concluded that in order to improve the unlatching performance of the slider the solenoid coil would have to be improved.

Test 18 (July 5, 1998)

Mechanism Specifications:

1. Compression-type coil spring with .016in wire size, .375in free length, k = 5.70 lb/in, and .180in OD (outside diameter). Spring has force specifications of .918lb with slider unlatched and .52lb with slider latched
2. .020in spring spacer in bottom of can
3. Double wound coil
4. Fan blade pusher-pin base geometry and pole piece
5. Green, plastic pole piece retaining spacer (between pole piece and ferrite)
6. Power Supply hooked through Dr. Umans' box; operating on 20ms (.020s) pulses, unlatch holding current = .400A, unlatching voltage = 35.0+V, Solenoid control box period = 8s @ 50% duty cycle

The compressor from Test 17 was removed from the air conditioning system in the heat transfer laboratory and the latching mechanism was disassembled. A new coil for the solenoid was wound. This coil was double wound using #28 wire (winding two wires side-by-side). The double winding effectively increased the amount of current the coil could receive while supplying it with the same unlatching voltage (the resistance of the coil was reduced). The block, can, slider, and solenoid were then assembled and placed out on the table for separate testing (not assembled onto the compressor). This was the first series of tests with the new double wound coil. 1. With the solenoid connected to Dr. Umans' control box the "bouncing" phenomena was observed again. This "bouncing" phenomena occurred over the whole range of holding currents and unlatching voltages (at least until the unlatching voltage was too low to move the slider to the unlatched position). 2. It was observed that if a small force was exerted on the slider (in the unlatching direction) the slider would latch and unlatch properly. This small force was representative of the small weight (.042lb) placed on the slider in Test 7 to eliminate the "bouncing" phenomena. It was concluded that in order to eliminate the "bouncing" problem the spring force should be reduced more. Therefore the .020in coil spring spacer in the bottom of the can was removed.

Test 19 (July 5, 1998)

Mechanism Specifications: same as those in Test 18 except that the .020in spring spacer in the bottom of the can was removed which affected the spring force

1. Compression-type coil spring with .016in wire size, .375in free length, k = 5.70 lb/in, and .180in OD (outside diameter). Spring has force specifications of .804lb with slider unlatched and .406lb with slider latched
2. No spring spacer in bottom of can
3. Double wound coil
4. Fan blade pusher-pin base geometry and pole piece
5. Green, plastic pole piece retaining spacer (between pole piece and ferrite)
6. Power Supply hooked through Dr. Umans' control box; operating on 20ms (.020s) pulses, unlatch holding current = .400A, unlatching voltage = 35.0+V, Solenoid control box period = 8s @ 50% duty cycle

The block, can, slider, and solenoid were assembled and placed out on the table for separate testing (not assembled onto the compressor). The slider successfully latched and unlatched. However, it was observed that if the unlatching voltage was reduced from maximum the slider would begin "bouncing" again. It was concluded that the "bouncing" problem had not been dealt with thoroughly and that further modifications to Dr. Umans' box may be needed to fix the problem.

Test 20 (July 7, 1998)

Mechanism Specifications:

1. Compression-type coil spring with .016in wire size, .375in free length, k = 5.70 lb/in, and .180in OD (outside diameter). Spring has force specifications of .918lb with slider unlatched and .52lb with slider latched
2. .020in spring spacer in bottom of can
3. Double wound coil
4. Fan blade pusher-pin base geometry and pole piece
5. Green, plastic pole piece retaining spacer (between pole piece and ferrite)
6. Power Supply hooked through Dr. Umans' box; Dr Umans' box modified to supply positive voltage or zero voltage to coil, unlatching voltage pulse width increased to 40ms (.040s), voltage zeroing pulse width (for slider to latch) still 20ms (.020s), unlatch holding current = .400A, unlatching voltage = 35.0+V, Solenoid control box period = 8s @ 50% duty cycle

It was discovered that Dr. Umans' control box operated by switching from a positive holding voltage to a negative unlatching voltage (for a 20ms pulse). The voltage then transitioned from a negative unlatching voltage back to a positive holding voltage. This sequence of voltage switches was designed to unlatch the slider. In order to for the slider to latch, the positive holding voltage was switched to zero for a 20ms pulse (the spring was now free to engage the slider into the latch). After the 20ms pulse the voltage was brought back to the positive holding voltage. This is illustrated in Figure 4.2 below.

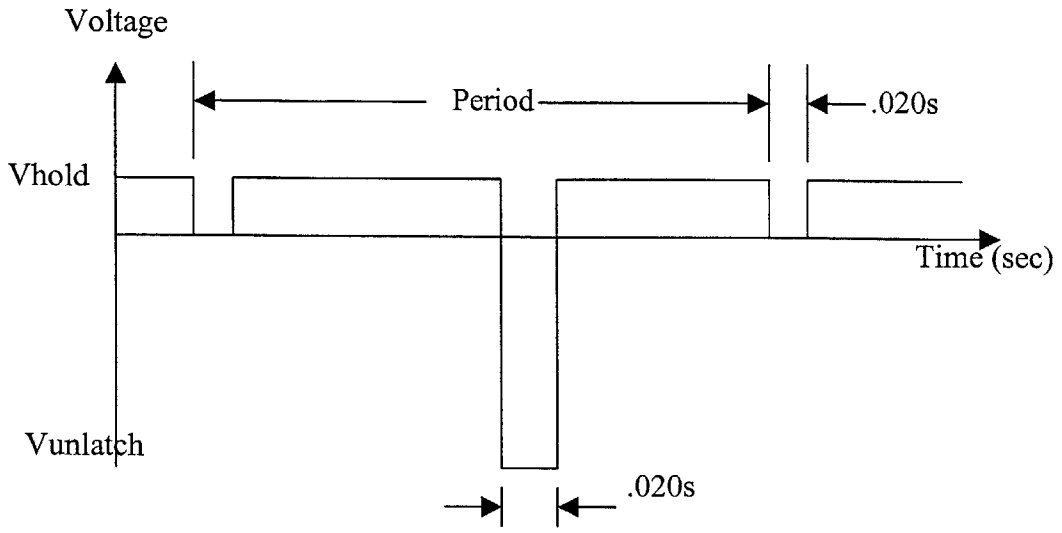

Figure 4.2 (This shows a plot of the voltage output vs time for Dr. Umans' control box. This output goes straight to the solenoid coil. Notice the transition from negative unlatching voltage to positive holding voltage.)

It was now thought that the "bouncing" phenomena could be explained by the transition from a negative unlatching voltage to a positive holding voltage. Even though the transition time through zero voltage is very small, it does give the coil spring a chance to move the slider some distance. Even if this distance is very small, the positive holding voltage may not have enough power to pull the slider back up against the pole piece. In order to correct this problem, Dr. Umans' redesigned the control scheme so that the voltage never transitions from a negative voltage through zero to a positive voltage. Also, the total time of the unlatching voltage pulse was doubled to .040s. The new control scheme is shown below in Figure 4.3.

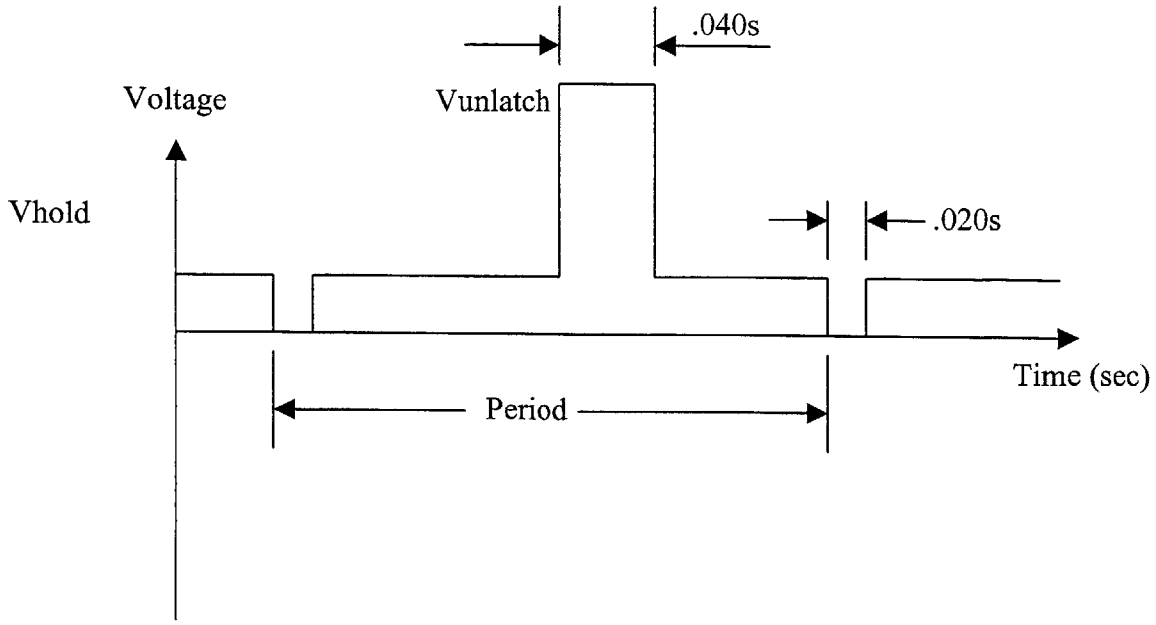

Figure 4.3 (This shows a plot of the new control scheme for voltage output vs time for Dr. Umans' control box. This output goes straight to the solenoid coil. Notice that there is no transition from negative to positive voltage.)

With this new control scheme and the specifications listed above, the block, can, slider, and solenoid were assembled and placed out on the table for separate testing (not assembled to the compressor). The slider successfully latched and unlatched.

Test 21 (July 7, 1998)

Mechanism Specifications: same as those in Test 20

The block, can, slider, and solenoid assembly from Test 20 was assembled onto the compressor. A hand-crank test was performed. The slider latched and unlatched successfully.

Test 22 (July 7, 1998)

Mechanism Specifications: same as those in Test 20 and Test 21

The compressor and latching mechanism from Test 21 were completely assembled into the air conditioning system in the heat transfer laboratory. Once again, the compressor was started with the slider in the latched position. The slider unlatched and latched successfully.

Conclusions of Tests 12 Through 22

It can be concluded from Tests 12 through 17 that the single wound solenoid coil was not strong enough to successfully unlatch the slider. There are important parameters that deserve discussion at this point. First, the bobbin that the coil was wound on was made of nylon. Nylon's heat resistance capability is not good. In fact, in almost every case that the mechanism was disassembled it was noticed that the nylon bobbin had melted. This heat damage can be attributed to both the operating temperature of the compressor and the power dissipation of the solenoid coil when the unlatching voltage pulse was applied. Another concern was the inability to change the physical size of the solenoid coil (make it bigger). This would obviously be a good solution to the problem. However, time constraints and the necessity to change the geometry parameters of several other mechanism parts prevented this solution from being a reality. Thus, in an effort to develop more unlatching force, the single wound coil was replaced by a double wound coil. As described in Test 18, the double wound coil increased the amount of current through the coil while maintaining the same voltage.

Tests 18 through 22 demonstrated that the real solution to the bouncing problem was to be found in the voltage control scheme to the solenoid coil. By preventing the coil voltage from transitioning from a negative voltage value to a positive voltage value, the bouncing phenomena was completely eliminated. However, even with the double wound design, the solenoid still was not developing enough force to extract the slider in one revolution of the compressor crankshaft. The new voltage control scheme therefore had to also incorporate a .040s unlatching voltage pulse (double what it was previously). The inability to unlatch the slider in one revolution of the compressor crankshaft can be explained with two conclusions. First, as mentioned for the slider engaging dynamics, the actual bump of the vane and vane stem was .017in and not the design value of .020in. Therefore the force needed to extract the slider in one revolution of the crankshaft will be more than the values calculated and experimentally determined in Chapter 2. Second, the latch cut-out geometry and the geometry of the slider latching surface result in less net clearance than the .017in of bump (on the order of .008in). This condition will also require a larger extraction force than that calculated in Chapter 2.

4.2 Thermodynamic Test Data Taken From An Air Conditioning System Utilizing The Latching Mechanism Compressor

The main objective of this section is to analyze the results of air conditioning system performance test data. This performance test data was taken and analyzed with the latching mechanism compressor installed in a duct-free split air conditioning system. The tests that are listed were all performed at United Technologies Carrier in Syracuse, New York. In addition to analyzing system performance, trends in refrigerant pressure and mass flow rate versus time will be analyzed. Compressor power consumption will also be analyzed closely (especially during the unload cycles). All the tests listed below will be listed according to the chronological order in which they actually occurred.

At this point it is important that the existing experimental setup in the Carrier test facility be explained. Two insulated and temperature controlled rooms were used in the testing of the system. The outdoor room contained the condensor, the compressor, the refrigerant flow meter, and both liquid and vapor return lines. The indoor room contained the evaporator and the evaporator air sampling unit. The evaporator air sampling unit was positively sealed to the air exiting the evaporator so that this air could be accurately sampled. The pressure in the air sampling unit was maintained at atmospheric pressure with the use of vacuum system connected to a control loop

PERFORMANCE CALCULATIONS:

The performance calculations were based on sets of experimental data. The first set of experimental data came from air side measurements. Air side measurements were made on evaporator entering and exiting air. The second set of experimental data came from refrigerant side measurements. Refrigerant pressure and temperature were measured at various points throughout the system enabling refrigerant state point properties to be calculated. All experimental data was taken with standard instrumentation (thermocouples, pressure transducers, etc) that was connected to a data acquisition system on a PC. LabView was the data acquisition software chosen.

Actual experimental measurements that were made of exiting evaporator air include wet bulb temperature, dry bulb temperature, and the pressure difference across the nozzle(s). The nozzle(s) were located in the air sampler but downstream of the air exiting the evaporator and downstream of the wet and dry bulb temperature measurements. The nozzle(s) were made of near ideal geometry and had been calibrated such that from a given pressure difference across the nozzle a flow rate could be calculated. There were a total of three nozzles each with a different throat diameter. Thus a combination of nozzles could be opened or shut off depending on how fast the evaporator fan was rotating (high, medium, or low setting). The low pressure on the downstream side of the nozzle was created by an air pump. This air pump was controlled using a feedback loop which measured the pressure in the air sampler unit. With this method, the pressure in the air sampler could be maintained at atmospheric thus creating an environment similar to the

evaporator discharging air into the atmosphere. Once these three measurements were made the relative humidity, enthalpy, and specific volume of the air exiting the evaporator could be calculated using psychometric relations. It is important to note that the relative humidity, enthalpy, and specific volume were calculated from average values of wet bulb temperature, dry bulb temperature, and nozzle pressure difference. Over a specific test cycle these experimentally measured values could change from one sample time to the next (especially with the compressor loading and unloading). An outdoor room air sampler was used to measure the wet bulb temperature and dry bulb temperature of the air entering the evaporator. Thus relative humidity, enthalpy, and specific volume of the air entering the evaporator were found using the same psychometric relations. Once again, average values of wet bulb temperature and dry bulb temperature were used.

The following performance parameters were calculated using air side data (data from the air entering and exiting the evaporator).

1. **airflow through the evaporator (cfm):** This parameter was calculated using the pressure difference across the nozzle(s) and the calculated value of specific volume of the air exiting the evaporator.

2. **Capacity, total (Btu/hr):** This value was calculated using the airflow (cfm) from **1**, the enthalpy difference between the exiting evaporator air and the entering evaporator air, and the specific volume of the air exiting the evaporator.

3. **Sensible Heat Ratio:** This value is found by dividing the sensible heat transfer (using dry bulb temperature difference) by the latent heat transfer (heat transfer from decrease in humidity ratio).

4. **Power (watts):** This value was measured using a power meter that was connected to the data acquisition system. It represents an average value of all the instantaneous power values sampled by the data acquisition system during one test cycle. Note: no air side data was used for the power measurement.

5. **Efficiency (EER):** This efficiency value is the Capacity, total (BTU/hr) from **2** divided by the Power (watts) from **4**.

6. **Coefficient of Performance (COP):** This efficiency value is the Capacity, total (BTU/hr) from **2** divided by the Power (BTU/hr) from **4**. Note that the power from **4** was converted from watts to BTU/hr for this calculation.

The following performance parameters were calculated using refrigerant side data. As was the case for the air side data, pressure and temperature of the R22 was measured at various points throughout the system. With this data, saturated refrigerant temperature,

saturated enthalpy, and state point enthalpy could be determined. Once again, average values of temperature and pressure were used to calculate the state point properties.

1. **Refrigerant Mass Flow Rate (lb/hr)** This parameter was calculated using the Capacity, total (BTU/hr) from the air side data and the calculated enthalpy difference between the compressor entering section and the condensor leaving section.

2. **Compressor Power (watts)** This value is found by subtracting a constant power value (the non-compressor watts) from the average Power described in **4** in the air side data performance parameters.

3. **Compressor Heat Factor (lb/watts)** This value is found by dividing the product of the Refrigerant Mass Flow (lb/hr) and the enthalpy difference (between compressor entering and condensor exiting) by the Compressor Power in **2**.

4. **Power Factor** This value is simply the product of the average values of instantaneous voltage and current divided by the Power from **4** in the air side data.

It is important to note that the non-compressor watts described in **2**, above, simply refers to all of the power consumed by the air conditioning system less the power consumed by the compressor. The details of determining the non-compressor watts will be covered in the first set of tests.

FIRST SET OF TESTS

This set of tests includes two types of tests at each operating condition of the latching mechanism. The first test is a "slow" test because the sampling rate of data is relatively slow. The second test is a "fast" test due to the much faster data sampling rate (once every tenth of a second). The fast test is also taken over a shorter time period (approximately 1 minute) to keep the magnitude of data to a reasonable level. The slow test is taken over approximately a 5 to 6 minute period of time. Plots of pressure versus time, mass flow rate versus time, etc. will come from the fast data. Performance data such as Capacity, COP, EER, etc. will come from the slow data. Data on evaporator and condensor fan power consumption are also included in this set of tests. Another important system parameter is the expansion device that was used upstream of the evaporator. The stock Italian duct-free spit system had an orifice-type expansion device located immediately downstream of the condensor. This device was cut out of the system and replaced with two adjustable needle-type orifice valves. The two needle valves were placed in parallel and were hand adjusted according to each test condition. Each needle valve had a micrometer type adjustment from 0.000in (valve fully closed) to .300in (valve fully open). The diameter of a fully open valve was .055in. A small sight glass was placed immediately upstream of the needle valves to verify whether there was any vapor entering the expansion valves or not.

Test 1 (August 26, 1998)

Table 4.4 (Configuration)

R22 (lb_m)	3.40
Indoor Fan Setting (Evaporator fan)	Hi
Compressor %	100 (compressor fully loaded)
Duty Period (Seconds)	n.a.
Non Compressor Power (watts)	195
Expansion Settings (Needle Valves)	2 valves fully open
Nozzle Area (ft^2)	.158

Note: The method by which Non Compressor Power was calculated is shown in Test 6.

Table 4.5 (Performance Parameters)

Air flow (cfm)	465.99	
Capacity, total (BTU/hr)	-16471.3	Corrected = -17764.5
Sensible Heat Ratio	-7.71	
Power (watts)	2234.6	
Efficiency (EER)	-7.37	Corrected = -7.95
Efficiency (COP)	-2.16	Corrected = -2.33

Note: Corrected capacity is found by dividing the product of the meter mass flow rate (lb/hr) and the Capacity value (BTU/hr) in the first column by the calculated mass flow rate. The meter mass flow rate and the calculated mass flow rate are listed in the table below. Both flow rates are refrigerant mass flow rates.

Table 4.6 (Balance Checks)

	Calculated (from R22 state point properties and Corrected air side, Tbl 4.5)	Meter (Values taken directly by measurement devices)
R22 Mass Flow Rate (lb/hr)	242.0	260.8
Compressor Power (watts)	2039.6	n.a.
Compressor Heat Factor (lb/watts)	.666	.72 (This value found by using the meter mass flow rate)
Power Factor	.946	n.a.

Comments: This test with the compressor fully loaded was performed to act as a reference for later tests. It was observed that it took approximately 20 minutes from the time the compressor was started until no vapor was seen in the sight glass. Also, it is important to note that the meter mass flow rate is higher than the mass flow rate calculated. When a correction factor was calculated to account for this difference, higher efficiency values were shown in Table 4.5 above. This correction calculation will continue to be used throughout this First Set Of Tests. It was later determined that the refrigerant mass flow rate was indeed higher than that calculated. The source of the error was inappropriate zeroing of the temperature transducers in the evaporator exit air sampler.

Test 2 (August 26, 1998)

Table 4.7 (Configuration)

R22 (lb_m)	3.40
Indoor Fan Setting (Evaporator fan)	Hi
Compressor %	50
Duty Period (seconds)	10
Non Compressor Power (watts)	195
Expansion Settings (Needle Valves)	2 valves fully open
Nozzle Area (ft^2)	.158

Note: The method by which Non Compressor Power was calculated is shown in Test 6.

Table 4.8 (Performance Parameters)

Air flow (cfm)	438.13	
Capacity, total (BTU/hr)	-10728.5	Corrected = -13680.6
Sensible Heat Ratio	-4.87	
Power (watts)	1351.5	
Efficiency (EER)	-7.94	Corrected = -10.12
Efficiency (COP)	-2.33	Corrected = -2.97

Note: Corrected capacity is found by dividing the product of the meter mass flow rate (lb/hr) and the Capacity value (BTU/hr) in the first column by the calculated mass flow rate. The meter mass flow rate and the calculated mass flow rate are listed in the table below. Both flow rates are refrigerant mass flow rates.

Table 4.9 (Balance Checks)

	Calculated (from R22 state point properties and Corrected air side, Tbl 4.8)	Meter (Values taken directly by measurement devices)
R22 Mass Flow Rate (lb/hr)	149.1	189.85
Compressor Power (watts)	1156.5	n.a.
Compressor Heat Factor (lb/watts)	.604	.769 (This value found by using the meter mass flow rate)
Power Factor	.811	n.a.

Comments: During this test vapor was noticed in the sight glass. The vapor followed an interesting cycle in that shortly after the compressor loaded more vapor was noticed flowing more quickly through the sight glass. This is believed to be from the transient vapor in the liquid line being forced through the system at a higher flow rate once the compressor became fully loaded.

Test 3 (August 26, 1998)

Table 4.10 (Configuration)

R22 (lb_m)	3.40
Indoor Fan Setting (Evaporator fan)	Hi
Compressor %	25
Duty Period (seconds)	10
Non Compressor Power (watts)	200
Expansion Settings (Needle Valves)	1 valve closed, 1 valve fully open
Nozzle Area (ft^2)	.158

Note: The method by which Non Compressor Power was calculated is shown in Test 6.

Table 4.11 (Performance Parameters)

Air flow (cfm)	448.7	
Capacity, total (BTU/hr)	-3857.4	Corrected = -7104.5
Sensible Heat Ratio	-2.83	
Power (watts)	865.7	
Efficiency (EER)	-4.45	Corrected = -8.21
Efficiency (COP)	-1.31	Corrected = -2.41

Note: Corrected capacity is found by dividing the product of the meter mass flow rate (lb/hr) and the Capacity value (BTU/hr) in the first column by the calculated mass flow rate. The meter mass flow rate and the calculated mass flow rate are listed in the table below. Both flow rates are refrigerant mass flow rates.

Table 4.12 (Balance Checks)

	Calculated (from R22 state point properties and Corrected air side, Tbl 4.11)	Meter (Values taken directly by measurement devices)
R22 Mass Flow Rate (lb/hr)	51.22	94.3
Compressor Power (watts)	665.7	n.a.
Compressor Heat Factor (lb/watts)	.34	.623 (This value found by using the meter mass flow rate)
Power Factor	.676	n.a.

Comments: Even with one of the needle valves completely closed and the other one fully open, vapor was noticed in the sight glass.

Test 4 (August 26, 1998)

Table 4.13 (Configuration)

R22 (lb_m)	3.40
Indoor Fan Setting (Evaporator fan)	Hi
Compressor %	25
Duty Period (seconds)	5
Non Compressor Power (watts)	195
Expansion Settings (Needle Valves)	1 valve closed, 1 valve fully open
Nozzle Area (ft^2)	.158

Note: The method by which Non Compressor Power was calculated is shown in Test 6.

Table 4.14 (Performance Parameters)

Air flow (cfm)	448.9	
Capacity, total (BTU/hr)	-4120.56	Corrected = -6832.1
Sensible Heat Ratio	-2.94	
Power (watts)	879.0	
Efficiency (EER)	-4.69	Corrected = -7.8
Efficiency (COP)	-1.37	Corrected = -2.28

Note: Corrected capacity is found by dividing the product of the meter mass flow rate (lb/hr) and the Capacity value (BTU/hr) in the first column by the calculated mass flow rate. The meter mass flow rate and the calculated mass flow rate are listed in the table below. Both flow rates are refrigerant mass flow rates.

Table 4.15 (Balance Checks)

	Calculated (from R22 state point properties and Corrected air side, Tbl 4.14)	Meter (Values taken directly by measurement devices)
R22 Mass Flow Rate (lb/hr)	54.13	88.7
Compressor Power (watts)	684.0	n.a.
Compressor Heat Factor (lb/watts)	.34	.560 (This value found by using the meter mass flow rate)
Power Factor	.673	n.a.

Comments: Even with one of the needle valves completely closed and the other one fully open, vapor was noticed in the sight glass.

Test 5 (August 26, 1998)

Table 4.16 (Configuration)

R22 (lb_m)	3.40
Indoor Fan Setting (Evaporator fan)	Hi
Compressor %	50
Duty Period (seconds)	5
Non Compressor Power (watts)	200
Expansion Settings (Needle Valves)	2 valves fully open
Nozzle Area (ft^2)	.158

Note: The method by which Non Compressor Power was calculated is shown in Test 6.

Table 4.17 (Performance Parameters)

Air flow (cfm)	435.2	
Capacity, total (BTU/hr)	-10842.5	Corrected = -13838
Sensible Heat Ratio	-4.90	
Power (watts)	1333.9	
Efficiency (EER)	-8.12	Corrected = -10.38
Efficiency (COP)	-2.38	Corrected = -3.04

Note: Corrected capacity is found by dividing the product of the meter mass flow rate (lb/hr) and the Capacity value (BTU/hr) in the first column by the calculated mass flow rate. The meter mass flow rate and the calculated mass flow rate are listed in the table below. Both flow rates are refrigerant mass flow rates.

Table 4.18 (Balance Checks)

	Calculated (from R22 state point properties and Corrected air side, Tbl 4.17)	Meter (Values taken directly by measurement devices)
R22 Mass Flow Rate (lb/hr)	151.67	194.1
Compressor Power (watts)	1133.9	n.a.
Compressor Heat Factor (lb/watts)	.58	.747 (This value found by using the meter mass flow rate)
Power Factor	.805	n.a.

Comments: Both valves were opened for this test and vapor was noticed in the sight glass.

Test 6 (August 27, 1998)

This test was performed in order to determine the non compressor power. It also was done in order to determine the power the indoor fan (evaporator) drew. The experimental set up for this test was very simple. The compressor was simply disconnected from the system and thus the power meter read the system power minus the compressor power (non compressor power). The non compressor power was measured with the supply power at two different voltage settings. The indoor or evaporator fan was also set at three different settings (low, medium, and high).

Table 4.19 (Power tests with the supply power at 231 volts)

Indoor Fan Speed Setting	Fan only (watts)	Non Compressor Power (includes fan only power) (watts)
Low	53	181
Medium	53	181
High	67	195

Table 4.20 (Power tests with the supply power at 235.5 volts)

Indoor Fan Speed Setting	Non Compressor Power (includes fan only power) (watts)
High	200

Comments: It should be noted that the 195 watts and 200 watts values are used in Tests 1 through 5 as the non compressor power. The decision to choose either the 195 watts value or the 200 watts value was based off the magnitude of the power supply voltage during the particular test being conducted.

Test 7 (August 31, 1998)

These tests were performed in order to determine the power consumption of the condensor (outdoor) fan. Several different size capacitors were tested with the condensor fan motor. Fan shaft rotational speed was also measured using a strobe light and pieces of aluminum foil attached to the fan blades. The results of these tests are shown below in Table 4.21.

Table 4.21 (Power tests on condensor fan motor. Supply voltage = 231V)

Fan Motor Capacitor Size (microFarad)	Fan shaft speed (RPM)	Fan Motor Power Consumption (watts)
No capacitor	935	130
5	503	135
4	405	53
3	307	34

Data plotted from test 3 is shown below in Figure 4.4. Included on this plot is compressor entering pressure, compressor leaving pressure, and outdoor liquid pressure (pressure at the exit of the condensor) as functions of time. Obviously, this plot is representative of the compressor cycling from loaded to unloaded. As the compressor loads and unloads, a cycling pressure magnitude is noticed from this plot for all three variables. The important conclusion that is drawn from this plot is that there is very little damping of the pressure transient from the compressor exit to the condensor exit.

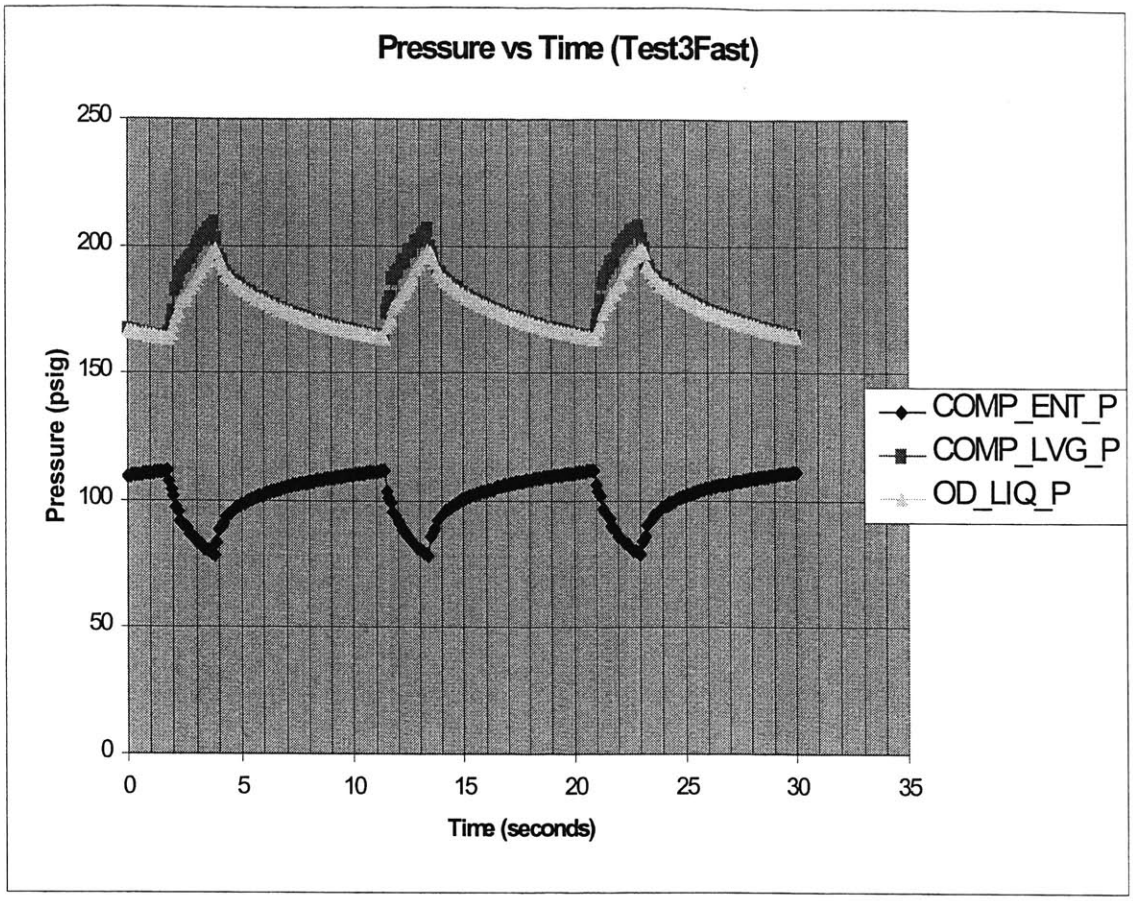

Figure 4.4 (This is a plot showing data taken from Test 3.)

Figure 4.5, below, is another plot of data from Test 3. This plot is representative of the exact same system conditions as shown in the plot in Figure 4.4. This plot shows the compressor entering pressure and the indoor liquid pressure (the pressure downstream of the needle-type expansion valves, but upstream of the evaporator) as functions of time. It is important to point out that there is noticeable damping of the pressure magnitude across the evaporator. However, the pressure transient of the indoor liquid remains in phase with the pressure change at the compressor inlet.

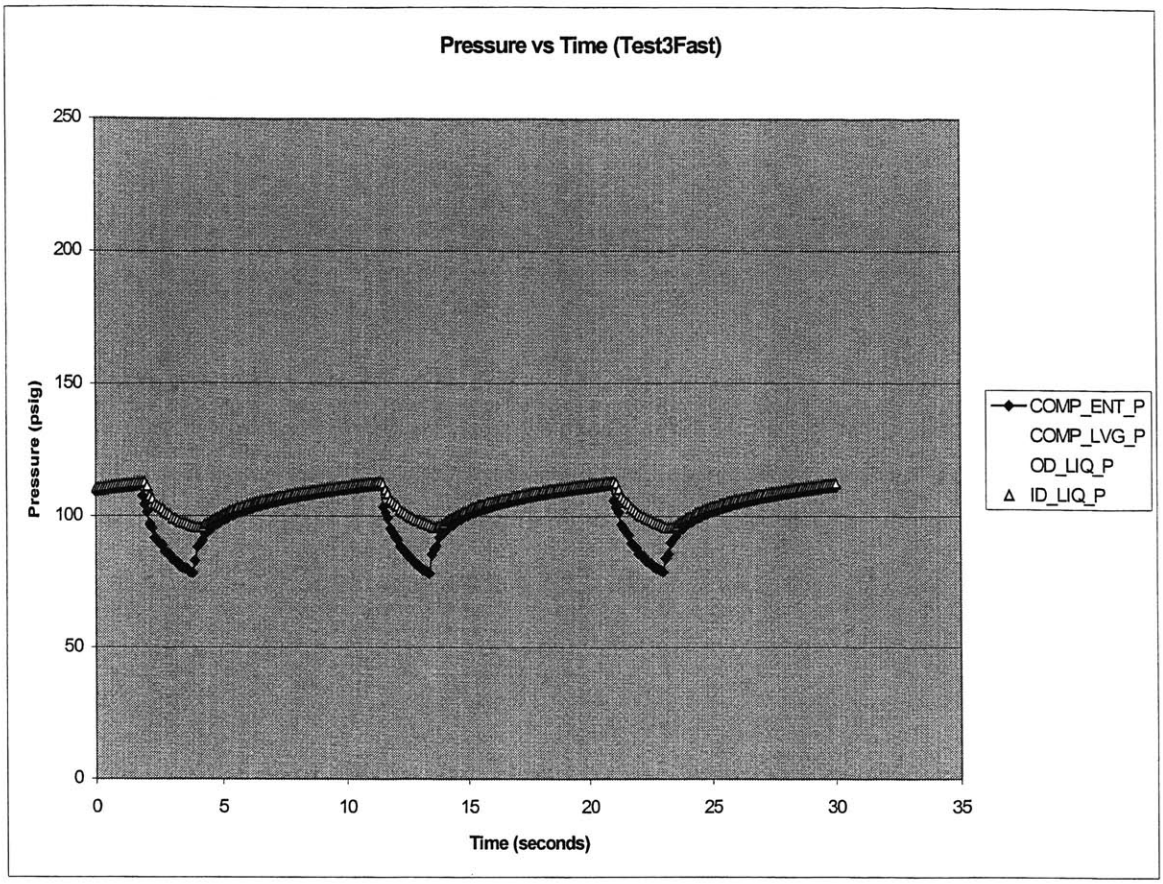

Figure 4.5 (This is a plot showing data taken from Test 3)

OVERALL CONCLUSIONS FROM THE FIRST SET OF TESTS

1. There was no significant pressure "damping" across the condensor. "Across the condensor" is defined from compressor exit to condensor exit.

2. There was a noticable pressure "damping" effect across the evaporator. "Across the evaporator" is defined from just upstream of the evaporator to just upstream of the compressor.

3. Compressor entering pressure and compressor leaving pressure average values are the same (approximately) for the 5 second period and 10 second period test runs. This is comparing test runs 2 and 5 (both @ 50% duty cycle) and test runs 3 and 4 (both at @ 25% duty cycle).

4. Condensor pressure drop is equal to approximately 6 psig for the 50% duty cycle tests. Condensor pressure drop is equal to approximately 3 psig for the 25% duty cycle tests.

5. Evaporator pressure drop (measured from just upstream of the evaporator to compressor inlet) is equal to approximately 15 psig for the 50% duty cycle tests. Evaporator pressure drop is equal to approximately 5 psig for the 25% duty cycle tests. It is important to note that the measured pressure drop includes the evaporator, approximately 25ft of vapor line, and the suction filter dryer.

6. There is not much difference in the efficiency values (COP and EER) between the two 50% duty cycle tests (test 2 and test 5).

7. There is not much difference in the efficiency values (COP and EER) between the two 25% duty cycle tests (test 3 and test 4).

8. The EER for the two 50% duty cycle tests (test 2 and test 5) is greater than the EER for test 1 (steady, fully loaded operation).

9. The EER for the two 25% duty cycle tests (test 3 and test 4) is less than the EER for test 1 (steady, fully loaded operation). This efficiency value could be much better if the unloaded watts could be reduced. i.e. reduce power to the compressor while it is unloaded.

10. Unloaded power = (minimum power – non compressor power)
    Test 5 = 417watts, Test 4 = 421watts, Test 2 = 424watts, Test 3 = 409watts

11. All the cycling tests had very low sub-cooling values. Vapor was observed in the liquid line sight glass for all cycling tests.

SECOND SET OF TESTS

The second set of tests once again includes "slow" and "fast" tests at each operating condition of the latching mechanism. Plots of pressure versus time, mass flow rate versus time, etc. will come from the fast data. These second set of tests have several improvements over the first set of tests. First, a watt-hour meter was installed to accurately keep track of the total power consumed by the system during each test. The first set of tests relied on averaging the values of instantaneous power measurements. Second, more R22 was added to the system in order to eliminate the vapor seen in the sight glass during the first set of tests. Last, a 40%, and 30% compressor duty cycle test was performed to better understand system performance parameters as a function of compressor duty cycle (percentage of time the compressor is loaded during a duty period setting).

Test 1 (August 31, 1998)

Table 4.22 (Configuration)

R22 (lbm)	3.62
Indoor Fan Setting (Evaporator fan)	Hi
Compressor %	25
Duty Period (seconds)	10
Non Compressor Power (watts)	195
Expansion Settings (Needle Valves)	1 valve closed, 1 valve at .275in of .300in
Nozzle Area (ft^2)	.0709

Table 4.23 (Performance Parameters)

	Initial Measurement	Air Corrected	From Watt-Hour Meter
Air Flow (cfm)	447.6		
Capacity, total (BTU/hr)	-5686.8	-6811.8	
Sensible Heat Ratio	1.051		
Power (watts)	868.5	868.5	855
Efficiency (EER)	-6.55	-7.84	-7.97
Efficiency (COP)	-1.92	-2.29	-2.36

Note: Air Corrected capacity is found by dividing the product of the meter mass flow rate (lb/hr) and the Capacity value (BTU/hr) in the first column by the calculated mass flow rate. The power value in the Watt-Hour meter column is a true power value (not averaged).

Table 4.24 (Balance Checks)

	Calculated (from R22 state point properties)	Meter (Values taken directly by measurement devices)
R22 Mass Flow Rate (lb/hr)	89.6	91.7
Compressor Power (watts)	673.5	660 (This value found by using Meter value from Table 4.23)
Compressor Heat Factor (lb/watts)	.548	.572 (This value found by using the meter mass flow rate and the meter power)
Power Factor	.707	n.a.

Comments: No vapor was noticed in the sight glass. It is important to point out here that the needle valves were hand adjusted at each test in order to eliminate vapor in the sight glass. This was done only for the second set of tests. Approximately ten minutes was

allowed between tests to make sure that, at the compressor duty cycle and duty period setting, no vapor was seen in the sight glass.

Test 2 (August 31, 1998)

Table 4.25 (Configuration)

R22 (lbm)	3.62
Indoor Fan Setting (Evaporator fan)	Hi
Compressor %	25
Duty Period (seconds)	5
Non Compressor Power (watts)	195
Expansion Settings (Needle Valves)	1 valve closed, 1 valve at .275in of .300in
Nozzle Area (ft^2)	.0709

Table 4.26 (Performance Parameters)

	Initial Measurement	Air Corrected	From Watt-Hour Meter
Air Flow (cfm)	447.4		
Capacity, total (BTU/hr)	-5906.2	-7031.2	
Sensible Heat Ratio	1.036		
Power (watts)	854.9	854.9	842
Efficiency (EER)	-6.91	-8.22	-8.35
Efficiency (COP)	-2.02	-2.41	-2.45

Note: Air Corrected capacity is found by dividing the product of the meter mass flow rate (lb/hr) and the Capacity value (BTU/hr) in the first column by the calculated mass flow rate. The power value in the Watt-Hour meter column is a true power value (not averaged).

Table 4.27 (Balance Checks)

	Calculated (from R22 state point properties)	Meter (Values taken directly by measurement devices)
R22 Mass Flow Rate (lb/hr)	92.8	91.2
Compressor Power (watts)	659.9	647 (This value found by using Meter value from Table 4.23)
Compressor Heat Factor (lb/watts)	.598	.600 (This value found by using the meter mass flow rate and the meter power)
Power Factor	.703	n.a.

Comments: No vapor was seen in the sight glass.

Test 3 (September 1, 1998)

Table 4.28 (Configuration)

R22 (lbm)	3.62
Indoor Fan Setting (Evaporator fan)	Hi
Compressor %	50
Duty Period (seconds)	10
Non Compressor Power (watts)	195
Expansion Settings (Needle Valves)	1 valve open, 1 valve at .215in of .300in
Nozzle Area (ft^2)	.0709

Table 4.29 (Performance Parameters)

	Initial Measurement	Air Corrected	From Watt-Hour Meter
Air Flow (cfm)	429.5		
Capacity, total (BTU/hr)	-11529.72	-12654.7	
Sensible Heat Ratio	.827		
Power (watts)	1333.16	1333.16	1278
Efficiency (EER)	-8.65	-9.49	-9.90
Efficiency (COP)	-2.53	-2.78	-2.90

Note: Air Corrected capacity is found by dividing the product of the meter mass flow rate (lb/hr) and the Capacity value (BTU/hr) in the first column by the calculated mass flow rate. The power value in the Watt-Hour meter column is a true power value (not averaged).

Table 4.30 (Balance Checks)

	Calculated (from R22 state point properties)	Meter (Values taken directly by measurement devices)
R22 Mass Flow Rate (lb/hr)	171.4	172.6
Compressor Power (watts)	1138.2	1083 (This value found by using Meter value from Table 4.23)
Compressor Heat Factor (lb/watts)	.682	.721 (This value found by using the meter mass flow rate and the meter power)
Power Factor	.834	n.a.

Comments: No vapor was seen in the sight glass.

Test 4 (September 1, 1998)

Table 4.31 (Configuration)

R22 (lbm)	3.62
Indoor Fan Setting (Evaporator fan)	Hi
Compressor %	50
Duty Period (seconds)	5
Non Compressor Power (watts)	195
Expansion Settings (Needle Valves)	1 valve open, 1 valve at .225in of .300in
Nozzle Area (ft^2)	.0709

Table 4.32 (Performance Parameters)

	Initial Measurement	Air Corrected	From Watt-Hour Meter
Air Flow (cfm)	432.1		
Capacity, total (BTU/hr)	-11891.3	-1316.25	
Sensible Heat Ratio	.816		
Power (watts)	1318.3	1318.3	1290
Efficiency (EER)	-9.02	-9.87	-10.09
Efficiency (COP)	-2.64	-2.89	-2.96

Note: Air Corrected capacity is found by dividing the product of the meter mass flow rate (lb/hr) and the Capacity value (BTU/hr) in the first column by the calculated mass flow rate. The power value in the Watt-Hour meter column is a true power value (not averaged).

Table 4.33 (Balance Checks)

	Calculated (from R22 state point properties)	Meter (Values taken directly by measurement devices)
R22 Mass Flow Rate (lb/hr)	176.3	176.6
Compressor Power (watts)	1123.3	1095 (This value found by using Meter value from Table 4.23)
Compressor Heat Factor (lb/watts)	.725	.745 (This value found by using the meter mass flow rate and the meter power)
Power Factor	.829	n.a.

Comments: No vapor was seen in the sight glass.

Test 5 (September 1, 1998)

Table 4.34 (Configuration)

R22 (lbm)	3.62
Indoor Fan Setting (Evaporator fan)	Hi
Compressor %	50
Duty Period (seconds)	2
Non Compressor Power (watts)	195
Expansion Settings (Needle Valves)	1 valve open, 1 valve at .245in of .300in
Nozzle Area (ft^2)	.0709

Table 4.35 (Performance Parameters)

	Initial Measurement	Air Corrected	From Watt-Hour Meter
Air Flow (cfm)	430.3		
Capacity, total (BTU/hr)	-12203.7	-13328.7	
Sensible Heat Ratio	.804		
Power (watts)	1316.8	1316.8	1270
Efficiency (EER)	-9.27	-10.12	-10.50
Efficiency (COP)	-2.72	-2.97	-3.08

Note: Air Corrected capacity is found by dividing the product of the meter mass flow rate (lb/hr) and the Capacity value (BTU/hr) in the first column by the calculated mass flow rate. The power value in the Watt-Hour meter column is a true power value (not averaged).

Table 4.36 (Balance Checks)

	Calculated (from R22 state point properties)	Meter (Values taken directly by measurement devices)
R22 Mass Flow Rate (lb/hr)	180.8	181.8
Compressor Power (watts)	1121.8	1075 (This value found by using Meter value from Table 4.23)
Compressor Heat Factor (lb/watts)	.750	.786 (This value found by using the meter mass flow rate and the meter power)
Power Factor	.815	n.a.

Comments: No vapor was seen in the sight glass.

Test 6 (September 1, 1998)

Table 4.37 (Configuration)

R22 (lbm)	3.62
Indoor Fan Setting (Evaporator fan)	Hi
Compressor %	40
Duty Period (seconds)	5
Non Compressor Power (watts)	195
Expansion Settings (Needle Valves)	1 valve open, 1 valve at .185in of .300in
Nozzle Area (ft^2)	.0709

Table 4.38 (Performance Parameters)

	Initial Measurement	Air Corrected	From Watt-Hour Meter
Air Flow (cfm)	432.5		
Capacity, total (BTU/hr)	-10152.9	-11277.9	
Sensible Heat Ratio	.885		
Power (watts)	1130.5	1130.5	1113
Efficiency (EER)	-8.98	-9.98	-10.13
Efficiency (COP)	-2.63	-2.92	-2.97

Note: Air Corrected capacity is found by dividing the product of the meter mass flow rate (lb/hr) and the Capacity value (BTU/hr) in the first column by the calculated mass flow rate. The power value in the Watt-Hour meter column is a true power value (not averaged).

Table 4.39 (Balance Checks)

	Calculated (from R22 state point properties)	Meter (Values taken directly by measurement devices)
R22 Mass Flow Rate (lb/hr)	152.7	152.7
Compressor Power (watts)	935.5	918 (This value found by using Meter value from Table 4.23)
Compressor Heat Factor (lb/watts)	.712	.726 (This value found by using the meter mass flow rate and the meter power)
Power Factor	.800	n.a.

Comments: No vapor was seen in the sight glass.

Test 7 (September 1, 1998)

Table 4.40 (Configuration)

R22 (lbm)	3.62
Indoor Fan Setting (Evaporator fan)	Hi
Compressor %	30
Duty Period (seconds)	5
Non Compressor Power (watts)	195
Expansion Settings (Needle Valves)	1 valve open, 1 valve at .100in of .300in
Nozzle Area (ft^2)	.0709

Table 4.41 (Performance Parameters)

	Initial Measurement	Air Corrected	From Watt-Hour Meter
Air Flow (cfm)	435.2		
Capacity, total (BTU/hr)	-8438.9	-9563.9	
Sensible Heat Ratio	.949		
Power (watts)	990.8	990.8	950
Efficiency (EER)	-8.52	-9.65	-10.07
Efficiency (COP)	-2.50	-2.83	-2.95

Note: Air Corrected capacity is found by dividing the product of the meter mass flow rate (lb/hr) and the Capacity value (BTU/hr) in the first column by the calculated mass flow rate. The power value in the Watt-Hour meter column is a true power value (not averaged).

Table 4.42 (Balance Checks)

	Calculated (from R22 state point properties)	Meter (Values taken directly by measurement devices)
R22 Mass Flow Rate (lb/hr)	126.3	119.3
Compressor Power (watts)	795.8	755 (This value found by using Meter value from Table 4.23)
Compressor Heat Factor (lb/watts)	.686	.683 (This value found by using the meter mass flow rate and the meter power)
Power Factor	.762	n.a.

Comments: No vapor was seen in the sight glass.

Pressure versus time data from test 5 is plotted below in order to demonstrate the magnitude of pressure damping across the evaporator. It should be noted that as the duty period is decreased, the magnitude of damping across the evaporator is increased. The plot of pressure versus time data across the condensor is not shown due to its similarity of that shown in Figure 4.4.

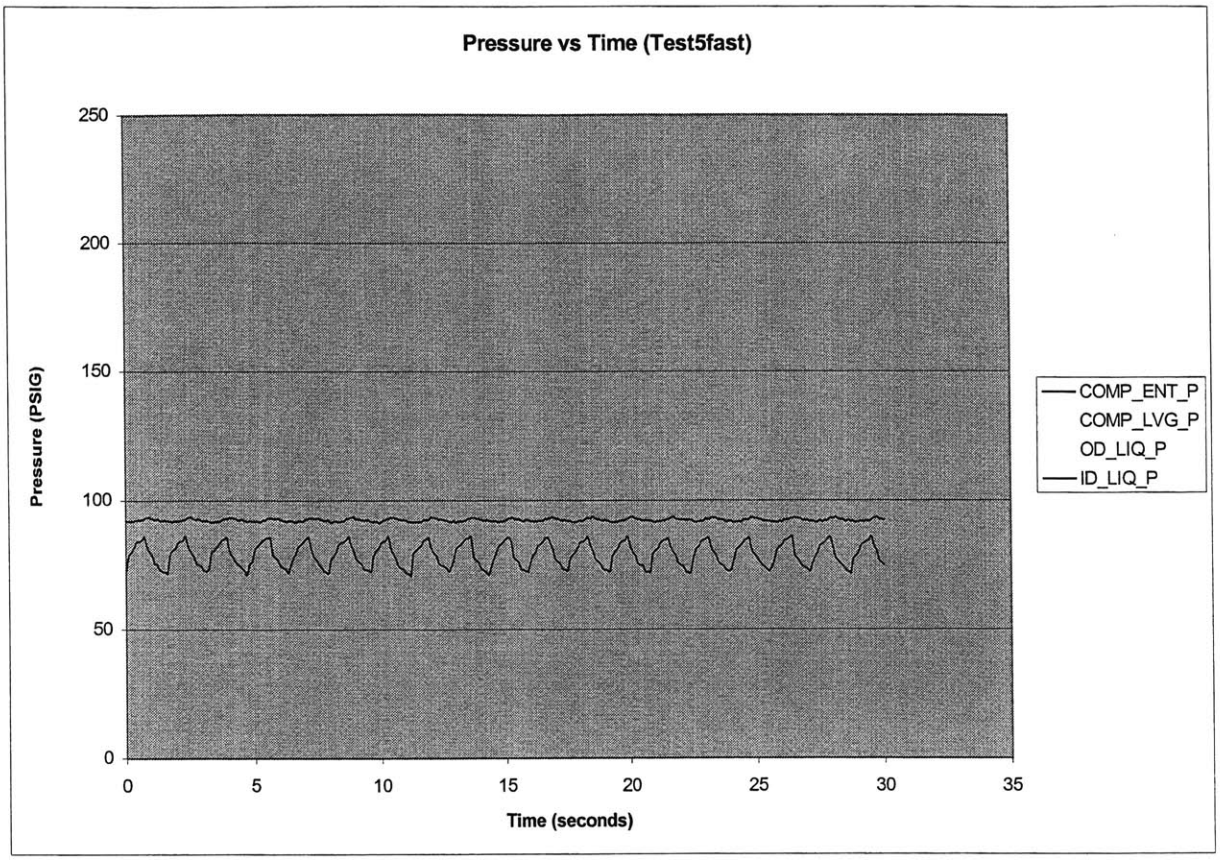

Figure 4.6 (This is a plot showing data taken from test 5. Notice the high damping across the evaporator shown by the indoor liquid pressure.)

OVERALL CONCLUSIONS FROM THE SECOND SET OF TESTS

1. There was no significant pressure "damping" across the condensor. "Across the condensor" is defined from compressor exit to condensor exit.

2. There was a noticable pressure "damping" effect across the evaporator. "Across the evaporator" is defined from just upstream of the evaporator to just upstream of the compressor. This "damping" effect became more noticeable on the 50% duty cycle tests as the period was reduced (from 10 sec to 5 sec to 2 sec). The pressure "damping" effect was also quite noticeable on Test 6 (40% duty cycle).

3. Compressor entering pressure and compressor leaving pressure average values are the same (approximately) for the two 25% duty cycle tests and the three 50% duty cycle tests. This is comparing test runs 1 and 2 (both at 25% duty cycle) and test runs 3, 4, and 5 (all three at 50% duty cycle). A general trend that is observed is that as the percentage of time that the compressor is loaded is decreased, the average compressor entering pressure becomes larger. Also, as the percentage of time that the compressor is loaded is decreased, the average compressor leaving pressure becomes smaller. Results from the 40% duty cycle test and the 30% duty cycle test support this conclusion.

4. Condensor pressure drop is equal to approximately 3 psig for the 25% duty cycle tests, 5 psig for the 50% duty cycle tests, 5 psig for the 40% duty cycle test, and 4 psig for the 30% duty cycle test.

5. Evaporator pressure drop (measured from just upstream of the evaporator to compressor inlet) is equal to approximately 5 psig for the 25% duty cycle tests, 14 psig for the 50% duty cycle tests, 11 psig for the 40% duty cycle test, and 7 psig for the 30% duty cycle test. It is important to note that the measured pressure drop includes the evaporator, approximately 25ft of vapor line, and the suction filter dryer.

6. There is not much difference in the efficiency values (COP and EER) between the two 25% duty cycle tests (test 1 and test 2).

7. There is not much difference in the efficiency values (COP and EER) between the three 50% duty cycle tests (test 3, test 4, and test 5).

8. There is not much difference in the efficiency values (COP and EER) between the 40% duty cycle test and the 30% duty cycle test.

9. It is important to note that while the difference in efficiency values (COP and EER) is small, a general trend of increasing efficiency is observed as the duty period is reduced. For example, when comparing test 3 and test 4 (both at 50% duty cycle), the COP increases from –9.902 to –10.09. This trend is consistent when looking at all the tests.

10. The EER for test 1 (Air Corrected) (25% duty cycle) is approximately equal to the EER for test 1 from the first set of tests (fully loaded operation). The EER for test 2 (25% duty cycle) is greater than the EER for test 1 from the first set of data.

11. The EER for test 3, test 4, and test 5 (50% duty cycle) is greater than the EER for test 1 from the first set of data (fully loaded operation).

12. The EER for test 5 (40% duty cycle) and the EER for test 6 (30% duty cycle) is greater than the EER for test 1 from the first set of data (fully loaded operation).

13. Unloaded power = (minimum power – non compressor power)
Test 1 = 403watts, Test 2 = 399watts, Test 3 = 400watts, Test 4 = 399watts
Test 5 = 402watts, Test 6 = 392watts, Test 7 = 391watts

5. CONCLUSION

This final chapter is intended to discuss design issues that were not addressed in previous chapters. These design issues are ones that need to be solved in order to fully implement the latching mechanism in a Carrier EDB-240 rotary compressor. Each issue will be presented briefly in the following sections along with suggestions on how to solve the associated problems.

5.1 NOISE

With the compressor unloaded, the rolling piston "bumps" the vane and vane stem displacing both pieces approximately .017in. A noise is created due to this bumping. There is some uncertainty as to exactly where this noise is coming from and how it is making it to the outside world (to a human's ear). A possible explanation is the compressor shell flexing due to the vane load being transmitted to it when the mechanism latches. In any case, the noise level was quickly determined to be unacceptable. A quick and obvious solution to the problem is to modify the latching mechanism such that it has no vane bump. However, this proves to be especially difficult in the sense that the self-timing feature of vane release at rolling piston top dead center would be eliminated. Even though this "no vane bump" mechanism appears to be a difficult mechanism to design, it appears to be the best solution to the noise problem.

5.2 UNLOADED POWER

Efficiency values (COP and EER) increased by running the compressor in variable capacity mode (latching and unlatching the vane and vane stem). However, simple cost estimates were later done by Dick Duell and Kevin Dunshee at Carrier and Dr. Steve Umans at MIT. These cost estimates showed that the efficiency values discovered in the test data would have to be increased in order for Carrier to regain the cost of implementing the latch mechanism and manufacturing it. An obvious way of doing this is to reduce to the power to the compressor motor while it is unloaded (vane and vane stem latched). Attempts were underway to experiment with this and get results, but due to lack of time no concrete experimental results were obtained. Also, care would have to be paid to the cost of implementing the electronic controls and hardware needed to cut power to the compressor while it is unloaded.

5.3 ADJUSTABLE EXPANSION VALVES (TXV'S)

As was discovered in testing the compressor at Carrier in an air conditioning system; the expansion valves needed to be adjusted every time the duty cycle and/or duty period of the latching mechanism were/was changed. Of course this operation would have to be done automatically by an electronically controlled TXV valve. The concern is that electronic TXV valves are expensive and would drive the total cost of the latching

mechanism and it's associated hardware to unacceptable levels. However, at this point there doesn't appear to be another solution available.

5.4 FAILURE DUE TO CYCLIC LOADING

Due to the design of the mechanism, cyclic loading of certain parts is unavoidable. It is the combination of high loads and very small cross sectional areas that raises serious concerns about the reliability and durability of the mechanism. The slider (or latch pin as it was later named) has a very small cross section and is expected to hold up to loads as high as 100lb. These loads can cycle on and off at rates of 60Hz. Over several years of operation the fatigue of small latch components (such as the slider) can become a major concern. In the prototype mechanism that was built at MIT and tested at MIT and Carrier, the slider material failed and broke into two pieces. It should be pointed out that the slider and the vane stem were made of type A2 air hardened tool steel. For the demonstration apparatus these parts were left in the annealed condition where as the design (see Section 2.6) was based on the hardened condition. In any case, a serious effort needs to be done in order to correctly size mechanism components and to make sure that they can withstand the high magnitude cyclic loads that they will encounter.

5.5 LATCHING MECHANISM MOUNTED INTERNALLY

The prototype latching mechanism that was designed and built at MIT was mounted externally to the compressor (vane stem protruded through the compressor shell). An external mounted latching mechanism would not be cost effective to manufacture in large quantities. Therefore the mechanism would have to be mounted inside the shell of the compressor. This does require significant design considerations since space constraints become more critical inside the shell. This is especially crucial since it was discovered that the solenoid coil could be physically larger in order to aid in the extracting of the slider. Also of importance is the precision tolerance requirements on the latching mechanism parts. Moving the latching mechanism inside the shell does not eliminate the precision tolerance issue that would have to be dealt with in order to achieve a cost effective design for manufacture and assembly.

REFERENCES

1. J. Meriam and L. Kraige, Engineering Mechanics, Volume Two, Dynamics, 3rd ed., John Wiley & Sons, Inc., 1992

2. William D. Callister, Jr., Materials Science And Engineering, An Introduction, 3rd ed., John Wiley & Sons, Inc., 1994

3. Ferdinand P. Beer and E. Russell Johnston, Jr., Mechanics Of Materials, 2nd ed., McGraw-Hill, Inc., 1992

4. Norman H. Beachley and Howard L. Harrison, Introduction To Dynamic System Analysis, Harper & Row, 1978

APPENDIX A: MATLAB CODE USED TO MODEL SLIDER DYNAMIC MOTION (CHAPTER 2, SECTION 4)

```
t  = 0;
tf = .00228;
tspan = [t0 tf];
x0 = [.110 0]'; %initial displ in ft .040in spacer + .070 slider travel

[t,x] = ode23 ('sliderderivaives', tspan, x0);

lent = length (t)

x1 = x(1:lent, 1)
x2 = x(1:lent, 2)

subplot (211)
plot (t, x1)
xlabel ('time (sec)')
ylabel ('displacement (in)')
title (['Displacement vs. Time: Lighter Mass, Spring, and FEA mag force'])

subplot (212)
plot (t, x2)
xlabel ('time (sec)')
ylabel ('velocity (in/sec)')
title (['Velocity vs. Time: Mass and Spring Only'])
```

```
function xdot = sliderderivatives (t, x)
a = 1463.8;
b = -244.1;
c = -4.3039;
d = 1.6902;
m = .00001381; % units in lb*s^2/in

%a = 0;
%b = 0;
%c = 2.0714; % units in lb*s^2/in
%d = -.5989;
%m = .00001825; % units in lb*s^2/in
A = a/m;
```

```
B = b/m;
C = c/m;
D = d/m;
xdot = [x(2); -A*(x(1))^3 – B*(x(1))^2 – C*(x(1)) –D];
```